RPL-TDR-64-108

TOTAL IMPULSE MEASURING SYSTEM FOR SOLID-PROPELLANT ROCKET ENGINE

PHASE I REPORT

JUNE 1963

SECOND PRINTING
AUGUST 1964

TECHNICAL DOCUMENTARY REPORT NO. RPL-TDR-64-108

AIR FORCE ROCKET RESEARCH LABORATORIES
AIR FORCE SYSTEMS COMMAND
UNITED STATES AIR FORCE
EDWARDS, CALIFORNIA

PROJECT NO. 3850, TASK NO. 3850306

PREPARED UNDER CONTRACT NO. AF04 (611)-8515

BY

V. C. PLANE

ROCKETDYNE
A DIVISION OF NORTH AMERICAN AVIATION, INC.
6633 CANOGA AVENUE, CANOGA PARK, CALIFORNIA

NOTICES

When Government drawings, specifications, or other data are used for any purpose other than in connection with a definitely related Government procurement operation, the United States Government thereby incurs no responsibility nor any obligation whatsoever; and the fact that the Government may have formulated, furnished, or in any way supplied the said drawings, specifications, or other data, is not to be regarded by implication or otherwise as in any manner licensing the holder or any other person or corporation, or conveying any rights or permission to manufacture, use, or sell any patented invention that may in any way be related thereto.

Copies of this report should not be returned to the Air Force Laboratories unless return is required by security considerations, contractual obligations, or notice on a specific document.

This report is releasable to the Office of Technical Services, Department of Commerce.

FOREWORD

This report was prepared by Rocketdyne, a Division of North American Aviation, Inc., Canoga Park, California, on Air Force Contract AF04(611)-8515 under Task No. 3850306 of Project No. 3850, "Total Impulse Measuring System for Solid-Propellant Rocket Engine (Research)." Contract AF04(611)-8515 consists of a program for the analysis and design (Phase I), fabrication and testing (Phase II), and installation and testing (Phase III), of an accurate (0.1%) solid-propellant total impulse measurement system for Edwards Air Force Base. This report is submitted to present the development status of the system, and constitutes the Phase I report in the over-all program. It was prepared by the Research Instrumentation Group of the Rocketdyne Research Department.

ABSTRACT

Discussion and results of the three main considerations comprising the initial (Phase I) effort are presented: (1) study and discussion of the use site and existing measurement system at EAFB, with recommendations for the installation of the Rocketdyne system; (2) general and applied mathematical analyses of spring-mass total impulse measurement systems; and (3) mechanical and electrical design of the Rocketdyne system to be constructed. Specific results of these separate but related program efforts are, respectively: (1) concurrence with the general approach taken in the existing EAFB system, but disagreement with some specific design, installation, and operational features of the system; (2) new and original methematical analyses whose results justify the Rocketdyne approach to the measurement problem; and (3) new and original mechanical and electrical component designs which set a new standard in accuracy and performance, producing an over-all error breakdown commensurate with program objectives.

TABLE OF CONTENTS

LIST OF ILLUSTRATIONS

LIST OF TABLES

SUMMARY

The final results of effort in the initial (Phase I) portion of the contract were twofold. First, production of a detailed design for the total impulse measuring system with the desired measurement capabilities was accomplished. The results of all associated analyses of this system indicate that its performance, in anticipated solid-propellant studies, will produce measurements with total errors not exceeding 0.1%. Second, the analytical development undertaken in support of the design effort produced general quantitative results useful in any design of spring-mass systems for transient thrust and total impulse measurement systems. The general trapezoidal excitation of both one- and two-degree-of-freedom systems, with viscous damping, was investigated, and the methods used to obtain the errors expressions and tabulations are applicable to comparatively short, as well as long engine operating durations. Consequently, the mathematical results obtained with this program are directly applicable, for example, to measurements associated with pulsed-mode operations of space engines. As a result, analytical and design experience was obtained that appears useful for future applications in dynamic force and impulse measurements.

The following specific subjects are discussed and/or analyzed:

1. Existing thrust integration system at EAFB;
2. Recommendations for installation of Rocketdyne-designed system at EAFB;
3. General mathematical discussion of the relationship between the integrated input and integrated output for certain linear dynamic systems;
4. Analytical dynamics of a spring-mass total impulse measurement system (one degree-of-freedom): theory and application;
5. Dynamic response of Rocketdyne thrust and total impulse measurement system (two degree-of-freedom): theory and application;

6. Theory and application of parallelogram compresion-type flexure suspension systems;

7. Detailed description of the design of mechanical and electrical system and components;

8. Determination of complete spring-mass system;

9. Description of the design of additional instrumentation developed for operational use with the total impulse measurement system.

EDWARDS AIR FORCE BASE THRUST INTEGRATION SYSTEM

INTRODUCTION

Discussions and use-site inspections with EAFB personnel have resulted in agreement regarding the general measurement system approach previously taken by EAFB in the design and construction of equipment and facilities for solid-propellant evaluation studies (BATES). A total impulse measuring system consisting of a precision strain-gage load cell supplying an analog signal to a voltage-controlled oscillator, to produce a proportional pulse repetition rate whose output is cumulatively registered by an electronic counter, is regarded as basically sound and accurate because of the continued development such equipment has received in recent years. However, very substantial improvement has been immediately realized in this method through concentrated design and analytical efforts directed at component and system refinement. As a result, specific design, installation, and operational features of the existing EAFB system appear undesirable and incompatible with the measurement objectives in this contract. A two-part discussion follows of practical instrumentation engineering considerations and their application to the EAFB system.

PART I: GENERAL DISCUSSION

Error Factors

The design of a high-precision recording system for low-level signals requires a knowledge of several factors which are not readily apparent. The three error-producing elements which are commonly neglected are: (1) contact resistance, (2) leakage, and (3) thermal emf.

Contact Resistance. Contact resistance is present whenever a coupling is introduced: connector, terminal strip, program board, switch, relay, etc. Variations in contact resistance are usually caused by dirt and by "dry

circuit" contacts. (Dry circuits occur when the current level is too low to remove oxidation and "powdering" of contact surfaces.) Resistance can be controlled by good maintenance and by choosing relays and switches which provide good wiping action between chemically stable contact materials. In most cases, contact resistance is not a serious problem, but it can become serious if it is disregarded.

Leakage. Leakage occurs wherever a signal lead wire is exposed, and it is present at those devices named in the foregoing paragraph on contact resistance. (Note: This is often called "leakage resistance," which makes it an inverted term. It is better to use "leakage" alone as a noun than to chance the confusion caused by "leakage" and "resistance" being of opposite inclination.) Although leakage can be caused by sloppy techniques (dirt, oil, finger tracks, etc.), it is most often the result of atmospheric humidity and is consequently variable. Its most annoying characteristic, however, is that it is very difficult to measure.

The reason for this measurement difficulty is that if a resistance-measuring device is placed across two terminals where moisture is suspected, the voltage from the device causes electrolysis of the moisture. Gas is formed at one terminal (at least), and the measurement shows the resistance of the gas film. The thickness of the gas film is determined by the amount of voltage across the terminals. This effect is shown in Table 1 which gives the leakage measured between four pairs of terminals on a moistened fanning (terminal) strip. The "low-voltage bridge" was assembled in the laboratory and designed to apply approximately the same voltage across the terminals as occurs from a transducer signal. It should be noted that a device like the Voltohmyst, with its 1.5-volt source, does not introduce sufficient error to be serious, but that the high-voltage source can give an extremely erroneous result.

The most serious problem caused by leakage occurs when a bridge network is used as a transducer. Leakage will reduce the sensitivity, and if it is unsymmetrical, it will change the balance point. Very little leakage is necessary; for example, using a 350-ohm, 3 mv volt bridge, 2.5 megohms across one leg represents 1% of unbalance.

TABLE 1

LEAKAGE MEASUREMENTS

Type of Device	Approximate Voltage From Source	Measured Resistance, ohms
Megger (Biddle)	150	500,000
Ohmmeter (Triplett)	45	100,000
Voltohmyst (RCA)	1.5	6,500
Low-Voltage Bridge (Lab Assembly)	0.01	3,200

Thermal Emf. Thermal emf is produced wherever dissimilar metals are in contact. Fortunately, these dissimilar metal contacts come in pairs and are opposite in direction, so that if the two contacts of the pair are at the same temperature, the thermal emf's will cancel. For example, a copper lead wire is connected to one brass lug of a switch. The other brass lug naturally connects to the copper wire continuation. Basically (disregarding the other metals in the switch), this becomes a copper-brass-brass-copper sequence, and the emf generated from copper to brass is equal and opposite to that generated from brass to copper, provided that the junction temperatures are equal. This is the function of Becquerel's Law for Intermediate Metals, which says that a dissimilar metal may be inserted in a line provided that the junctions are at the same temperature.

However, the insistance on no ΔT (temperature difference) between junctions should be noted. The emf generated by a t/c (thermocouple) system is $\alpha(\Delta T)$, in which α is the difference in potential between the metals in the thermal emf series. When a t/c is used for measuring temperature, α should be as high as is practical, but in any interconnections carrying low emf, α should be low enough so that $\alpha(\Delta T)$ will be negligible, or care should be taken to keep ΔT low. At one time, constantan was widely used for winding resistors, and these resistors created a severe problem. When connected into a copper line, two copper constantan t c's were formed and a slight ΔT between the ends of the resistor produced considerable

voltage, because for copper-constantan, α is about 20 microvolts per F of ΔT. Resistors are now usually made of manganin, evanohm, etc., which have a low value of α with copper. Regardless, design should consider that a series of elements (switches, resistors, relays, etc.) in a low-level signal line can accumulate enough emf errors to produce appreciable signal error. Whenever possible, such items as span and balance controls should be put in the high-voltage (power) lines to a bridge transducer and not in the low-level (signal) lines.

As an example, tests for thermal emf through the normally closed contacts of a certain relay showed that it produced one microvolt per F of change in ambient temperature. When the coil was activated, the heat from the coil was sufficient to produce 8 microvolts through the closed contacts after it had stabilized. This is a particularly severe case, but all the relays tested showed some thermal effect.

The zero balance control can be an awkward source of thermal emf's. This control is often necessary to bridge circuits, but is awkward because the control is usually a slidewire (VDR) which is a mass of dissimilar materials: brass terminals, resistance wire, and contact slider (usually a mixture of graphite and metal). There is one way that the control wiring can be designed to minimize its effect. First, the VDR should be connected between the power input terminals, not between the signal terminals. Second, it should use a limiting resistor of as high a resistance as possible. In Fig. 1, R_b is the transducer bridge resistance, R_s is the VDR (zero control) and R_i is the limiting resistor. When wired in the fashion shown,

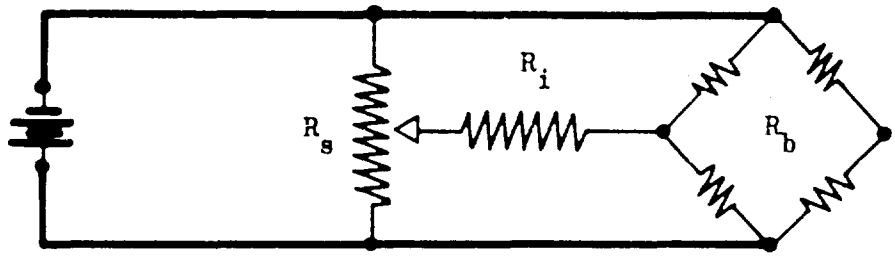

Figure 1. Transducer Circuit

the emf's developed at the three VDR terminals will either be in the power input circuit in which microvolts are negligible compared to volts, or will be isolated by the ratio of R_i to R_b. For this reason, R_i should be

as large as possible. It can be calculated by using the maximum unbalance condition which occurs when the R_s slider is at either end, thus putting R_i across one leg of R_b. For a 350-ohm, 3 mv/volt transducer, 500,000 ohms for R_i will provide more than ±5% zero control, which is adequate because commercial transducers are ±2% (or better) zero balance. Any transducer which is very far beyond its zero balance specification has something basically wrong, and should be removed from service for repair. If R_i is 500,000, then the effect of the thermal emf from the zero control will be reduced by the factor 350/500,000 or 0.07%, and can be neglected.

The worst single source of thermal emf error is the strain-gage transducer. By their nature, the strain wires and the copper lead wires form t/c's, but these are partially compensated for by Becquerel's Law. The gage wires, however, have a finite dimension and the t/c junctions are displaced far enough so that the signal terminals can be at different temperatures (i.e., ΔT is not zero), and this may be complicated by the presence of internal zero and modulus resistors. If the transducer can be located in a protective temperature-controlled box (e.g., pressure transducers) the problem is not serious, but a load cell measuring force from an operating thrust chamber is quite vulnerable. Radiated heat from the flame can reflect from surrounding elements, convected heat can be carried by swirling air, and conducted heat can be transmitted from the chamber through the supports. The most aggravating characteristic of this problem is that it varies indeterminably during the test and causes errors which cannot be corrected.

There is a simple test to determine the presence of thermal emf. It requires that a motor be fired without taking data. For example, if a load cell circuit is in question, the motor is mounted in preparation for firing (the longest practical duration should be used). A sensitive zero-center recorder (e.g., -1 to +1 millivolt)is connected to the signal terminals, and the power is removed from the transducer input. The system is now set up to record any undesirable emf's. The recorder input terminals are then shorted together and either the recorder is adjusted to zero or the pen mark is noted as zero input. Then the short is removed. Any resulting movement of the pen will show initial thermal emf. With the recorder running, 10 minutes should be allowed to record prerun thermals, then the

motor should be run, waiting 10 to 15 minutes afterward to allow stabilization. The record will show the thermal emf's: prerun, run, and postrun. This test will be indicative of the presence of thermal emf's, and should not be used for correction (thermal errors are highly nonpredictable), but should be used to determine whether redesign is necessary.

System Complexity

Except for the force transducer, the error elements discussed above are caused by complexity; complexity is in turn usually caused by efforts to provide flexibility. In attempting to produce a measuring system, it is advisable to remember that flexibility and precision are not compatible, especially in low-voltage circuits. Ideally, a strain-gage bridge should be coupled to its conditioning equipment with four well-insulated wires with copper-to-copper solder connections at each end. This is, of course, impossible because it is usually necessary to have zero-balance controls and simulation devices. However, it is possible to eliminate all unnecessary interconnections such as fanning strips, connectors, relays, and switches, thereby reducing to a minimum the possibility of thermal emf and leakage errors.

PART II: SPECIFIC APPLICATION TO EXISTING BATES SYSTEM

Thrust Integration System

The complete data system as installed at EAFB is impossible to analyze for the probability of error because there is no way of determining the effects of the various environments to which it is exposed, especially heat, humidity, and cleanliness. However, the various areas in which error could occur can be discussed, including an estimate of the amount of error which can be produced in each.

Calibration. A mechanical loading calibrator is incorporated in the system. No detailed study of this unit was made, but in general, it should be adequate within the limits imposed by the load cell. Any calibrator, however, should be periodically checked for accuracy against some standard (a proving ring should be suitable for this case). A device which uses mechanical linkages is susceptible to variation with use. This unit should be accurate within 0.25%.

Load Cell. This unit is the key element in the system, and unfortunately is also the most susceptible to short-term errors. In severe cases, the load cell can be as much as 2% in error for short periods. A test to determine its thermal susceptibility was described in Part I, in the discussion of thermal emf.

Interconnections. Conversation with operating personnel indicated the presence of four or five connections. These could be reduced to two. Thermal emf errors are small in these cases (less than 0.1% in any case), but they can accumulate. The most serious problem with interconnections is the possible presence of leakage between uninsulated terminals, and this is often uncontrollable because temperature fluctuations cause a connector housing to "breathe" humid air, thereby depositing moisture. Errors of 3% have been found in "waterproof" connectors which were not properly tested.

Bridge Completion Unit. Apparently, the equipment furnished by B & F was originally designed for flexibility to avoid the extra cost of an individual design for each problem. It is usable with one-, two-, and four-arm bridges, and is supplied with the necessary boards for completing each bridge. Although these boards are within a rack in the recording center, there is still a possibility of some leakage error. Although the possibility is small, such flexibility should be avoided.

Zero Balance Control. This control is a VDR properly located between the power leads with a limiting resistor to isolate the control from the bridge. However, to make this unit usable with bridges of different resistances and

sensitivites, the isolating resistor is 5000 ohms. This value will give reasonable isolation, but the control becomes extremely sensitive. For a 350-ohm, 3-mv/volt bridge, this control gives ±500% variation in zero. A resistor of 100,000 to 250,000 ohms would be adequate. The error from this unit is probably negligible unless the control knob was accidentally touched or vibrated after calibration. Wiper motion between wires could cause appreciable error because of its sensitivity.

Resistance Simulation ("R-Cal") Switch. There is probably no error in this device, but two factors should be considered. It is a "dry" circuit (i.e., low current) and contact resistance should be monitored, and any thermal gradients between the switch terminals should be avoided. Wiping action of the contacts should keep the resistance low, and there does not seem to be any heat-producing element near the switch.

Voltage Calibration. The switch to supply calibrated voltage to the VCO input is subject to the comments of the foregoing paragraph.

Data Recording and Reduction

The manner in which the data are recorded and reduced can affect accuracy as much as any other single factor. Figure 2 shows the beginning and end of a thrust-time curve. (The steady-state period is omitted.) As the system is operated, a gating signal is used to turn the recorder "on" when the level reaches 10% of design, and "off" when it returns to 10% at cutoff. In this way, the force indicated from the igniter is not recorded. However, this introduces several chances for further error. The idea is predicated on the assumption that ignition and burnout characteristics are the same for all grains.

With ideal conditions, the grain surface will ignite uniformly, and thrust will build up rapidly, leaving only a small area (lined shading in Fig. 2) before the gate "on" time; but if ignition spreads slowly, a larger thrust-time area is lost (dotted shading). Burnout is even more critical, because

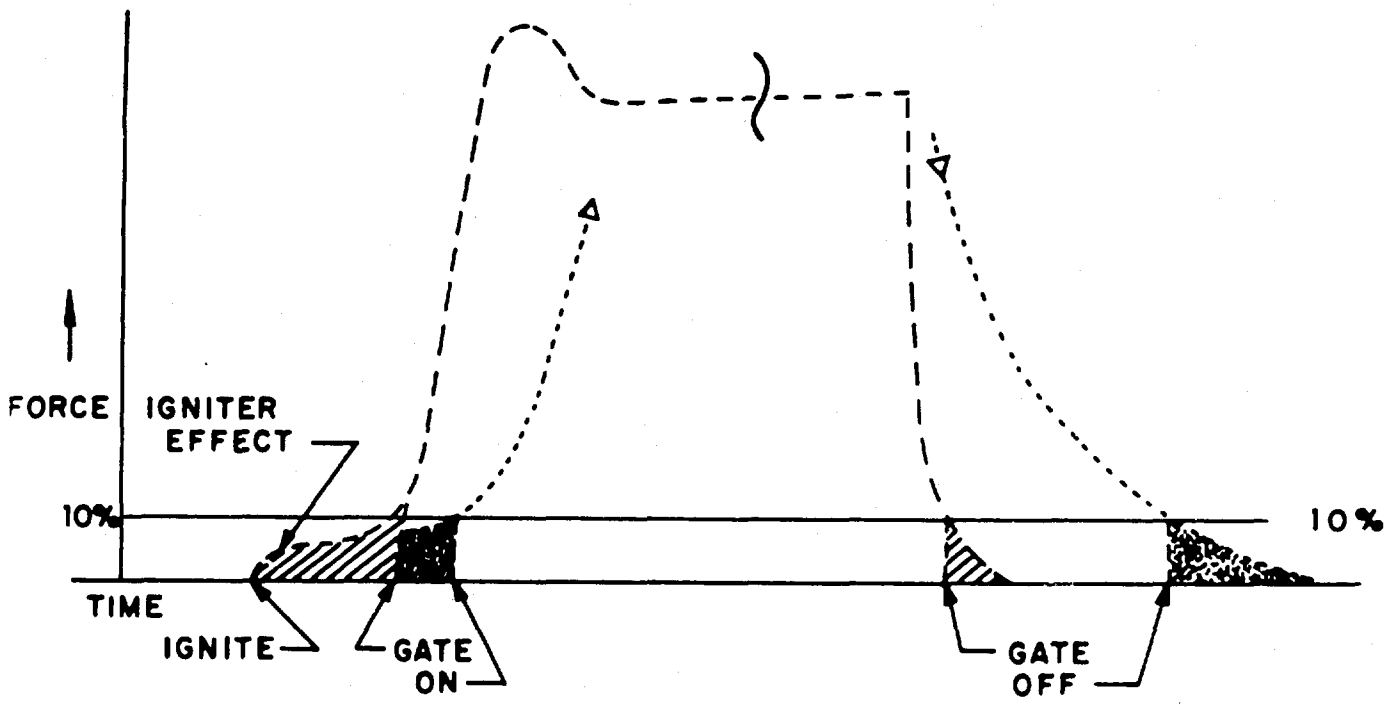

Figure 2. Thrust Analog

no two grains will burn to the case at all points in the same manner. The lined shading again shows an ideal case, but because there are always small pockets left as burnout approaches, it would be expected that considerable energy is left even though the thrust is below the 10% level as shown by the dotted area. Thus, a biased error is produced which is variable and consequently uncorrectable.

Another error which can occur is the activation level of the gate. This is controlled by another system (transducer plus conditioning equipment), and its use could easily add as much error as is introduced by the igniter. The burnout level is particularly doubtful because the heat from the burning grain can produce nonuniform temperature distribution in the pressure transducer, and this can produce not only thermal emf's but will not permit the temperature compensation to operate properly. The latter is predicated on uniform temperatures throughout the sensing element.

A more controllable method of making these measurements would be to test each igniter type for the amount of impulse it adds and use that value as a correction. The total impulse could then be recorded and the igniter impulse subtracted. This would give much better precision, because the variable errors would be reduced as much as possible and one biased but measureable error would be added. The correction for igniter thrust need not be highly accurate because it is a small part of the total.

Without analyzing a large number of high-speed analog records of firings, it is impossible to determine the amount and variability of error introduced by gating the recorder. However, the error will be greater for small grains than for large ones, thereby producing an untraceable variation in specific impulse (I_s). Furthermore, I_s is always in error in the negative direction, which prejudices performance with respect to design; i.e., the system can never record all of the available performance.

An element which might have been a factor in the decision to use the 10% gating level is a-c noise. The voltage-controlled pulse rate generator has a characteristic which must not be neglected; it does not respond to negative voltages. Consequently, if pure ac is fed to it, it will count only the positive portion and will not subtract counts for the negative, so that the result looks like a positive dc. This characteristic means that if the complete curve is integrated and if a-c noise is on the signal line at the beginning and end of the run (near zero dc), it will produce an error. There are three different ways that this error can be eliminated without introducing further errors, but such a design is beyond the scope of this discussion.

INSTALLATION REQUIREMENTS OF ROCKETDYNE SYSTEM

CONCRETE TEST PAD

A concrete test pad of sufficient size, strength, and flatness is necessary for the proper support of the Rocketdyne-designed system. The complete test stand has over-all dimensions of approximately 20 feet in length, 5 feet in width, and 5 feet in height, and is composed of two in-line sections having approximately 13- and 7-foot lengths, respectively. The sections weigh about 18,000 and 4000 pounds, respectively, and four lifting eye-bolts are supplied with each section. All points on the surface of the supporting section of concrete should be within 1/4 inch of a horizontal surface so that alignment and leveling problems of the system are not too severe. The design and configuration of the two existing test stand mounting beams, 24 inches apart and imbedded in the concrete of the BATES test pad, are considered satisfactory for the Rocketdyne system. Consequently, the system was designed taking into consideration an identical type of tiedown. A cross-sectional area of an imbedded BATES tiedown beam is shown in Fig. 3.

ELECTRICAL POWER AND WIRING REQUIREMENTS

Satisfactory operation of the hydraulic calibrator and the strain-gage load cell during calibration and measurement operations requires an adequate quantity, size, and configuration of wiring, and a suitable type of electrical power. A minimum of 12 No. 18 wires in two shielded cables of 6 wires each are required for operation of the load cell, and 25 No. 18 wires and 1 No. 8 wire are required for operation of the Ruska hydraulic calibrator.

Electrical power required at the test stand, from an EAFB source, is 10 amperes of unregulated 24-vdc. Regulated d-c power for the operation of the load cell and calibrator will be supplied from rack-mounted sources located in the test control room enclosure supplied by Rocketdyne. The 12 No. 18 wires in two shielded cables of 6 wires each required for the load cell should be in a separate conduit from all other wiring, so that all

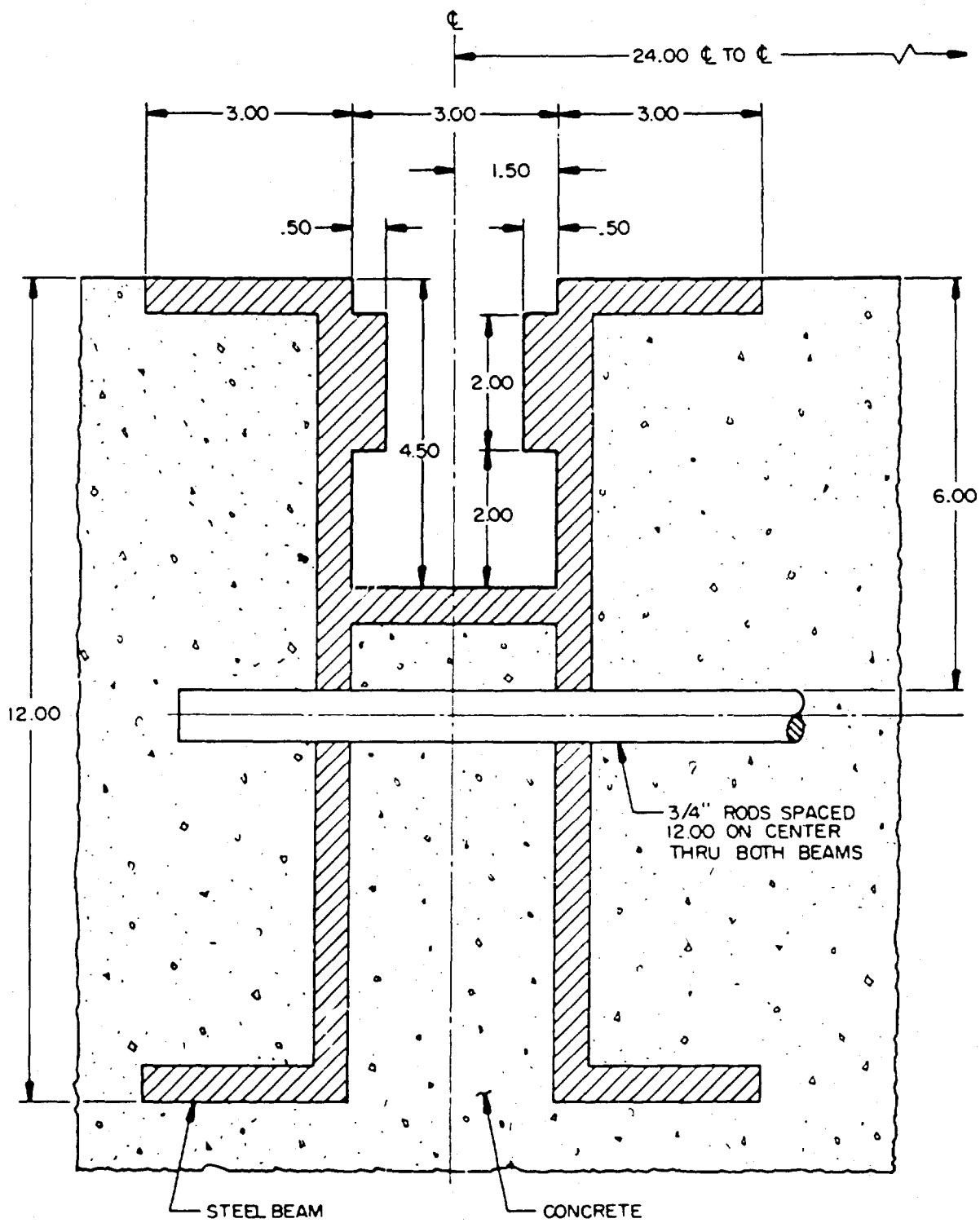

Figure 3. Cross Section of Test Stand Tie-Down Beam

possible electrical interference be avoided. All instrumentation wiring, both for load cell and calibrator, should pass through a waterproof junction box located in the ground about 25 feet from the test pad. The junctions in this box of the load cell wiring should be the only breaks in the load cell cables between the load cell connections at the test stand, and the chassis connections on the rack-mounted units in the control room. This single break in each load cell cable, although undesirable from a measurement accuracy standpoint, is needed for practical rewiring purposes in the event of a motor failure resulting in the destruction of wiring in the vicinity of the test pad. All cable connectors should be of the Bendix waterproof type. Both of the cable connections at the load cell should use Bendix socket connectors No. 10-72614-6S, and the junction box connectors in each load cell cable should consist of Bendix pin connector No. 10-169114-6P and socket connector No. 10-72614-6S. The Ruska calibrator control wiring connectors in the waterproof junction box should consist of Bendix pin connector No. 10-72128-12P and socket connector No. 10-72628-12S for the 25 No. 18 wires, and pin No. 10-72115-3P and socket No. 10-72615-3S for the single No. 8 wire.

GRAVITY MEASUREMENT

Accurate total impulse measurements, by the Rocketdyne system, require calibration of the measuring system by the hydraulic calibrator. Because very accurate dead weights will be used to produce the precise hydraulic pressures utilized to obtain the calibrating forces, a knowledge of the specific value of the acceleration due to gravity, at the test site, is required so that the weights can be properly fabricated. In accordance with these considerations, Rocketdyne requested and received from EAFB the local g value, to six significant figures, at Test Pad No. 5, Solid Motor Test Area, Rocket Propulsion Laboratory. The measurement was performed on 18 January 1963 and was determined to be 979.477 cm/sec^2. This value of g was utilized in the design of the calibrating weights by the Ruska Instrument Company, manufacturers of the hydraulic calibration system.

INTRODUCTORY DISCUSSION

Mathematical analysis is an essential part of any adequate effort to design and build a total impulse measurement system possessing the accuracy required in the contractural effort. Without this analysis, all design and construction effort would be based solely upon qualitative judgment resulting from a combination of previous trial-and-error experience and guess-work. Its application ranges from its use to determine both general and specific guidelines during the system design phase to its use in an accurate and detailed evaluation of the system after its construction. The objective of all mathematical analysis undertaken in this contractual effort was the mathematical characterization of the system for the purpose of a quantitative determination of its behavior in the performance of its measuring function. The analyses presented in this section of the report consist not only of static equilibrium considerations needed in motor suspension flexure system design and constructional alignment operations, but also of dynamic response determinations of the mechanical system to transient force excitations similar to thrust outputs encountered in rocket motor propellant tests. Accordingly, the range and type of analyses reflect the variety of inquiries directed, at various times, to the design aspects of the over-all constructional problem, and the sequence of the following mathematical efforts corresponds to their actual chronological occurrence.

The first mathematical effort was concerned with a general treatment of the relationship between the actual and measured impulse for certain linear dynamic systems, including a preliminary discussion of the impulse errors incurred by less-than-infinite integrations of indicated displacements. No numerical examples were undertaken in this initial effort because its purpose was a general discussion and elaboration of the basic idea underlying the measuring function. The second mathematical effort was concerned exclusively with trapezoidally shaped force-time excitations of a one spring-mass system viscously damped. Its purpose was to obtain some numerical results with a system-excitation combination which approximated an actual thrust-measuring system and rocket motor. The results of this undertaking provided the initial quantitative indication of the adequacy of the

mechanical system design. The third mathematical effort was concerned with a more accurate and detailed study of the actual measurement system, consisting of a series-connected massive concrete block, a thrust-measuring load cell, and the motor and mount assembly. The representation of the system in this study was the most advanced model undertaken in the Phase I effort. Its purpose was the determination of the effects on the impulse measurement error of such characteristics as concrete-block compliance, variable motor mass (propellant burning), nonviscous damping, and nonlinear force-displacement calibrations because of load-cell aging and/or imposed bending moments. The results of this advanced study provided the greater part of the justification of the design employed in the designed system.

The last of the mathematical developments contained in this report was undertaken to provide an analytical approach to the flexure system design of the motor suspension. The result of this effort was the determination of a suitable combination of flexure system and load cell mechanical stiffnesses that effectively isolated the load cell from extraneous forces and moments that would degrade its basically linear performance. The application of the results to the flexure design thereby minimized the problem of nonlinearities in the system calibration.

ANALYTICAL DYNAMICS: GENERAL EXPRESSIONS

INTRODUCTION AND SUMMARY

Some elementary observations are presented regarding the relationship between the integrated input and integrated output of certain simple types of linear dynamic systems. An application of these considerations is the solid-propellant total impulse measurement system designed by research instrumentation personnel. The material presented constitutes an elaboration of some comments made in Ref. 1 on the relationship between the total applied impulse and total measured impulse of such a system.

Three basic mathematical models are considered which represent increasing levels of generality: a simple model which is appropriate for initial design studies of the total impulse measurement system, and two more general models which may be needed in subsequent analyses.

Model 1

Model 1, a damped spring-mass system, is shown schematically in Fig. 4 and is described by the second-order differential equation

$$m\frac{d^2x(t)}{dt^2} + b\frac{dx(t)}{dt} + kx(t) = f(t),\ t \geq 0, \tag{1}$$

where the input force $f(t) \equiv 0$ for $t < 0$, and the displacement $x(t)$ of the mass m is subject to the initial conditions

$$\left.\begin{aligned} \frac{dx(t)}{dt} &= c_2 \\ x(t) &= c_1 \end{aligned}\right\} \text{ at } t = 0 \tag{2}$$

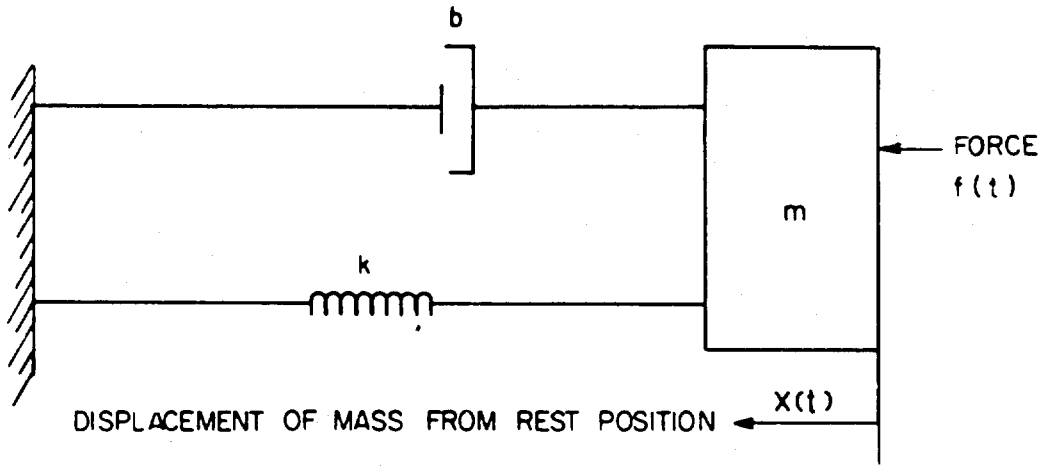

Figure 4. Schematic of Damped Spring-Mass System

Model 2

Model 2 is a system described by an nth order linear constant-coefficient differential equation:

$$a_n \frac{d^n x(t)}{dt^n} + a_{n-1} \frac{d^{n-1} x(t)}{dt^{n-1}} + \ldots + a_0 x(t) = f(t), \quad t \geq 0, \qquad (3)$$

where

$a_0 \neq 0$, $f(t) \equiv 0$ for $t < 0$, and the displacement $x(t)$ is subject to the initial conditions

$$\left.\begin{aligned} \frac{d^{n-1} x(t)}{dt^{n-1}} &= c_n \\ \frac{d^{n-2} x(t)}{dt^{n-2}} &= c_{n-1} \\ &\vdots \\ x(t) &= c_1 \end{aligned}\right\} \quad \text{at } t = 0 \qquad (4)$$

Model 3

Model 3 is a general linear time-invariant stable (physically realizable) dynamic system with impulse response (or weighting) function $W_3(t)$ and frequency response function $Y_3(w)$, subject to zero initial conditions. This model includes as special cases systems such as the above, whose input force and resulting displacement are related by ordinary linear differential equations with constant coefficients. Variable coefficient systems are excluded because they are not time-invariant.

For each model, what is of interest is the relationship between the integrated actual input force,

$$I_A = \int_0^\infty f(t)dt \tag{5}$$

and the integrated displacement indicated by the spring,

$$I_M = \int_0^\infty x(t)dt \tag{6}$$

For the case of an idealized total impulse measurement system, the integrated input I_A represents the total impulse generated by the rocket motor (the "total applied impulse") and the integrated output I_M is a measure of the total impulse measured by the system (the "total measured impulse"). The indicated limits of integration in Eq. 5 and 6 extend over all time $0 \leq t \leq \infty$, although in practice, the applied force $f(t)$ vanishes for $t > T$, where T is the duration of the run, and $x(t)$ is essentially zero after some later time.

For the three models under consideration, the following is shown:

$$\text{Model 1:} \quad I_M = K_1 I_A + K_1(mc_2 + bc_1)$$

$$\text{Model 2:} \quad I_M = K_2 I_A + K_2(a_n c_n + a_{n-1} c_{n-1} + \ldots + a_1 c_1)$$

$$\text{Model 3:} \quad I_M = K_3 I_A \tag{7}$$

where the quantities K_1, K_2, and K_3 appearing in Eq. 7 are system constants given by

$$K_1 = \frac{1}{k}$$

$$K_2 = \frac{1}{a_o}$$

$$K_3 = \int_o^\infty W(t)dt \tag{8}$$

These results are valid provided that the input $f(t)$ is a sufficiently well-behaved function and each of the systems is stable (Ref. 2). The conditions required of the input will undoubtedly always be satisfied by thrust functions.

RESULTS

Before deriving the results stated in Eq. 7 and 8, some alternative formulas are presented for the constants K_1, K_2, and K_3 and some of their practical implications are discussed. It should be noted first that under zero initial conditions the terms enclosed with parentheses in Eq. 7 drop out, and for each of the three systems the relationship between the total measured impulse and total applied impulse is of the form

$$I_M/I_A = K \tag{9}$$

where K is a constant determined by the system. Equation 9 implies that whenever the system is excited under zero initial conditions by an input $f(t)$, the ratio of the total measured impulse to the total applied impulse is a constant which does not depend on the specific form of the input. Moreover, this relationship indicates one way in which the constant K may, in principle, be determined experimentally. If possible, an input with known total impulse I_A would be applied (the pointwise behavior of the input need not be known), I_M would be measured, and the ratio I_M/I_A would be computed. Such an experiment, which may be described as a total impulse calibration procedure, would be repeated with sufficient frequency to obtain a

statistically reliable estimate of the constant K. Measurement analysis of the "constant" K could then be performed in the usual manner.

A second way (as an alternative to Eq. 8) can now be considered, in which the constants K_1, K_2, and K_3 in Eq. 7 may be interpreted. This will lead to another characterization which has possible practical applications. The three systems under consideration possess frequency response functions $Y_1(\omega)$, $Y_2(\omega)$, and $Y_3(\omega)$ which determine the effect of the systems on the various frequency components of the inputs. For models 1 and 2, the frequency response functions $Y_1(\omega)$ and $Y_2(\omega)$ may be expressed explicitly in terms of the coefficients in the differential equations describing the systems. In fact, the following is true (Ref. 2):

$$Y_1(\omega) = \frac{1}{m(i\omega)^2 + b(i\omega) + k},$$

$$Y_2(\omega) = \frac{1}{a_n(i\omega)^n + a_{n-1}(i\omega)^{n-1} + \ldots + a_1(i\omega) + a_o}. \tag{10}$$

From Eq. 8 and 10, it follows that

$$\begin{aligned} K_1 &= Y_1(0) \\ K_2 &= Y_2(0) \end{aligned} \tag{11}$$

The constant K_3 may be written in a similar form. For if $Y_3(\omega)$ denotes the frequency response function of system 3, then in terms of the system impulse response function $W_3(t)$,

$$Y_3(\omega) = \int_0^\infty W_3(t)e^{-i\omega t}\,dt, \tag{12}$$

and evaluating Eq. 12 at zero frequency ($\omega = 0$) gives

$$Y_3(0) = \int_0^\infty W_3(t)\,dt \tag{13}$$

Hence, from Eq. 8 and 13,

$$K_3 = Y_3(0) \tag{14}$$

Each of the constants appearing in Eq. 7 is therefore of the form

$$K = Y(0) , \tag{15}$$

where $Y(0)$ is the system frequency response function $Y(\omega)$ evaluated at zero frequency.

The above discussion also indicates a third way of describing the constants K_1, K_2, and K_3. All three systems possess impulse response fun ctions which are related to their frequency response functions in the manner

$$Y(\omega) = \int_0^\infty W(t)e^{-i\omega t}\, dt \tag{16}$$

That is, the frequency response function is the Fourier transform of the impulse response function. For $\omega = 0$ in Eq. 16

$$Y(0) = \int_0^\infty W(t)dt \tag{17}$$

Thus, from Eq. 15 and 17 it can be seen that each of the constants in Eq. 7 equals the total time integral of the system's impulse response function,

$$K = \int_0^\infty W(t)dt \tag{18}$$

It is well known (Ref. 2) that if the input $f(t)$ is taken to be a true unit step

$$u(t) = \begin{cases} 0 \text{ for } t < 0 \\ 1 \text{ for } t \geq 0 \end{cases}$$

then the corresponding response $U(\tau)$ at time τ is given simply by

$$U(\tau) = \int_0^\tau W(t)dt \qquad \tau \geq 0 \tag{19}$$

where $W(t)$ is the system impulse response function. Allowing τ to become arbitrarily large in Eq. 19 gives

$$\lim_{\tau \to \infty} U(\tau) = \int_0^\infty W(t)dt \ . \tag{20}$$

From Eq. 18 and 20 it follows that the constants K_1, K_2, and K_3 may be described as the steady-state values of the responses of the systems to unit step inputs. This last characterization of the constants appearing in Eq. 7 indicates another way in which they may, in principle, be determined experimentally. A step input would be applied to the system (subject to zero initial conditions, for example) and the input would be maintained at a constant level until the measured response became essentially constant. If the step has height $A \neq 1$, then the value of the steady-state response is to be divided by A to obtain the constant K. Again, such a procedure would be repeated sufficiently to form a statistically reliable estimate of the constant K and its variability.

It should be noted in passing that if it is not possible to apply a true step input to the system but only a ramp function

$$f(t) = \begin{cases} 0 \text{ for } t < 0 \\ \alpha t \text{ for } 0 \leq t \leq t_0 \\ A \text{ for } t_0 \leq t \end{cases}$$

then the above procedure (measuring the steady-state value of the response as an estimate of the constant K) may still be applied. A step input is preferable, however, because it can be shown that the experimental error arising from not being able to pass to the limit $\tau \to \infty$, but instead taking as an estimate of K the response $x(\tau_0)$ at some large time τ_0, is smaller for a step input than for a corresponding ramp input. The difference in the errors for the two types of input becomes small as τ_0 increases, however, and therefore should provide no practical difficulties in the application of this method.

DERIVATION OF RESULTS

In this discussion, the results expressed in Eq. 7 and 8 of the introduction are demonstrated. Model 3 is used first because the result for this case is almost a matter of definition and also is used in the other two cases.

Model 3

A linear time-invariant stable dynamic system is characterized by its impulse response function $W(t)$, which represents the response of the system to a unit-impulse applied at time $t = 0$. For such a system, the response $x(t)$ to an input $f(t)$, with zero initial conditions, is given in terms of the impulse response function $W(t)$ by

$$x(t) = \int_0^t W(\tau) f(t - \tau) d\tau \tag{21}$$

Here it is assumed for simplicity that the system is physically realizable (the response depends only on the past of the input and not on its future) and that the input vanishes for $t < 0$. It is also assumed that the system possesses a frequency response function

$$Y(\omega) = \int_0^\infty W(t) e^{-i\omega t} dt$$

and that the input $f(t)$ has a Fourier transform*

$$F_f(\omega) = \int_0^\infty f(t) e^{-i\omega t} dt \tag{22}$$

*For example, a function $f(t)$, defined for $t \geq 0$, possesses a Fourier transform if it is continuous (except possibly for a finite number of jumps) and if $\int_0^\infty |f(t)| dt$ exists. To avoid complications, it is assumed from this point that these conditions are met by the inputs. Note that the latter requirement follows automatically from the first if $f(t)$ vanishes for all t greater than some $T > 0$, which will certainly be true for all inputs to the total impulse measurement system.

Then, if $F_x(\omega)$ denotes the Fourier transform of the output, the frequency domain relationship (corresponding to Eq. 21) is

$$F_x(\omega) = Y(\omega)F_f(\omega) \tag{23}$$

Now, if $F_x(\omega)$, $Y(\omega)$, and $F_f(\omega)$ are evaluated at $\omega = 0$,

$$F_x(0) = \int_0^\infty x(t)dt = I_M$$

$$Y(0) = \int_0^\infty W(t)dt$$

$$F_f(0) = \int^\infty f(t)dt = I_A \tag{24}$$

Hence, from Eq. 23 and 24

$$I_M = \left(\int_0^\infty W(t)dt \right) I_A \tag{25}$$

which is the desired result. It can be observed again that

$$\int_0^\infty W(t)dt = Y(0)$$

Model 1

Considering now the linear second-order constant coefficient differential equation, 1, with initial conditions Eq. 2: every solution $x(t)$ of Eq. 1 for $t \geq 0$ is of the form

$$x(t) = h(t) + y(t) \tag{26}$$

where $h(t)$ is the solution of the homogeneous equation

$$m \frac{d^2h(t)}{dt^2} + b \frac{dh(t)}{dt} + kh(t) = 0, \quad t \geq 0 \tag{27}$$

satisfying the initial conditions $dh(t)/dt = c_2$ and $h(t) = c_1$ at $t = 0$, and where $y(t)$ is a particular solution of the nonhomogeneous equation (Eq. 1) with zero initial conditions for $y(t)$. Here it is assumed that the input is sufficiently well-behaved so that it possesses a Fourier transform given by Eq. 22. Corresponding to the decomposition (Eq. 26), the total measured impulse I_M may be split into two parts:

$$I_M = I_{Mh} + I_{My} \tag{28}$$

where

$$I_{Mh} = \int_0^\infty h(t)dt \tag{29}$$

is the contribution to I_M arising from $h(t)$ and

$$I_{My} = \int_0^\infty y(t)dt \tag{30}$$

is the contribution to I_M arising from $y(t)$. Although for the total impulse measurement system it seems appropriate to assume zero initial conditions (in which case $h(t)$ is identically zero and $I_M = I_{My}$), the expression (Eq. 7) for I_M which is obtained i valid in the general case.

Considering first the contribution I_{Mh} to I_M which is associated with the given initial conditions, the solution $h(t)$ of Eq. 27 may easily be expressed in explicit form in terms of the parameters m, b, and k (for example, in Ref. 2), but it is not necessary to deal with such explicit solutions to derive the result (Eq. 7). It need only be shown that by virtue of the assumption that the system is stable (a condition ensured by the assumption $b/m > 0$), the solution $h(t)$ as well as its first derivative $dh(t)/dt$ approaches zero as t becomes arbitrarily large.

With this in mind, Eq. 27 is integrated over the interval $0 \leq t \leq \tau$ to obtain

$$m \int_0^\tau \frac{d^2h(t)}{dt^2}\, dt + b \int_0^\tau \frac{dh(t)}{dt}\, dt + k \int_0^\tau h(t)dt = 0$$

and therefore

$$(mh'(\tau) + bh(\tau)) - (mh'(0) + bh(0)) + k\int_0^\tau h(t)dt = 0$$

where $dh(t)/dt$ has been denoted by $h'(t)$. Thus

$$\int_0^\tau h(t)dt = \frac{1}{k}(mh'(0) + bh(0)) - \frac{1}{k}(mh'(\tau) + bh(\tau)) \tag{31}$$

Now, because $h'(\tau)$ and $h(\tau)$ approach zero as $\tau \to \infty$, Eq. 31 becomes, for arbitrarily large τ,

$$I_{Mh} = \int_0^\infty h(t)dt = \frac{1}{k}(mc_2 + bc_1) \tag{32}$$

where the initial values c_2 and c_1 have been substituted for $h'(0)$ and $h(0)$. As anticipated, $I_{Mh} = 0$ for zero initial conditions ($c_2 = c_1 = 0$).

Considering the contribution to I_M arising from $y(t)$, because system 1 is a linear time-invariant stable dynamic system with frequency response function

$$Y_1(\omega) = \frac{1}{m(i\omega)^2 + b(i\omega) + k} \tag{33}$$

the result obtained for model 3 may be applied to conclude that

$$I_{My} = \int_0^\infty y(t)dt = Y_1(0)\, I_A$$

But $Y_1(0) = 1/k$, as seen from Eq. 33, and therefore

$$I_{My} = \frac{1}{k}\, I_A \tag{34}$$

Thus, summing I_{Mh} as given by Eq. 32 and I_{My} as given by Eq. 34,

$$I_M = \frac{1}{k} I_A + \frac{1}{k}(mc_2 + bc_1) \tag{35}$$

which is the desired expression for model 1. Alternatively, if Eq. 35 is solved for I_A,

$$I_A = kI_M - (mc_2 + bc_1) \tag{36}$$

Before continuing to model 2 consider, briefly, the errors which result from not being able to perform the integration

$$\int_0^\infty x(t)dt = I_M \tag{37}$$

over the infinite range $0 \leq t \leq \infty$. The situation will be restricted to where $f(t)$ vanishes outside of an interval $0 \leq t \leq T$ (for total impulse measurement T is the full duration of the run). Similar remarks will apply to the more general case of model 2.

Supposing the response $x(t)$ is known only over the time interval $0 \leq t \leq t_o$, where $t_o > T$, then what is of interest is the error

$$\delta_M = I_M - \int_0^{t_o} x(t)dt \tag{38}$$

made in approximating I_M by $\int_0^{t_o} x(t)dt$ and also the error δ_A made in determining I_A from Eq. 36 when $\int_0^{t_o} x(t)dt$ is used in place of I_M. The latter error is given by

$$\delta_A = k\,\delta_M \tag{39}$$

and is easily seen by subtracting

$$k \int_0^{t_o} x(t)dt - (mc_2 + bc_1)$$

from the right side of Eq. 36.

Then, from Eq. 37 and 38

$$\delta_M = \int_0^\infty x(t)dt - \int_0^{t_o} x(t)dt = \int_{t_o}^\infty x(t)dt \tag{40}$$

Because $f(t) \equiv 0$ for $t \geq t_o$, $x(t)$ is a solution of the homogeneous equation

$$m \frac{d^2x(t)}{dt^2} + b \frac{dx(t)}{dt} + kx(t) = 0, \quad t \geq t_o \tag{41}$$

The problem of determining δ_M as given by Eq. 40 from the differential equation (Eq. 41) is entirely similar to the problem of determining I_{Mh} from Eq. 27. Here the initial time $t = 0$ is replaced by t_o, and the initial conditions $dh(t)/dt = c_2$, $h(t) = c_1$ at $t = 0$ are replaced by $dx(t)/dt = x'(t_o)$, $x(t) = x(t_o)$ at $t = t_o$.

Reasoning as before, the expression

$$\delta_M = \frac{1}{k} (mx'(t_o) + bx(t_o)) \tag{42}$$

is obtained instead of that given by Eq. 32. Also, from Eq. 39 and 42,

$$\delta_A = mx'(t_o) + bx(t_o) \tag{43}$$

It can be observed further that by virtue of Eq. 36, 38, and 42

$$I_A = k \int_0^{t_o} x(t)dt + (mx'(t_o) + bx(t_o)) - (mx'(0) + bx(0)) \tag{44}$$

or, if zero initial conditions $x'(0) = x(0) = 0$ are assumed,

$$I_A = k \int_0^{t_o} x(t)dt + (mx'(t_o) + bx(t_o)) \tag{45}$$

The quantities $\int_0^{t_o} x(t)dt$ and $x(t_o)$ which appear in Eq. 42, 43, and 45 are directly measurable from recorded data, and presumably the parameters m, b, and k would also be known. If $x'(t_o)$ could be estimated from given data, or if $x'(t_o)$ were known to be nearly zero, then in principle δ_M, δ_A, and I_A could be determined from Eq. 42, 43, and 45. It should be noted that under the assumptions made in this section, $x'(t_o)$ and $x(t_o)$ will approach zero for $t_o \to \infty$.

Model 2

The proof of the result (eq. 7) for system 2 may be carried out in a manner entirely similar to that for system 1. The solution $x(t)$ of Eq. 3, with initial conditions (Eq. 4), is represented as the sum of solution $h(t)$ of the homogeneous equation (with initial conditions, (Eq. 4)) and the solution $y(t)$ of the original nonhomogeneous equation (Eq. 3) having zero initial conditions. Again, splitting I_M into two parts,

$$I_M = I_{Mh} + I_{My}$$

The result for model 3 is applied to conclude that

$$I_{My} = Y_2(0)\, I_A$$

where $Y_2(0)$ is the frequency response function of system 2 evaluated at $\omega = 0$. Because, as noted earlier,

$$Y_2(\omega) = \frac{1}{a_n(i\omega)^n + a_{n-1}(i\omega)^{n-1} + \ldots + a_1(i\omega) + a_o}$$

Then, $Y_2(0) = 1/a_o$ and therefore

$$I_{My} = \frac{1}{a_o}\, I_A \tag{46}$$

To determine I_{Mh}, the homogeneous equation

$$a_n h^{(n)}(t) + a_{n-1} h^{(n-1)}(t) + \ldots + a_o h(t) = 0$$

is integrated over the interval $0 \le t \le \tau$ to obtain

$$\int_0^\tau h(t)dt = \frac{1}{a_o}\,(a_n c_n + a_{n-1}\, c_{n-1} + \ldots + a_1 c_1)$$
$$- \frac{1}{a_o}\,(a_n h^{(n-1)}(\tau) + a_{n-1} h^{(n-2)}(\tau) + \ldots + a_1 h(\tau)\ )$$

where $h^{(j)}(t) = d^j h(t)/dt^j$ and $c_j = h^{(j-1)}(0)$; $j = 1, 2, \ldots, n$. If this system is stable in the dynamic sense,* then as $\tau \to \infty$ the terms within the second pair of parentheses approach zero, and

$$I_{Mh} = \int_0^\infty h(t)dt = \frac{1}{a_o}\left(a_n c_n + a_{n-1}\, c_{n-1} + \ldots + a_1 c_1\right) \qquad (47)$$

Thus, from Eq. 46 and 47 the desired result is obtained:

$$I_M = \frac{1}{a_o} I_A + \frac{1}{a_o}\left(a_n c_n + a_{n-1}\, c_{n-1} + \ldots. + a_1 c_1\right) \quad .$$

*For this purpose it is sufficient to assume that the (generally complex) roots of $a_n\lambda^n + a_{n-1}\lambda^{n-1} + \ldots + a_1\lambda + a_o = 0$ have negative real parts. For model 1, which corresponds to the case $n = 2$ in model 2, the assumption $b/m > 0$ which was made is equivalent to the assumption that the roots of $m\lambda^2 + b\lambda + k = 0$ have negative real parts.

FREE VIBRATION WITH VISCOUS DAMPING

With reference to Fig. 5, a spring-suspended mass, m, is considered free to vibrate vertically in a medium offering a viscous resistance, i.e., a resisting force proportional to the first power of the velocity. Such resistance is usually termed viscous damping. The mass of the spring itself is considered small compared with the suspended mass, so that the discussion is concerned with the motion of a single particle. In this case, if the mass, m, be displaced any distance, x, (within the elastic range of the spring) from its position of equilibrium and then released, it will begin to move under the action of a resultant force.

$$X = -kx - c\dot{x} \tag{48}$$

where

k = spring constant = force necessary to produce unit extension of the sprin
c = coefficient of damping = magnitude of the viscous resistance at unit velocity.

Newton's second law of motion states that when a force acts upon a given particle, that force produces an accceleration of the particle in the direction of the force and proportional to its magnitude. For the force expressed by Eq. 48, the equation of motion becomes:

$$m\ddot{x} = -kx - c\dot{x} \tag{49}$$

Dividing through by m and introducing the notations

$$\frac{k}{m} = \omega^2 \text{ and } \frac{c}{m} = 2n \tag{50}$$

the equation may be written in the form

$$\ddot{x} + 2n\dot{x} + \omega^2 x = 0 \tag{51}$$

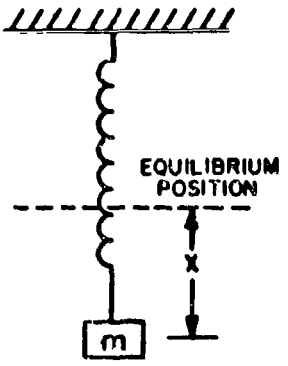

Figure 5. Simple Spring-Mass System, Free Vibration

Thus, for free vibrations with viscous damping a linear differential equation with constant coefficients is obtained.

As a trial solution of Eq. 51, take

$$x = Ce^{rt} \tag{52}$$

where

r = a constant.

Substituting this trial function for x in Eq.51 results in the auxiliary equation:

$$r^2 + 2nr + \omega^2 = 0 \tag{53}$$

This equation determines two values of r for which expression(52) can satisfy Eq. 51:

$$r_1 = -n + \sqrt{n^2 - \omega^2}$$

$$r_2 = -n - \sqrt{n^2 - \omega^2} \tag{54}$$

Hence, the general solution of Eq. 51 becomes:

$$x = Ae^{r_1 t} + Be^{r_2 t} \tag{55}$$

where

A and B = arbitrary constants of integration.

To attach any physical significance to this solution, two distinct cases must be distinguished, depending on whether the radical $\sqrt{n^2 - \omega^2}$ in Equation 54 is real or imaginary, in other words whether $n > \omega$ or $n < \omega$. Equation 50 indicates that this depends on the relative magnitudes of the damping coefficient, c and the spring constant, k. Generally speaking, a large coefficient of damping and a small spring constant will result in real values of r_1 and r_2, while, for the reverse of these conditions, r_1 and r_2 will be complex numbers.

Case I, $n > \omega$

In this case r_1 and r_2 have real values. To evaluate the constants A and B in the general solution(Eq 55)the initial conditions of the motion must be known. Assuming, as a particular case, that

$$x = x_0, \ \dot{x} = 0, \text{ when } t = 0 \tag{56}$$

it is found by direct substitution into Eq. 55 and its first derivative with respect to time that:

$$A = -\frac{r_2 x_0}{r_1 - r_2} \quad , \quad B = +\frac{r_1 x_0}{r_1 - r_2} \tag{57}$$

For these values, Eq. 55 becomes:

$$x = \frac{x_0}{r_1 - r_2}\left(r_1 e^{r_2 t} - r_2 e^{r_1 t}\right) \tag{58}$$

In connection with this solution, it should be noted that both r_1 and r_2 are negative, r_2 being numerically the larger. Thus the displacement x has the same sign as x_0 and approaches zero as a limit when t becomes infinitely

large. The motion is not a vibration at all but simply one in which the suspended mass, after its initial displacement, gradually creeps back toward the equilibrium position but takes theoretically infinite time to get there. It results from the fact that the damping coefficient is too large compared with the spring constant and is sometimes of practical interest in connection with certain types of electrical measuring instruments such as the galvanometer. In the case where $n = \omega$, aperiodic motion is also obtained, and the corresponding value of the damping coefficient $c = 2nm$ becomes

$$c_{crit} = 2\omega m \tag{59}$$

and is called critical damping.

Case 2, $n < \omega$

More often, the case is encountered where $n < \omega$ so that the roots r_1 and r_2 are complex. In discussing this case, it will be convenient to change the form of Eq.55 to indicate more clearly its physical significance. Remembering that the concern now is only with the case where $n < \omega$, let

$$\omega^2 - n^2 = \omega_1^2 \tag{60}$$

Then expressions in Eq. 54 become

$$\left.\begin{aligned} r_1 &= -n + i\omega_1 \\ r_2 &= -n - i\omega_1 \end{aligned}\right\} \tag{61}$$

where

$$i = \sqrt{-1}$$

and Eq.55 may be written in the form

$$x = e^{-nt}\left(Ae^{i\omega_1 t} + Be^{-i\omega_1 t}\right) \tag{62}$$

Using the known relations

$$\left.\begin{aligned} e^{iz} &= \cos z + i \sin z \\ e^{-iz} &= \cos z - i \sin z \end{aligned}\right\} \tag{63}$$

Eq. 55, in turn, may be written in the form

$$x = e^{-nt} (C_1 \cos \omega_1 t + C_2 \sin \omega_1 t) \tag{64}$$

where

C_1 and C_2 = new arbitrary constants.

To evaluate these constants, assume now the initial conditions

$$x = x_0 \ , \ \dot{x} = \dot{x}_0, \text{ when } t = 0 \tag{65}$$

Then substituting Eq. 65 into Eq. 64, together with its first derivative with respect to time, there is obtained

$$C_1 = x_0 \text{ and } C_2 = \frac{\dot{x}_0}{\omega_1} + \frac{nx_0}{\omega_1} \tag{66}$$

and the solution becomes

$$x = e^{-nt} \left[x_0 \cos \omega_1 t + \left(\frac{\dot{x}_0 + nx_0}{\omega_1} \right) \sin \omega_1 t \right] \tag{67}$$

The general solution (64) can be represented in another form by using the relation

$$\cos (\theta - \varphi) = \cos\theta \cos\varphi + \sin\theta \sin\varphi \tag{68}$$

to obtain

$$x = Ae^{-nt} \cos (\omega_1 t - \alpha) \tag{69}$$

where

$$A = \sqrt{C_1^2 + C_2^2}$$

$$\alpha = \tan^{-1}\frac{C_2}{C_1}$$ = new forms of the arbitrary constants.

Using the values of C_1 and C_2 from expressions (66) these new constants become

$$A = \sqrt{x_0^2 + \left(\frac{\dot{x}_0 + nx_0}{\omega_1}\right)^2} \tag{70}$$

and

$$\alpha = \tan^{-1}\left(\frac{\dot{x}_0}{x_0\omega_1} + \frac{n}{\omega_1}\right) \tag{71}$$

A displacement-time curve plotted from Eq.69 is seen to be vibratory in nature and represents so-called damped free vibrations. Equation (67) is therefore the expression for the vibratory effects of any initial displacement x_0 or initial velocity $\dot{x}_0$, when $t = 0$.

FORCED VIBRATION, GENERAL DISTURBING FORCE

While damped free vibrations are important, there are many cases for which the differential equation of motion(51) of a spring-suspended mass in Fig. 6a takes the more general form:

$$\ddot{x} + 2n\dot{x} + \omega^2 x = q = f(t) \tag{72}$$

where

$q = \frac{Q}{m}$ = the disturbing force per unit of suspended mass.

In dealing with this equation, a procedure somewhat different from that used previously will be followed. Referring to Fig. 6b, it is assumed that the disturbing force, q, per unit of mass is given by a curve AB. At any instant,

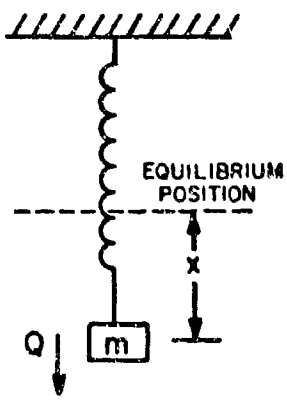

Figure 6a. Spring-Mass System, Forced Vibration

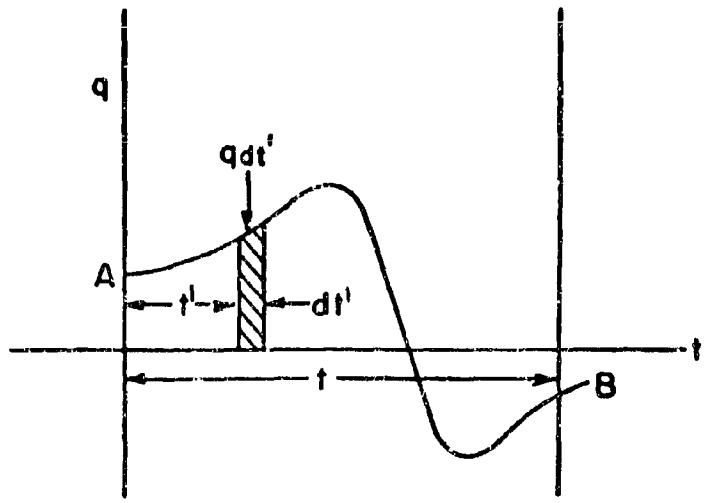

Figure 6b. Force-Time Analog

t', consider one elemental impulse q dt' as represented by the shaded strip in the diagram. This one impulse imparts to each unit of mass an instantaneous increase in velocity $d\dot{x} = q\,dt'$, regardless of what other forces, such as the spring force, may be acting on it, and regardless of its displacement and velocity at the instant t'. Treating this increment of velocity as if it were an initial velocity (at the instant t') and using Eq. 67, it is concluded that the corresponding displacement of the spring-suspended mass at any later time, t, will be

$$dx = e^{-n(t-t')} \frac{q\,dt'}{\omega_1} \sin \omega_1 (t-t') \tag{73}$$

Since each impulse q dt' between t' = 0 and t' = t has a like effect, there is obtained, as a result of the continuous action of the disturbing force q, the total displacement

$$x_1 = \frac{1}{\omega_1} \int_0^t q e^{-n(t-t')} \sin \omega_1 (t-t')\,dt' \tag{74}$$

This expression still does not include the effect of any initial displacement x_0 or initial velocity $\dot{x}_0$, when t = 0. These effects, however, are exactly

those represented by Eq.67 ; hence, for a complete solution of Eq. 72, there is obtained

$$x = e^{-nt}\left[x_0 \cos \omega_1 t + \left(\frac{\dot{x}_0 + nx_0}{\omega_1}\right)\sin \omega_1 t\right] + \frac{1}{\omega_1}\int_0^t qe^{-n(t-t')} \sin \omega_1 (t-t')dt' \tag{75}$$

At first glance it might appear that the first term in this expression represented free vibrations and the last term forced vibrations, but this is not quite the case. Actually the first term represents only the effect of initial displacement and initial velocity; the last term represents the complete effect of the disturbing force $q = f(t')$. The disturbing force produces, on its own account, both free and forced vibrations and all this together is accounted for by the integral in Eq. 75 , i.e., by the solution (74). For this reason, Eq. 74 and 75 are especially useful in studying the early effects of a disturbing force before damping has had time to dissipate the free vibrations.

For convenience in further calculations, it will be helpful to transform the integral in Eq. 75 as follows: Using the relation

$$\sin (\omega_1 t - \omega_1 t') = \sin \omega_1 t \cos \omega_1 t' - \cos \omega_1 t \sin \omega_1 t' \tag{76}$$

The complete solution is given as

$$\begin{aligned} x = {} & e^{-nt}\left[x_0 \cos \omega_1 t + \left(\frac{\dot{x}_0 + nx_0}{\omega_1}\right)\sin \omega_1 t\right] \\ & + \frac{e^{-nt}\sin \omega_1 t}{\omega_1}\int_0^t qe^{nt'} \cos \omega_1 t' \, dt' \\ & - \frac{e^{-nt}\cos \omega_1 t}{\omega_1}\int_0^t qe^{nt'} \sin \omega_1 t' \, dt' \end{aligned} \tag{77}$$

Application of this expression to rectangular and trapezoidal force-time inputs will now be made.

APPLICATION OF METHOD TO RECTANGULAR AND TRAPEZOIDAL FORCE-TIME INPUTS

RECTANGULAR FORCE-TIME INPUT

Application of Eq. 77 for a rectangular force-time input to the spring-mass system provides a relatively simple demonstration of the mathematical method and the results obtained by its use. Although stepped inputs are not encountered in actual rocket engine performance evaluations, they are employed for test stand dynamic evaluation tests by the use of fracture links and snapped wires. Figure 7 shows the shape of the input force-time curve. The constant-level force duration is arbitrarily taken to be great enough to dissipate essentially all oscillation of the system produced during the up-step by the damping (always present in some degree) by the time the down-step occurs at the input force termination. Separate evaluations of Eq. 77 for the two steps are made because of the difference in initial conditions and load existing at the instants the two steps occur.

Figure 7. Force-Time Input, Rectangular

Case 1, Stepped Loading

Initial conditions at $t = 0$ are $x_0 = 0$, $\dot{x}_0 = 0$, and $q = \frac{F_0}{m}$ is constant during the loaded phase. The subsequent displacement, x, of the mass, m, using Eq. 77 is

$$x = \frac{F_0 e^{-nt}}{m\omega_1}\left[\sin \omega_1 t \int_0^t e^{nt'} \cos \omega_1 t' dt' - \cos \omega_1 t \int_0^t e^{nt'} \sin \omega_1 t' \, dt'\right] \tag{78}$$

from which is obtained

$$x = \frac{F_0 e^{-nt}}{m\omega_1 (n^2+\omega_1^2)}\left[\omega_1 e^{nt} - n \sin \omega_1 t - \omega_1 \cos \omega_1 t\right] \tag{79}$$

Multiplying this displacement equation by the spring constant, k, and utilizing the relations

$$kx = F \ , \ \omega^2 = \frac{k}{m} \ , \ \frac{\omega^2}{n^2+\omega_1^2} = 1 \tag{80}$$

where

F = force indicated by the spring

there re ults

$$F = F_0 \left(1 - \frac{n}{\omega_1} e^{-nt} \sin \omega_1 t - e^{-nt} \cos \omega_1 t\right) \tag{81}$$

By integration of Eq. 81 for the duration of the applied step loading an expression is obtained relating the impulses of the actual input force and the force measured by the spring.

$$\int_0^t F \, dt = F_0 \left[\int_0^t dt - \frac{n}{\omega_1} \int_0^t e^{-nt} \sin \omega_1 t \, dt - \int_0^t e^{-nt} \cos \omega_1 t \, dt\right] \tag{82}$$

Since the actual impulse in this case is $I_A = F_0 t$, Eq. 35, using the notation for measured impulse, $I_M = \int_0^t F dt$, provides the expression

$$I_M - I_A = - \frac{F_0}{n^2+\omega_1^2} \left[\left(\frac{\omega_1^2 - n^2}{\omega_1}\right) e^{-nt} \sin \omega_1 t - 2ne^{-nt} \cos \omega_1 t + 2n\right] \tag{83}$$

Equation 83 indicates that the difference between the actual and measured impulses (error), for the duration of the stepped loading, is a function of the force level, the damping, the damped natural frequency and the force duration time.

Case 2, Stepped Unloading

Taking t = 0 at the instant of system unloading the initial conditions are taken to be $x_0 = \frac{F_o}{k}$, $\dot{x}_0 = 0$, and q = 0. Although a zero initial velocity, at the stated displacement, would theoretically require an infinite time to obtain, by damping, subsequent to an upstep, it is entirely realistic and practical to regard it obtained in a finite time. Fox example, examination

of the derivative of Eq. 79 shows that $\dot{x} \leq 10^{-46}$ in/sec in 2 seconds after a 10,000-pound stepped load is applied to a 175 cps system damped only 5 percent of critical damping.

The subsequent displacement, x, of mass, m, again using Eq. 77 in which these values are substituted, is seen to be:

$$x = \frac{F_0 e^{-nt}}{k}\left[\cos \omega_1 t + \frac{n}{\omega_1} \sin \omega_1 t\right] \tag{84}$$

Again utilizing the relations $kx = F$, $I_M = \int_0^t F dt$ there results

$$I_M = \frac{F_0}{n^2 + \omega_1^2}\left[\left(\frac{\omega_1^2 - n^2}{\omega_1}\right) e^{-nt} \sin \omega_1 t - 2ne^{-nt} \cos \omega_1 t + 2n\right] \tag{85}$$

and since $I_A = 0$ for periods subsequent to the stepped unloading, Eq. 85 represents the error incurred during the time t after the down-step. By inspection of Eq. 83 and 85 it is seen that the two impulse errors associated with a rectangular force-time input are equal in magnitude and opposite in sign, for <u>equal</u> integration times subsequent to the two steps, and result in a <u>zero net overall measurement error</u> by the system due to mechanical response. The only restrictions incorporated in the foregoing application were (1) a constant-level force duration long enough to obtain essentially static equilibrium by the time of the down-step and, (2) an equal integration time after the down-step. Of course, equal-time integrations for stepped loading and unloading of the system and the statement $\dot{x}_o = 0$ at the time of the down-step are equivalent to stating that the system is once again in static equilibrium by the end of the integration performed after unloading. The purpose of the foregoing exercise was to examine the relation between system design-excitation and measurement errors, through a breakdown of the over-all integration into separate integrations.

TRAPEZOIDAL FORCE-TIME INPUT

The use of Eq. 77 for the more general case of trapezoidal force-time inputs consists of its successive use with each of the four separate phases of the system excitation, identified by reference to Fig. 8. Phase numbering is based on symmetry considerations rather than on chronological order. The force-time input excitation consists of two ramps, one up and one down, separated by an intermediate constant-level force whose duration is again great enough to obtain essentially static equilibrium at the time of occurrence of the down-ramp. Force-time inputs of this type provide useful analytical approximations to rocket motor thrust-time curves.

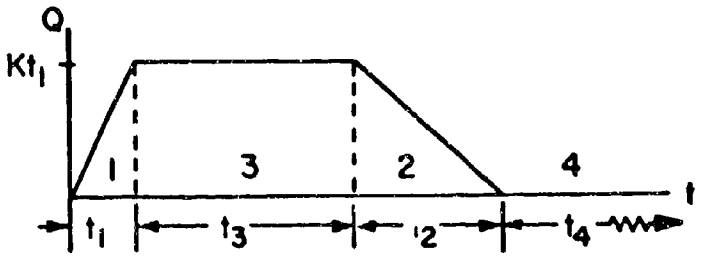

Figure 8. Force-Time Input, Trapezoidal

Phase 1: Startup Ramp

Initial conditions are $x_0 = \dot{x}_0 = 0$, and the excitation force is $Q = Kt$, where K is the slope of the ramp, during the time period $0 \leq t \leq t_1$. On substitution of these expressions into Eq. 77, the displacement x of the mass m during phase 1 is given by:

$$x = \frac{Ke^{-nt}}{\omega_1 m}\left[\sin \omega_1 t \int_0^t t' e^{nt'} \cos \omega_1 t' \, dt' - \cos \omega_1 t \int_0^t t' e^{nt'} \sin \omega_1 t' \, dt'\right] \tag{86}$$

which results in

$$x = \frac{Ke^{-nt}}{\omega_1 m}\left[\frac{\omega_1 t \, e^{nt}}{n^2 + \omega_1^2} - \frac{2n\omega_1 e^{nt} - (n^2 - \omega_1^2) \sin \omega_1 t - 2n\omega_1 \cos \omega_1 t}{(n^2 + \omega_1^2)^2}\right] \tag{87}$$

On multiplying this equation by the spring constant, k, and utilizing the relations given in Eq. 80 there is obtained the expression:

$$F = Kt + \frac{2Kn(e^{-nt}\cos\omega_1 t - 1)}{n^2 + \omega_1^2} + \frac{K(n^2 - \omega_1^2)\, e^{-nt}\sin\omega_1 t}{\omega_1(n^2 + \omega_1^2)^2} \qquad (88)$$

The expression relating the impulses of the applied and measured startup forces is obtained by integration of Eq. 88 to time t_1, that is,

$$\int_0^{t_1} F dt = K\int_0^{t_1} t dt - \frac{2Kn}{n^2 + \omega_1^2}\int_0^{t_1} dt + \frac{K(n^2-\omega_1^2)}{\omega_1(n^2+\omega_1^2)}\int_0^{t_1} e^{-nt}\sin\omega_1 t dt +$$

$$\frac{2Kn}{n^2 + \omega_1^2}\int_0^{t_1} e^{-nt}\cos\omega_1 t\, dt \qquad (89)$$

The integrated result, utilizing the expressions for measured and actual impulse during phase 1, respectively $I_M = \int_0^{t_1} F dt$ and $I_A = \frac{Kt_1^2}{2}$, provides the error expression:

$$E_1 = I_A - I_M = \frac{2Knt_1}{n^2+\omega_1^2} + \frac{K}{(n^2+\omega_1^2)^2}\left[\frac{n(n^2-3\omega_1^2)}{\omega_1} e^{-nt_1}\sin\omega_1 t_1 + \right.$$

$$\left.(3n^2 - \omega_1^2)\, e^{-nt_1}\cos\omega_1 t_1 - 3n^2 + \omega_1^2\right] \qquad (90)$$

Eq. 90 shows that the impulse error incurred <u>during</u> the startup phase is a function of the slope of the startup ramp, the damping, the damped natural frequency, and the startup duration time.

<u>Phase 2, Cutoff Ramp</u>

Initial conditions are $x_0 = \frac{Kt_1}{k}$, $\dot{x}_0 = 0$ essentially, and the excitation force is $Q = \frac{Kt_1}{t_2}(t_2 - t)$ during the time period $0 \leq t \leq t_2$. As before, the statement $\dot{x}_0 = 0$ is considered entirely realistic for the contemplated system and its excitation. It will be demonstrated later that no measureable error is incurred by stating $\dot{x}_0 = 0$ at this point of the contemplated trapezoidal excitation of the planned total impulse measurement system.

On substitution of these expressions in Eq. 77, the displacement x of the mass m during phase 2 is given by:

$$x = \frac{Kt_1}{k} e^{-nt}\left[\cos \omega_1 t + \frac{n}{\omega_1} \sin \omega_1 t\right] + \frac{Kt_1 e^{-nt} \sin \omega_1 t}{\omega_1 m} \int_0^t e^{nt'} \cos \omega_1 t' dt' -$$

$$\frac{Kt_1 e^{-nt} \cos \omega_1 t}{\omega_1 m} \int_0^t e^{nt'} \sin \omega_1 t' dt' - \frac{Kt_1 e^{-nt} \sin \omega_1 t}{\omega_1 m t_2} \int_0^t t' e^{nt'} \cos \omega_1 t' dt' +$$

$$\frac{K t_1 e^{-nt} \cos \omega_1 t}{\omega_1 m t_2} \int_0^t t' e^{nt'} \sin \omega_1 t' dt' \qquad (91)$$

which results in:

$$x = \frac{Kt_1 e^{-nt}}{k}\left[\cos \omega_1 t + \frac{n}{\omega_1} \sin \omega_1 t\right] + \frac{Kt_1 e^{-nt}}{\omega_1 m}\left[\frac{\omega_1 e^{nt}}{n^2+\omega_1^2} - \frac{n \sin \omega_1 t + \omega_1 \cos \omega_1 t}{n^2 + \omega_1^2} - \right.$$

$$\left. \frac{\omega_1 t e^{nt}}{t_2(n^2+\omega_1^2)} + \frac{2n\omega_1 e^{nt} - (n^2 - \omega_1^2) \sin \omega_1 t - 2n\omega_1 \cos \omega_1 t}{t_2(n^2 + \omega_1^2)^2}\right] \qquad (92)$$

On multiplying this equation by the spring constant k and again utilizing the relations given in Eq. 80 there is obtained the expression:

$$F = Kt_1 - \frac{t_1}{t_2}\left[Kt + \frac{2Kn(e^{-nt} \cos \omega_1 t - 1)}{n^2 + \omega_1^2} + \frac{K(n^2 - \omega_1^2) e^{-nt} \sin \omega_1 t}{\omega_1 (n^2 + \omega_1^2)^2}\right] \qquad (93)$$

The expression relating the impulses of the applied and measured cutoff forces is obtained by integration of Eq. 93 to time t_2, i.e.,

$$\int_0^{t_2} F\,dt = Kt_1 \int_0^{t_2} dt - K\left(\frac{t_1}{t_2}\right)\int_0^{t_2} t\,dt + \frac{2Kn}{n^2+\omega_1^2}\left(\frac{t_1}{t_2}\right)\int_0^{t_2} dt -$$

$$\frac{K(n^2-\omega_1^2)}{\omega_1(n^2+\omega_1^2)}\left(\frac{t_1}{t_2}\right)\int_0^{t_2} e^{-nt}\sin\omega_1 t\,dt -$$

$$\frac{2Kn}{n^2+\omega_1^2}\left(\frac{t_1}{t_2}\right)\int_0^{t_2} e^{-nt}\cos\omega_1 t\,dt \qquad (94)$$

The integrated result, utilizing the expressions for measured and actual impulse during phase 2, respectively

$$I_M = \int_0^{t_2} F\,dt \text{ and } I_A = \frac{Kt_1t_2}{2},$$

provides the error expression:

$$E_2 = I_A - I_M = -\frac{2Knt_1}{n^2+\omega_1^2} - \left(\frac{t_1}{t_2}\right)\frac{K}{(n^2+\omega_1^2)^2}\left[\frac{n(n^2-3\omega_1^2)}{\omega_1}e^{-nt_2}\sin\omega_1 t_2 + \right.$$

$$\left.(3n^2-\omega_1^2)\,e^{-nt_2}\cos\omega_1 t_2 - 3n^2+\omega_1^2\right] \qquad (95)$$

Comparison of the two error expressions for phases 1 and 2, Eq. 90 and 95 shows that complete cancellation of the two errors occurs for symmetrical startup and cutoff ramps (i.e., $t_1 = t_2$). With asymmetrical ramps, (i.e., $t_1 \neq t_2$), incomplete cancellation, in general, results in a net impulse measurement error during these two phases of the system excitation. Similar results are now obtained for phases 3 and 4.

Phase 3, Constant-Level Force

Initial conditions of this phase are obtained from the displacement expression (Eq. 87)and its derivative, at the instant of termination of phase 2. The result is:

$$x_0 = \frac{K}{\omega_1 m(n^2 + \omega_1^2)}\left[\omega_1 t_1 + \frac{(n^2 - \omega_1^2)e^{-nt_1}\sin \omega_1 t_1 + 2n\omega_1 e^{-nt_1}\cos \omega_1 t_1 - 2n\omega_1}{n^2 + \omega_1^2}\right]$$

$$\dot{x}_0 = \frac{K}{\omega_1 m\ (n^2 + \omega_1^2)}\left[\omega_1 - \frac{\omega_1(n^2+\omega_1^2)e^{-nt_1}\cos \omega_1 t_1 + n(n^2+\omega_1^2)e^{-nt_1}\sin \omega_1 t_1}{n^2 + \omega_1^2}\right] \quad (96)$$

The excitation force is $Q = Kt_1$ during the time period $0 \leq t \leq t_3$. On substitution of these expressions into Eq.77 , multiplication of the resulting equation by the spring constant, k, and use of the expressions in Eq. 80, the expression for the measured force, F, during phase 3 is:

$$F = K\left[\left(\frac{C_1}{\omega_1} - t_1\right)e^{-nt}\cos \omega_1 t + \left(\frac{C_2 + nC_1}{\omega_1^2} - \frac{nt_1}{\omega_1}\right)e^{-nt}\sin \omega_1 t + t_1\right] \quad (97)$$

where C_1 and C_2 are, respectively, the bracketed terms in Eq. 96 for x_0 and $\dot{x}_0$. The impulse of the measured force F during phase 3 is obtained by the integration of Eq. 97 to time t_3. The resulting expression, utilizing the relations $I_M = \int_0^{t_3} F\,dt$ and $I_A = K t_1 t_3$ for the measured and actual impulses, respectively, provides the error expression for phase 3, as shown following.

$$E_3 = I_A - I_M$$

$$= \frac{-K}{\omega_1(n^2+\omega_1^2)^2}\Big[n(n^2 - 3\omega_1^2)(e^{-nt_1}\sin \omega_1 t_1 + e^{-nt_3}\sin \omega_1 t_3) +$$

$$\omega_1(3n^2 - \omega_1^2)(e^{-nt_1}\cos \omega_1 t_1 + e^{-nt_3}\cos \omega_1 t_3) +$$

$$\omega_1(\omega_1^2 - 3n^2)\, e^{-n(t_1 + t_3)}\cos \omega_1(t_1 + t_3) +$$

$$n(3\omega_1^2 - n^2)\, e^{-n(t_1 + t_3)}\sin \omega_1 (t_1 + t_3) +$$

$$\omega_1 (\omega_1^2 - 3n^2)\Big] \qquad (98)$$

Equation 98 shows that the impulse error incurred during the constant-level phase is a function of the system-excitation parameters previously stated for phases 1 and 2 plus the constant-level duration time t_3.

Phase 4, Post-Cutoff Period

Initial conditions of this phase are obtained from the displacement expression (Eq. 92) and its derivative, at the instant of termination of phase 2. The result is:

$$x_0 = \frac{Kt_1}{k}\left[\frac{(\omega_1^2 - n^2)}{\omega_1 t_2(n^2 + \omega_1^2)}e^{-nt_2}\sin \omega_1 t_2 + \frac{2n(1 - e^{-nt_2}\cos \omega_1 t_2)}{t_2(n^2 + \omega_1^2)}\right]$$

$$\dot{x}_0 = \frac{Kt_1}{k}\left[\frac{-e^{-nt_2}\cos \omega_1 t_2}{t_2} + \frac{ne^{-nt_2}\sin \omega_1 t_2}{\omega_1 t_2} - \frac{1}{t_2}\right] \qquad (99)$$

The excitation force during the post-cutoff period is, of course, zero. On substitution of these expressions into Eq. 77, multiplication of the resulting equation by the spring constant, k, and use of the expressions in Eq. 80, the expression for the measured force, F, during phase 4 is:

$$F = Kt_1\left[C_3\, e^{-nt}\cos \omega_1 t + \left(\frac{C_4 + nC_3}{\omega_1}\right)e^{-nt}\sin \omega_1 t\right] \qquad (100)$$

where C_3 and C_4 are, respectively, the bracketed quantities in Eq. 99 for x_0 and $\dot{x}_0$.

The impulse of the measured force, F, during phase 4 is obtained by the integration of Eq. 100 to time t_4. The resulting expression, utilizing the relations $I_M = \int_0^{t_4} F\, dt$, $I_A = 0$, for the measured and actual impulses, respectively, provides the error expression for phase 4:

$$
\begin{aligned}
E_4 &= I_A - I_M \\
&= \left(\frac{t_1}{t_2}\right) \frac{K}{\omega_1 (n^2 + \omega_1^2)^2} \Big[n(n^2 - 3\omega_1^2)\ (e^{-nt_2} \sin \omega_1 t_2 + e^{-nt_4} \sin \omega_1 t_4) \ + \\
&\quad \omega_1 (3n^2 - \omega_1^2)\ (e^{-nt_2} \cos \omega_1 t_2 + e^{-nt_4} \cos \omega_1 t_4) \ + \\
&\quad \omega_1 (\omega_1^2 - 3n^2)\ e^{-n(t_2 + t_4)} \cos \omega_1 (t_2 + t_4) \ + \\
&\quad n(3\omega_1^2 - n^2)\ e^{-n(t_2 + t_4)} \cos \omega_1 (t_2 + t_4) \ + \\
&\quad \omega_1\ (\omega_1^2 - 3n^2) \Big]
\end{aligned}
\tag{101}
$$

The similarity of the error expressions for phases 1 and 2, and for phases 3 and 4, suggests their joint consideration, and useful simplification is obtained by expressing the damping parameter, n, and the damped natural frequency ω_1 in terms of the damping ratio $h = \frac{c}{c_{crit}}$ and undamped natural frequency ω. With reference to Eq. 50 and 59, the following expressions are obtained:

$$
\begin{aligned}
n &= \omega h \\
\omega_1 &= \omega \sqrt{1 - h^2}
\end{aligned}
\tag{102}
$$

The use of these relations in the sum of Eq.90 and 95 esults in the error expression for phases 1 and 2:

$$E_1 + E_2 = \frac{K}{\omega^2\sqrt{1-h^2}} \left\{\left[\quad h\,(3-4h^2)\, e^{-\omega h t_1} \sin \omega t_1 \sqrt{1-h^2} + \right.\right.$$

$$\left. \sqrt{1-h^2}\,(4h^2-1)\,(e^{-\omega h t_1} \cos \omega t_1 \sqrt{1-h^2} - 1)\right] -$$

$$\frac{t_1}{t_2}\left[- \quad h\,(3-4h^2)\, e^{-\omega h t_2} \sin \omega t_2 \sqrt{1-h^2} + \right.$$

$$\left.\left. \sqrt{1-h^2}\,(4h^2-1)\,(e^{-\omega h t_2} \cos \omega t_2 \sqrt{1-h^2} - 1)\right]\right\} \qquad (103)$$

Because the actual impulse for phases 1 and 2 is given by

$$I_{A1-2} = 1/2\, K t_1^2 + 1/2\, K\, t_1 t_2 = \frac{K t_1}{2}(t_1 + t_2)$$

$$= \frac{K t_1 t_2}{2}\left(\frac{t_1}{t_2} + 1\right) \qquad (104)$$

the fractional error for phases 1 and 2 is

$$F_{1,2} = \frac{E_1 + E_2}{I_{A1-2}} = \frac{2(E_1 + E_2)}{K\, t_1 t_2 \left(\frac{t_1}{t_2} + 1\right)} \qquad (105)$$

and on using the notations

$$H_1 = \sqrt{1-h^2}$$

$$H_2 = \frac{h(3-4h^2)}{\sqrt{1-h^2}} \qquad (106)$$

$$H_3 = 4h^2 - 1$$

the fractional error for phases 1 and 2 is expressed by

$$F_{1,2} = \frac{-2}{\omega^2 t_1 t_2 (\frac{t_1}{t_2} + 1)} \left\{ H_2 e^{-\omega h t_1} \sin \omega H_1 t_1 - H_3 (e^{-\omega h t_1} \cos \omega H_1 t_1 - 1) - \right.$$

$$\left. \frac{t_1}{t_2} \left[H_2 e^{-\omega h t_2} \sin \omega H_1 t_2 - H_3 (e^{-\omega h t_2} \cos \omega H_1 t_2 - 1) \right] \right\} \qquad (107)$$

Similarly, for phases 3 and 4

$$E_3 + E_4 = \frac{-K}{\omega^2 \sqrt{1 - h^2}} \left\{ - h(3 - 4h^2)(e^{-\omega h t_1} \sin \omega t_1 \sqrt{1 - h^2} + e^{-\omega h t_3} \sin \omega t_3 \sqrt{1-h^2} \right.$$

$$\sqrt{1 - h^2} (4h^2 - 1)(e^{-\omega h t_1} \cos \omega t_1 \sqrt{1 - h^2} + e^{-\omega h t_3} \cos \omega t_3 \sqrt{1 - h^2}) -$$

$$\sqrt{1 - h^2} (4h^2 - 1) e^{-\omega h (t_1 + t_3)} \cos \omega (t_1 - t_3) \sqrt{1 - h^2} +$$

$$h(3 - 4h^2) e^{-\omega h (t_1 + t_3)} \sin \omega (t_1 + t_3) \sqrt{1 - h^2} - \sqrt{1 - h^2} (4h^2 - 1) -$$

$$\frac{t_1}{t_2} \left[- h (3 - 4h^2)(e^{-\omega h t_2} \sin \omega t_2 \sqrt{1 - h^2} + e^{-\omega h t_4} \sin \omega t_4 \sqrt{1 - h^2}) + \right.$$

$$\sqrt{1 - h^2} (4h^2 - 1)(e^{-\omega h t_2} \cos \omega t_2 \sqrt{1 - h^2} + e^{-\omega h t_4} \cos \omega t_4 \sqrt{1 - h^2}) -$$

$$\sqrt{1 - h^2} (4h^2 - 1) e^{-\omega h (t_2 + t_4)} \cos \omega (t_2 + t_4) \sqrt{1 - h^2} +$$

$$h(3 - 4h^2) e^{-\omega h (t_2 + t_4)} \sin \omega (t_2 + t_4) \sqrt{1 - h^2} -$$

$$\left. \left. \sqrt{1 - h^2} (4h^2 - 1) \right] \right\} \qquad (108)$$

Because the actual impulse for phases 3 and 4 is given by

$$I_{A3-4} = K\, t_1 t_3 \tag{109}$$

he fractional error for phases 3 and 4 is

$$F_{3,4} = \frac{E_3 + E_4}{I_{A3-4}} = \frac{E_3 + E_4}{K\, t_1\, t_3} \tag{110}$$

nd on again using the notations in Eq.106 the fractional error for phases
and 4 is expressed by

$$\begin{aligned}
{}_{3,4} = \frac{1}{\omega^2 t_1 t_3} \Big\{ & H_2 \left(e^{-\omega h t_1} \sin \omega H_1 t_1 + e^{-\omega h t_3} \sin \omega H_1 t_3 - e^{-\omega h (t_1+t_3)} \cos \omega H_1 (t_1+t_3) \right) - \\
& H_3 \left(e^{-\omega h t_1} \cos \omega H_1 t_1 + e^{-\omega h t_3} \cos \omega H_1 t_3 - e^{-\omega h (t_1+t_3)} \cos \omega H_1 (t_1+t_3) - 1 \right) - \\
& \frac{t_1}{t_2} \Big[H_2 \left(e^{-\omega h t_2} \sin \omega H_1 t_2 + e^{-\omega h t_4} \sin \omega H_1 t_4 - e^{-\omega h (t_2+t_4)} \cos \omega H_1 (t_2+t_4) \right) - \\
& H_3 \left(e^{-\omega h t_2} \cos \omega H_1 t_2 + e^{-\omega h t_4} \cos \omega H_1 t_4 - e^{-\omega h (t_2+t_4)} \cos \omega H_1 (t_2+t_4) - 1 \right) \Big] \Big\}
\end{aligned} \tag{111}$$

DISCUSSION

A discussion of the over-all measurement error is appropriate at this point. To begin, it should be stated that a methematical integration of an indicated force-time curve performed to an infinite time will show that no error occurs in the measurement of total impulse of any kind of excitation of a spring-mass system. The purpose of this analysis, however, is to obtain the expression for the error that is incurred for finite integrations of indicated forces by a spring-mass system trapezoidally excited. It is therefore reasonable to examine the sum of Eq. 103 and 108 (total error) to determine if it does vanish for an infinite post-cutoff integration time, t_4. Accordingly, for $t_4 = \infty$,

$$E_T = E_1 + E_2 + E_3 + E_4 = \frac{K}{\omega^2}\left[H_2\left(e^{-\omega h t_3}\sin \omega t_3\sqrt{1-h^2} - e^{-\omega h(t_1+t_3)}\sin \omega (t_1+t_3)\sqrt{1-h^2}\right) - H_3\left(e^{-\omega h t_3}\cos \omega t_3\sqrt{1-h^2} - e^{-\omega h(t_1+t_3)}\cos \omega (t_1+t_3)\sqrt{1-h^2}\right)\right] \qquad (112)$$

Inspection of Eq. 112 for total measurement error shows that $E_{total} \rightarrow 0$ as $t_1 + t_3 \rightarrow t_3$. The accuracy of Eq. 112 for the contemplated measurement system and a very rapid transient excitation is demonstrated by the fact that $E_T \leq 1.3 \times 10^{-95}$ lb sec for $t_4 = \infty$, for a 175-cps system, damped 10% critical, subjected to a startup ramp of 10,000 pounds in 5 milliseconds followed by a constant-level force duration of 2 seconds.

Therefore, for all practical purposes, Eq. 103 and 108 regarded either separately, or jointly for total error, quantitatively show the relationship between measurement system-design parameters and total impulse measurement errors incurred by finite times of integration for general trapezoidal excitations. The only limitation imposed on the entire mathematical development of these expressions is the statement of static equilibrium at the time of the excitation downramp, and the insignificance

of the error resulting from this assumption for the planned system and its excitation was demonstrated.

Because percentage errors are usually more desirable than absolute errors, Eq. 107 and 111 are of more interest for measurement purposes. Values of error obtained by the use of these equations, when multiplied by 100, will be in the desired form.

A few statements regarding the actual use of such a measurement system are appropriate. Examination of the error expressions shows that the actual operation of the system described will be governed by the level of error that can be tolerated. The percentage of error incurred in the total measurement, as shown by the sum of Eq. 107 and 111, is a function of the system's natural frequency, ω, and damping ratio, h, the excitation symmetry ratio, t_1/t_2, and the individual values of t_1, t_2, t_3, and t_4. All of these design and excitation parameters, except t_4, are beyond control of the system's operator, once a measurement system is constructed and put in use. Consequently, the duration of the post-cutoff integration time will be the controlling operational factor in holding measurement errors below a desired level.

Any decision regarding the amount of post-cutoff integration time, t_4, is consequently dependent upon the shape of the input excitation curve, if errors are to be held to the desired level with the constructed system.

ANALYTICAL DYNAMICS OF THE ROCKETDYNE THRUST AND TOTAL IMPULSE MEASUREMENT SYSTEM

INTRODUCTION

In studies associated with the design of the thrust total impulse measure ment system for use at EAFB, it was desirable to develop a mathematical model which more adequately describes the dynamic response characteristics of this thrust measurement system. The development and analysis of such a model is described herein.

Because the system which was investigated possessed nonlinear character-istics, it was necessary to adopt a numerical approach for the solution of the resulting equations of motion. However, if several appropriate simpli-fying assumptions are made, it is possible to solve the equations in closed form for a special case which is outlined in the following analysis.

MATHEMATICAL MODEL

In systems of this type, it is customary to describe the mathematical model by means of a network of springs and dashpots. In particular, the thrust measurement system may be represented by two springs and dashpots as shown in Fig. 9.

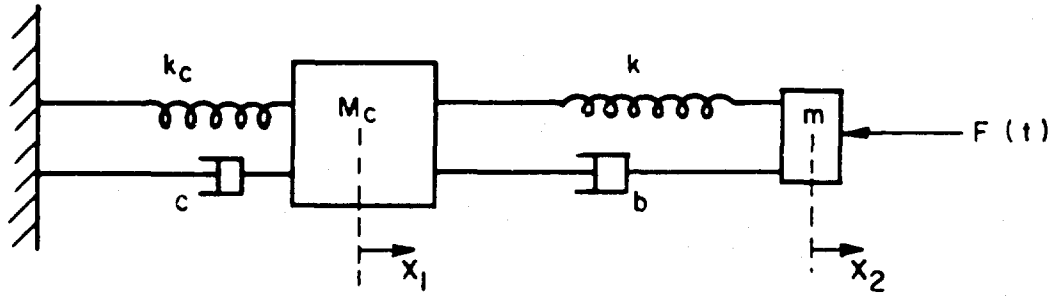

Figure 9 . Two-Degree-of-Freedom System

In Fig. , the concrete block and load cell have been replaced by equivalent springs and dashpots. The nomenclature is as follows:

M_c = mass of the concrete block

k_c = spring constant for the block evaluated on the basis of shear deflection produced by a thrust

m = mass of entire motor and mount assembly

k = spring constant for load cell

b,c = damping coefficients (including windage effects) of the cell and block, respectively

$F(t)$ = applied thrust

x_1, x_2 = the displacements of the block and load cell, respectively, from their equilibrium positions

It should be noted here that M_c, k_c, and k are assumed to be constants,* whereas m, b, and c are variable quantities given in the form

$$m \quad m(t)$$
$$b \quad b(\dot{x}_2)$$
$$c \quad c(\dot{x}_1)$$

DIFFERENTIAL EQUATIONS OF MOTION FOR THE SYSTEM

The equations of motion are derived by Lagrange's method, beginning with the expressions for the kinetic and potential energies of the system as given by

$$T = \frac{1}{2} M_c \dot{x}_1^2 + \frac{1}{2} m \dot{x}_2^2$$
$$V = \frac{1}{2} k_c x_1^2 + \frac{1}{2} k (x_2 - x_1)^2 \qquad (113)$$

*Variable k is treated in the final section of this discussion.

The resisting forces may be assumed in the form

$$f_1 = c(\dot{x}_1)\dot{x}_1$$

$$f_2 = b(\dot{x}_2)\dot{x}_2 \qquad (114)$$

Thus, in terms of the quantities T, V, and f_i, Lagrange's equations of motion may be written as

$$\frac{d}{dt}\left(\frac{\partial T}{\partial \dot{x}_i}\right) - \frac{\partial T}{\partial x_i} + \frac{\partial V}{\partial x_i} + f_i = Q_i \qquad i = 1,2 \qquad (115)$$

where Q_i = externally applied forces. With the aid of Eq. 113 and 114, the coupled equations of motion for the system are

$$M_c \ddot{x}_1 + (k_c + k)x_1 - kx_2 + c(\dot{x}_1)\dot{x}_1 = 0$$

$$\frac{d}{dt}(m\dot{x}_2) + k(x_2 - x_1) + b(\dot{x}_2)\dot{x}_2 = -F(t) \qquad (116)$$

There are two sets of initial conditions associated with the system (Eq. 116) to be considered in the present analysis:

$$\begin{array}{lll} 1. & \dot{x}_1(0) = 0 & \dot{x}_2(0) = 0 \\ & x_1(0) = 0 & x_2(0) = 0 \\ 2. & \dot{x}_1(0) = 0 & \dot{x}_2(0) = 0 \\ & x_1(0) = u_1 & x_2(0) = u_2 \end{array} \qquad (117)$$

EVALUATION OF SPRING CONSTANT

The concrete block is assumed to act as a beam built in at one end with a concentrated load acting at the free end shown as follows.

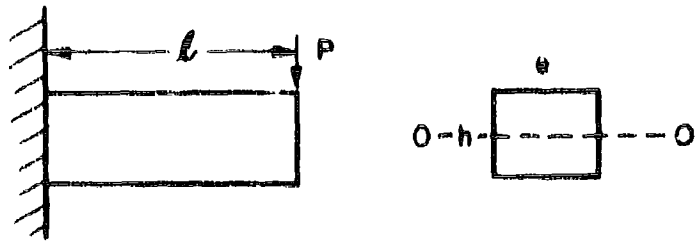

By definition, the spring constant for the beam is

$$k_c = P/\delta \tag{118}$$

where δ is the static deflection due to a load P. Because the cross-sectional dimensions of the block are of the order of magnitude of the length of the block, the deflection due to the effect of shear must be included in addition to that due to bending.

From Ref. 5, the following expression is obtained for δ:

$$\delta = \frac{P\ell^3}{3E_c I}\left[1 + 0.71\,(h/\ell)^2 - 0.10\,(h/\ell)^3\right] \tag{119}$$

where

E_c = Young's modulus for reinforced concrete

ℓ = length of beam

I = moment of inertia of cross-section about axis 00

$= \frac{(eh)(h/2)^2}{3} = eh^3/12$

Thus, the equivalent spring constant for the concrete block is given by

$$\begin{aligned} k_c &= P/\delta \\ &= 3E_c I/\ell^3\left[1 + 0.71(h/\ell)^2 - 0.10(h/\ell)^3\right] \\ &= (1/4)E_c(h/\ell)^3\, e/\left[1 + 0.71(h/\ell)^2 - 0.10(h/\ell)^3\right] \end{aligned} \tag{120}$$

A computer program has been written to solve the coupled system (Eq. 116) for a wide variety of functions $m(t)$, $F(t)$, $b(\dot{x})$, and $c(\dot{x})$. Parameter studies and impulse error estimates using this program will be described subsequently.

SPECIAL CASE: ONE DEGREE OF FREEDOM, VISCOUS DAMPING, AND TIME-VARYING MASS

If the assumption is made that the concrete block is so "stiff" that its motion can be neglected, then the system of equations (Eq. 4) reduces to a single-degree-of-freedom system given by

$$\frac{d}{dt}(m\dot{x}_2) + kx_2 + b(\dot{x}_2)\dot{x}_2 = -F(t) \tag{121}$$

In addition, if the damping factor $b(\dot{x}_2) = b = \text{constant}$, and $m(t)$ is assumed in the form $m = m_0 - at$, $t < m_0/a$, $a > 0$, the above equation is linearized and closed-form solutions are possible.

Considering, therefore, the linearized equation

$$(m_0 - at)\ddot{x}_2 + (b - a)\dot{x}_2 + kx_2 = -F(t) \tag{122}$$

write $s = m_0 - at$

Thus, Eq. 122 reduces to

$$s\,x_2'' + a_1 x_2' + a_2 x_2 = a_3 \bar{F}(s) \tag{123}$$

where primes denote differentiation with respect to s.

$$a_1 = (a-b)/a$$

$$a_2 = k/a^2$$

$$a_3 = -1/a^2$$

$$\bar{F}(s) = F\left(\frac{m_0 - s}{a}\right)$$

Equation 123 may be identified with an inhomogeneous Bessel's equation of a special kind. The homogeneous solution $(x_2)_H$ of Eq. 123 is

$$(x_2)_H = \left[AJ_\nu(\beta\sqrt{s}) + BY_\nu(\beta\sqrt{s})\right]s^{(1-a_1)/2} \tag{124}$$

where J_ν and Y_ν are respectively Bessel functions of first and second kind of order ν.

$$\nu = b/a$$
$$\beta = (2/a)\sqrt{k}$$

Applying the method of variation of constants, the general solution to Eq. 123 is:

$$x_2(s) = s^{b/2a}\Big[AJ_\nu(\beta\sqrt{s}) + BY_\nu(\beta\sqrt{s}) - \pi a_3 J_\nu(\beta\sqrt{s}) \int_{m_o}^{s} \bar{F}(y)y^{-b/2a}Y_\nu (\beta\sqrt{y})dy + \pi a_3 Y_\nu(\beta\sqrt{s}) \int_{m_o}^{s} \bar{F}(y)y^{-b/2a}J_\nu(\beta\sqrt{y})dy\Big] \tag{125}$$

In terms of the time t, this may be written as

$$x_2(t) = (m_o-at)^{b/2a}\Big[AJ_\nu(\beta\sqrt{m_o-at}) + BY_\nu(\beta\sqrt{m_o-at})\Big]$$
$$+ \pi a_3 a(m_o-at)^{b/2a}J_\nu(\beta\sqrt{m_o-at}) \int_o^t (m_o-a\tau)^{-b/2a}F(\tau)Y_\nu(\beta\sqrt{m_o-a\tau})d\tau$$
$$- \pi a_3 a(m_o-at)^{b/2a}Y_\nu(\beta\sqrt{m_o-at}) \int_o^t (m_o-a\tau)^{-b/2a}F(\tau)J_\nu(\beta\sqrt{m_o-a\tau})d\tau \tag{126}$$

The constants A and B are now to be determined from the initial conditions stated earlier in Eq. 117.

Case 1

$$\dot{x}_2(0) = 0 = x_2(0)$$

It is readily shown for these conditions that A = B = 0, and thus the solution is given by

$$x_2(t) = \pi\, a_3 a (m_o - at)^{b/2a}\Big[J_\nu(\beta\sqrt{m_o-at}) \int_o^t (m_o-a\tau)^{-b/2a} F(\tau) Y_\nu(\beta\sqrt{m_o-a\tau})d\tau$$

$$- Y_\nu(\beta\sqrt{m_o-a\tau}) \int_o^t (m_o-a\tau)^{-b/2a} F(\tau) J_\nu(\beta\sqrt{m_o-a\tau})d\tau\Big] \qquad (127)$$

Case 2

$$\dot{x}_2(0) = 0 \qquad x_2(0) = u_2$$

These conditions yield

$$(m_o)^{b/2a}\Big[AJ_\nu(\beta\sqrt{m_o}) + BY_\nu(\beta\sqrt{m_o})\Big] = u_2$$

$$(b/2a)(-a)(m_o)^{(b/2a)-1}\Big[AJ_\nu(\beta\sqrt{m_o}) + BY_\nu(\beta\sqrt{m_o})\Big]$$

$$+ (m_o)^{b/2a}\Big[AJ_\nu'(\beta\sqrt{m_o-at})\cdot\frac{\beta(-a)}{2\sqrt{m_o-at}} + BY_\nu'(\beta\sqrt{m_o-at})\cdot\frac{\beta(-a)}{2\sqrt{m_o-at}}\Big]_{t=0} = 0$$

Solving for A and B obtains

$$A = (\pi\,\beta u_2/2)(m_o)^{(a-b)/2a} Y_{\nu-1}(\beta\sqrt{m_o})$$

$$B = -(\pi\,\beta u_2/2)(m_o)^{(a-b)/2a} J_{\nu-1}(\beta\sqrt{m_o}) \qquad (129)$$

Thus, $x_2(t)$ is given by

$$x_2(t) = (m_o-at)^{b/2a}(\pi\beta u_2/2)(m_o)^{(a-b)/2a}\Big[J_\nu(\beta\sqrt{m_o-at})Y_{\nu-1}(\beta\sqrt{m_o})$$

$$- Y_\nu(\beta\sqrt{m_o-at})J_{\nu-1}(\beta\sqrt{m_o})\Big]$$

$$+ \pi a_3 a (m_o-at)^{b/2a}\Big[J_\nu(\beta\sqrt{m_o-at}) \int_o^t (m_o-a\tau)^{-b/2a} F(\tau) Y_\nu(\beta\sqrt{m_o-a\tau})d\tau$$

$$- Y_\nu(\beta\sqrt{m_o-at})\int_o^t (m_o-a\tau)^{-b/2a} F(\tau) J_\nu(\beta\sqrt{m_o-a\tau})d\tau\Big]$$

The solution for this special case should provide some insight in interpreting the results of the numerical treatment of the general case (Eq. 116).

MODIFICATION OF EQUATIONS OF MOTION FOR VARIABLE SPRING CHARACTERISTICS

If the load cell spring exhibits nonlinearities, the equations of motion derived earlier must be modified by assuming first that the force-displacement relation for the spring is given in the form

$$f = kx + \alpha x^3$$

where k and α are constants to be determined from information given by the load cell manufacturer or from direct static calibration.

Thus, the potential energy stored in the load cell spring now becomes

$$V_s = \int_o^{x_2-x_1} f\, dx$$

$$= \frac{1}{2} k(x_2-x_1)^2 + \frac{1}{4} \alpha(x_2-x_1)^4 \qquad (131)$$

With this modification of the potential energy, the revised equations of motion are:

$$M_c\ddot{x}_1 + c(\dot{x}_1)\dot{x}_1 + (k_c+k)x_1 - kx_2 - \alpha(x_2-x_1)^3 = 0$$

$$\frac{d}{dt}(m\dot{x}_2) + b(\dot{x}_2)\dot{x}_2 + k(x_2-x_1) + \alpha(x_2-x_1)^3 = -F(t) \qquad (132)$$

The coupled equations (Eq. 132) represent a two-degree-of-freedom system, with the specified general type of nonlinear damping, the load cell spring of which has the specified general type of nonlinear force-displacement characteristic.

DESCRIPTION OF COMPUTER PROGRAM

Introduction

An IBM 7094 computer program has been written which numerically integrates the preceding equations of motion (Eq. 132), determines the cumulative impulse, and estimates the error in the latter. The program includes a main program and four subprograms, all written in FORTRAN. In operation, the main program simply calls the principal subprogram, SOLVDE, once for each set of data. A brief indication of the operations performed within each subprogram is given below.

SOLVDE

SOLVDE is a subroutine-type subprogram which serves the dual purpose of an executive routine and an integration routine. It is executive in that it "reads in" the input data and control cards, prints out headings and results according to the control cards, and calls the other subprograms. In solving the differential equations, it uses Runge-Kutta type integration formulas. A Runge-Kutta technique was selected for convenience of starting the solution and because of its natural stability property (such techniques are always stable for a sufficiently small step size). Because various forms of the integration formulas are given in the literature (Ref. 6 and 7), the formulas are written as follows, in vector notation, with no further discussion. The coupled equations of motion are written as one equation:

$$\ddot{x} = G(t, x, \dot{x}) \tag{133}$$

where x, $\dot{x}$, $\ddot{x}$, and G = two-dimensional vectors. The given initial condition on the displacement is:

$$x(t_o) = x_o \tag{134}$$

The step-wise integration is performed accordingly as

$$x_{n+1} = x_n + h\dot{x}_n + \frac{h}{6}(A + B + C)$$

$$\dot{x}_{n+1} = \dot{x}_n + \frac{1}{6}(A + 2B + 2C + D) \qquad (135)$$

where

$$A = hG(t_n, x_n, \dot{x}_n)$$

$$B = hG\left(t_n + \frac{h}{2}, \; x_n + \frac{h}{2}\dot{x}_n, \; \dot{x}_n + \frac{A}{2}\right)$$

$$C = hG\left(t_n + \frac{h}{2}, \; x_n + \frac{h}{2}\dot{x}_n + \frac{h}{4}A, \; \dot{x}_n + \frac{B}{2}\right)$$

$$D = hG\left(t_n + h, \; x_n + h\dot{x}_n + \frac{h}{2}B, \; \dot{x}_n + C\right) \qquad (136)$$

and h = the step size.

RTSID

RTSID is a function-type subprogram which is called by SOLVDE to evaluate the right side of Eq. 129. It has arguments i, t, x_1, x_2, $\dot{x}_1$, and $\dot{x}_2$, and hence evaluates the i^{th} component (i = 1,2) of G at the specified values of time and of both components of x and $\dot{x}$. The proper evaluation requires information regarding the time variation of the system parameters and input excitation. For the system-excitation combination under consideration, the mathematical expressions for time dependence were:

1. Mass of entire motor and mount assembly:

$$m(t) = \begin{cases} m_o - at & \text{for} \quad t \leq t_B \\ m_o - at_B & \text{for} \quad t \geq t_B \end{cases}$$

where

m_o = initial mass

a = burning rate of propellant

t_B = cutoff time

2. Thrust excitation (trapezoidal):

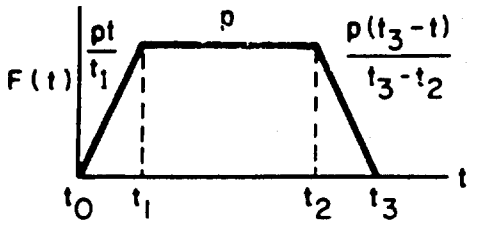

$$F(t) = \begin{cases} \dfrac{pt}{t_1} & \text{for} \quad t \leq t_1 \\ p & \text{for} \quad t_1 \leq t \leq t_2 \\ \dfrac{p(t_3-t)}{t_3 - t_2} & \text{for} \quad t_2 < t < t_3 \\ 0 & \text{for} \quad t_3 \leq t \end{cases}$$

where p, t_1, t_2, and t_3 = inputs to the program.

If a more general thrust function is desired, it can be put into the program in tabular form. A modified version of RTSID has been written which evaluates F(t) by linearly interpolating this table. In all other respects the two versions of RTSID are identical. The trapezoid in the above figure used by the modified version by inputting the table given as follows:

t	F(t)
o	o
t_1	p
t_2	p
t_3	o
t_4	o

where t_4 must be at least as large as Nh; N is the number of integration steps of size h.

Damping

The damping functions $b(\dot{x}_2)$ and $c(\dot{x}_1)$ associated respectively with the motor-load cell combination and the concrete block, were expressed in the following form:

$$b_i(\dot{x}_i) = A_i \tanh (B_i \dot{x}_i) + C_i \qquad (i = 1,2) \qquad (137)$$

This expression is versatile in that either a constant damping coefficient, c_i, can be used ($A_i = 0$), or the function can become arbitrarily close to a step function with a discontinuity at $\dot{x}_1 = 0$.

IMPULS

IMPULS is a subroutine type of subprogram which computes the cumulative impulse to time T, mathematically expressed by

$$I(T) = \int_0^T (k \left| x_2(t) - x_1(t) \right| + \alpha \left| x_2(t) - x_1(t) \right|^3) dt \qquad (138)$$

and which also estimates the error incurred, expressed by

$$E(T) = \int_T^\infty (k \left| x_2(t) - x_1(t) \right| + \alpha \left| x_2(t) - x_1(t) \right|^3) dt \qquad (139)$$

where $T \geq t_3$ and k and α are defined by the force-displacement relation

$$f = kx + \alpha x^3 \qquad (140)$$

It should be emphasized that the kind of error identified is the error incurred only by failure to mathematically integrate to infinity to obtain the maximum value of I(t). A mathematical integration inherently compensates for the nonlinear force-displacement characteristic of the system. An electronic integration of an indicated force-time plot, by means of only a voltage-controlled oscillator and a counter, cannot separate the errors incurred by departure from calibration linearity from the errors incurred

by premature termination of integration. Additional information would necessarily have to be supplied with an electronic integration of a system possessing a nonlinear force-displacement characteristic, if accurate measurements of total impulse are to be achieved. Considerable complication of equipment would be involved with the necessary automatic electronic compensation. Hence, all possible effort was made in the system design to obtain a load cell and voltage-controlled oscillator with the highest possible degree of linearity, in order to avoid this type of system complexity. To obtain information regarding the error associated with an electronic integration of a thrust signal obtained from a system exhibiting a nonlinear calibration, the computer program included integrations of the expression for several values of departure from a linear characteristic, specifically:

$$E_1 = \int_0^{\infty} \alpha \left| x_2(t) - x_1(t) \right|^3 dt \qquad (141)$$

in which several values of α are utilized. The practical usefulness of this kind of computation results from a judgment of the allowable error of this type, before a load-cell replacement or system mechanical realignment is required.

Additional remarks are appropriate to the discussion of the "normal" type of error, obtained by termination of the integration.

The integrand of Eq. 138 oscillates about zero, for $t \geq t_3$, with the area of each lobe smaller in magnitude than the preceding one and eventually tending to zero. For this reason $I(T)$ can be treated as a convergent alternating series if the values of the integration limit, T, are required to correspond to zero values of the integrand. The maximum error term of the series is the area $A(T)$ of the next lobe, so that the impulse error (Eq. 139) is related as follows:

$$\left| E(T) \right| \leq \left| A(T) \right| \qquad (142)$$

The output of the IMPULS subprogram is a table of the values of time T, corresponding to the zero values of the integrand, and the corresponding values of $I(T)$, $A(T)$, and $100\ A(T)/I(T)$. The latter value is the percent

of error in the measured total impulse associated with termination of the integration. The trapezoidal rule is used for the integration. Hence, if the step size used is too large, the computed values of A(T) may not be monotomically decreasing in magnitude. However, if the integration in SOLVDE has been stable, the computed values of A(T) will manifest a general decreasing trend.

CRTOUT

According to previous options, determined by input parameters, SOLVDE can call the subroutine CRTOUT to give cathode ray tube displays of the deflection of the load cell and, if desired, of the deflection of the concrete block. Each display is photographed so that the results are preserved on 9-inch by 9-inch photographs. CRTOUT determines the scaling, density of the points, etc., according to input parameters. The points are connected with lines using library tape subprograms.

APPLICATION OF THEORY TO THE ROCKETDYNE SYSTEM

Numerous combinations of design and operational parameters have been processed in the computer program to make a preliminary determination of the accuracy of the measurement of total impulse. The various parameter values used in these determinations represent the best possible estimates, prior to the actual construction and testing of the measurement system, of these variables. The parameter values listed in Case 1A below were regarded as nominal values and most of the computer "runs" for case 1 consisted of varying one of these parameters while holding the others at the nominal values. To conserve computing time, t_3 was held at two seconds for most of the runs because the worst percent errors are associated with the shortest excitation times, other parameters being held constant. Input excitation times of 5 and 10 seconds were also computed with appropriate corresponding values of t_1, t_2, and propellant burning rate (a). The parameter values and associated impulse error results listed in Case 1B are restricted to those of linear (viscous) damping, linear load-cell displacement characteristics, and variable motor mass during excitation. Case 2 contains

values associated with nonlinear system calibrations and nonlinear damping, together with the associated impulse measurement errors.

Case 1: Linear (viscous) damping and linear system calibration

A. Nominal values of parameters (Run No. 1)

M_c = mass of concrete block, 357 slugs (11,500 pounds)

k_c = spring constant of concrete block, 1.02×10^9 lb/ft (50 times stiffer than load cell)

c_1 = constant damping of concrete block, 1.812×10^5 lb sec/ft (damping ratio = 0.175)

c_2 = constant damping of load cell, 1.2×10^3 lb sec/ft

k = spring constant of load cell, 2.04×10^7 lb/ft

m_o = initial mass of motor and mount assembly, 15.55 slugs (500 pounds)

$m_o - at_b$ = terminal mass of motor and mount assembly, 13.35 slugs (430 pounds)

p = amplitude of applied thrust, 10^4 pounds

t_1 = rise time of applied thrust, 0.005 second

t_2 = cutoff of applied thrust, 1.95 seconds

t_3 = total time of applied thrust, 2 seconds

$x(0), \dot{x}(0)$ = initial conditions, 0

The results obtained with the above nominal values of parameters are given in the accompanying plots (Fig. 10 and 11) of load cell and concrete block displacement and in Table 2. An error of only 0.00117% is incurred by terminating the integration concurrently with motor burnout (2 seconds).

B. Other values of parameters (all those not listed were held at the nominal values): all listed errors are those incurred by terminating integration at burnout (2 seconds).

Run No. 2

c_1 = concrete block damping, 1.208×10^5 lb sec/ft (30% less than nominal)

Impulse error (at 2-seconds integration time): -0.00118%

Run No. 3

c_1 = concrete block damping, 2.416×10^5 lb sec/ft (30% more than normal)

Run No. 4

k_c = concrete block spring constant, 6.12×10^7 lb/ft (only 3 times stiffer than load cell)

c_1 = concrete block damping, 4.44×10^4 lb sec/ft (damping ratio = 0.175)

Impulse error (at 2-seconds integration time): -0.00009%

Run No. 5

k_c = concrete block spring constant, 4.08×10^9 lb/ft (200 times stiffer than load cell)

c_1 = concrete block damping, 3.624×10^5 lb sec/ft (damping ratio = 0.175)

Impulse error (at 2-seconds integration time): -0.00108%

Run No. 6

c_2 = load cell damping, 1.029×10^3 lb sec/ft (damping ratio = 0.030)

Impulse error (at 2-seconds integration time): -0.00119%

Run No. 7

c_2 = load cell damping, 1.371×10^3 lb sec/ft (damping ratio = 0.040)

Impulse error (at 2-seconds integration time): -0.00115%

Run No. 8

k = load cell spring constant, 1.8×10^7 lb/ft

c_2 = load cell damping, 1.125×10^3 lb sec/ft (damping ratio = 0.035)

Impulse error (at 2-seconds integration time): -0.00117%

Run No. 9

p = amplitude of applied thrust, 1500 pounds

Impulse error (at 2-seconds integration time): -0.00117%

Run No. 10

t_1 = rise time of applied thrust, 0.025 seconds

t_2 = cutoff of applied thrust, 4.925 seconds

t_3 = total time of applied thrust, 5.000 seconds

a = propellant burning rate, 0.4467 slugs/sec

Impulse error (at 5-seconds integration time): 0.00031%

Run No. 11

t_1 = rise time of applied thrust, 0.050 seconds

t_2 = cutoff time of applied thrust, 9.90 seconds

t_3 = total time of applied thrust, 10.00 seconds

a = propellant burning rate, 0.2222 slugs/sec

Impulse error (at 10-seconds integration time): -0.00006%

Case 2: Nonlinear damping and/or nonlinear system calibration

Run No. 12 (nonlinear load cell damping)

A_2 = maximum change in load cell damping, 342.9 lb sec/ft

B_2 = rapidity of change in load cell damping, 10^{29} sec/ft (damping ratio is 0.035 ±0.010)

Impulse error (at 2-seconds integration time):, -0.0011%

Run No. 13 (nonlinear force-displacement relation)

Nonlinearity coefficient, -7.5×10^{10} lb/ cu ft

Impulse error (at 2-seconds integration time): -0.088%
(error caused by using linear calibration)

Run No. 14 (nonlinear force-displacement equation)

Nonlinear coefficient, -15×10^{12} lb/cu ft

Impulse error (at 2-seconds integration time): -1.82%
(error caused by using linear calibration)

Run No. 15 (both damping and force-displacement, nonlinear)

A_2 and B_2 same as in Run No. 12

Same as Run No. 14

Impulse error same as in Run No. 14

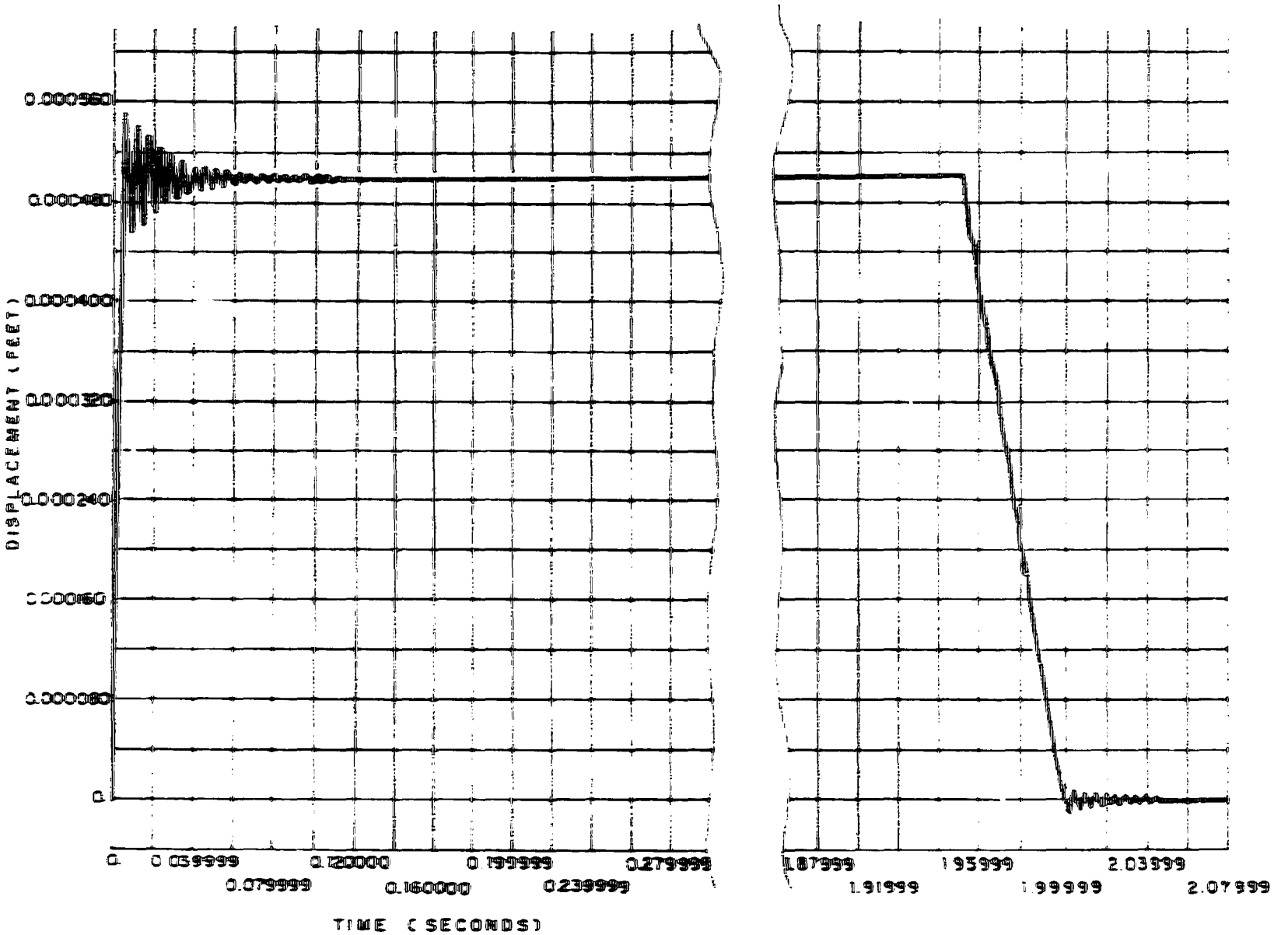

Figure 10. Load Cell Response (Case 1A)

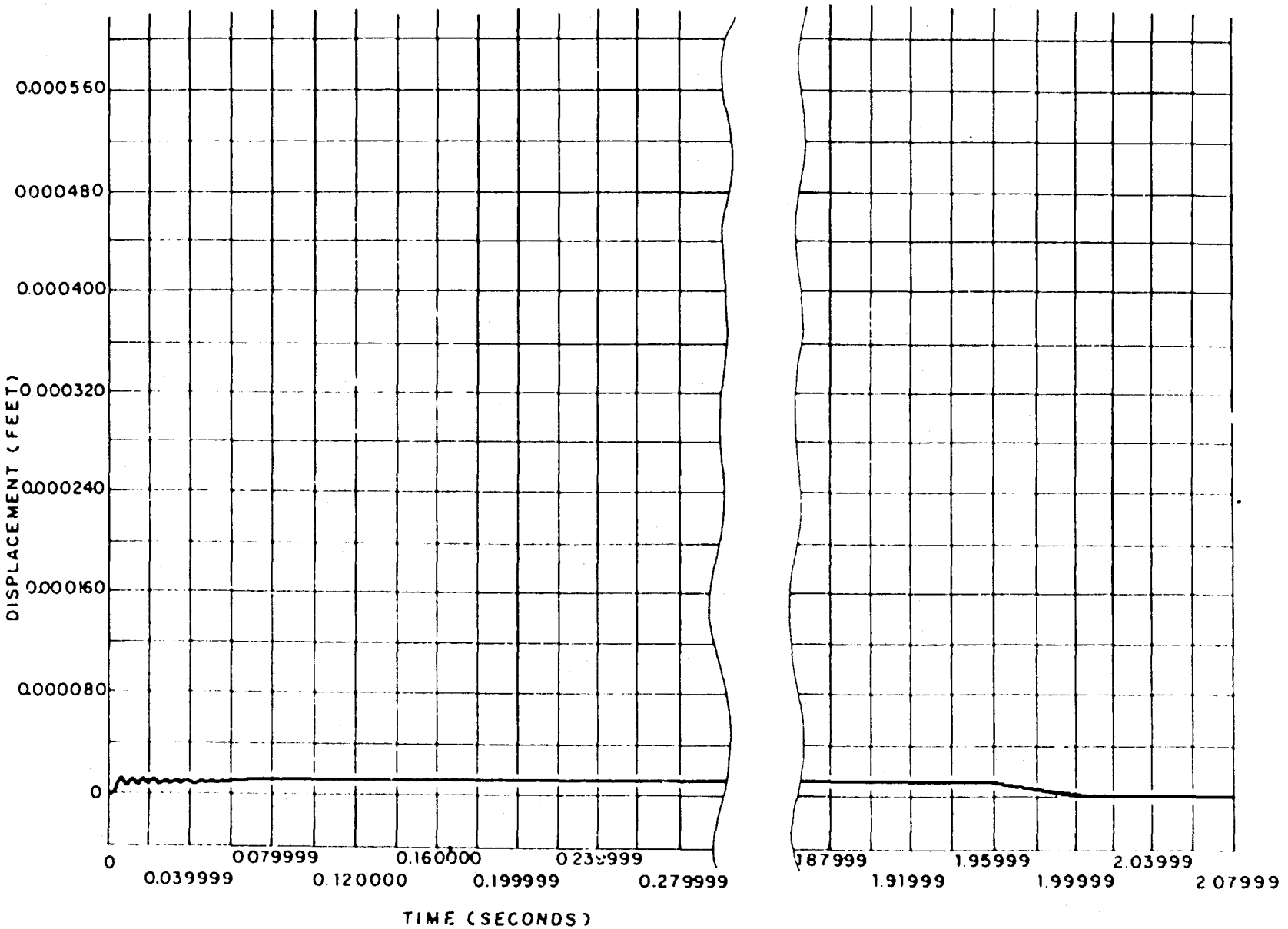

Figure 11. Abutment Response (Case 1A)

TABLE 2

TOTAL IMPULSE MEASUREMENT DATA

(CASE 1A: NOMINAL)

Integration Time, seconds	Cumulative Impulse, lb sec	Error, lb sec	Error, %
2.0000	19725.2	-0.23	-0.00117
2.0025	19725.0	0.20	0.00103
2.0050	19725.2	-0.18	-0.00090
2.0075	19725.0	0.15	0.00078
2.0100	19725.2	-0.13	-0.00067
2.0125	19725.0	0.13	0.00064
2.0155	19725.2	-0.10	-0.00051
2.0180	19725.1	0.089	0.00045
2.0205	19725.2	-0.078	-0.00039
2.0230	19725.1	0.067	0.00034
2.0255	19725.1	-0.063	-0.00032
2.0285	19725.1	0.050	0.00026
2.0310	19725.1	-0.045	-0.00023
2.0335	19725.1	0.039	0.00020
2.0360	19725.1	-0.034	-0.00017
2.0385	19725.1	0.032	0.00016
2.0415	19725.1	-0.025	-0.00013
2.0440	19725.1	0.022	0.00011
2.0465	19725.1	-0.020	-0.00010
2.0490	19725.1	0.017	0.00009
2.0515	19725.1	-0.015	-0.00007
2.0540	19725.1	0.014	0.00007
2.0570	19725.1	-0.011	-0.00006
2.0595	19725.1	.0098	0.00005
2.0620	19725.1	--.0086	-0.00004
2.0645	19725.1	.0074	0.00004
2.0670	19725.1	- .0070	-0.00004
2.0700	19725.1	.0055	0.00003
2.0725	19725.1	- .0049	-0.00002
2.0750	19725.1	.0043	0.00002

TABLE 2

(Continued)

Integration Time, seconds	Cumulative Impulse, lb sec	Error, lb sec	Error, %
2.0775	19725.1	-.0037	-0.00002
2.0800	19725.1	.0032	0.00002
2.0825	19725.1	-.0030	-0.00002
2.0855	19725.1	.0025	0.00001
2.0880	19725.1	-.0022	-0.00001
2.0905	19725.1	.0019	0.00001
2.0930	19725.1	-.0016	-0.00001
2.0955	19725.1	.0015	0.00001
2.0985	19725.1	-.0012	-0.00001
2.1010	19725.1	.0011	0.00001
2.1035	19725.1	-.0095	-0.00000
2.1060	19725.1	-.0082	0.00000
2.1085	19725.1	-.0077	-0.00000

THEORY AND APPLICATION OF PARALLELOGRAM COMPRESSION-TYPE FLEXURE SUSPENSION SYSTEMS

INTRODUCTION

Analysis of compression-type flexure suspension systems was made primarily for design clarification purposes so that a suitable suspension system could be provided for the BATES motor in the Rocketdyne-designed test stand. The need for such analysis was established by the dual design objectives of high system dynamic response to transient thrust forces, and a high degree of linearity in the measurement system indications of static forces. These two objectives resulted in the proposed use of a load cell having no compliant in-line flexures or ball joints with a motor suspension system whose operational deflections resulted in suitably small load cell bending stresses. The objectives were accomplished through the use of a flexure system whose static translational and rotational stiffnesses were suitably related to those of the load cell. The design criterion was based on the load cell electrical response to the bending moments imposed on it by mechanical system distortions resulting from motor thrusts and weight changes, calibration forces, and thermal expansions. Accordingly, mathematical expressions of the flexure system translational and rotational stiffnesses as functions of flexure component and system dimensions were derived. The complementary stiffnesses of the proposed load cell and its associated electrical responses were obtained from its designer, the Baldwin-Lima-Hamilton Corporation. The load cell-flexure system combination was then examined to determine the flexure system dimensions which produced a force and moment distribution yielding the necessary low level of load cell bending moment associated with the needed low level of measurement error. The results of this process consequently yielded the proposed flexure system design, and the steps in this process will now be discussed.

DERIVATION OF FLEXURE SYSTEM STIFFNESS EQUATIONS

With reference to the figure below and Fig. 12, the following equation in which E = Young's modulus and δ = deflection, have been developed for a flexure-strut combination.

Vertical Stiffness

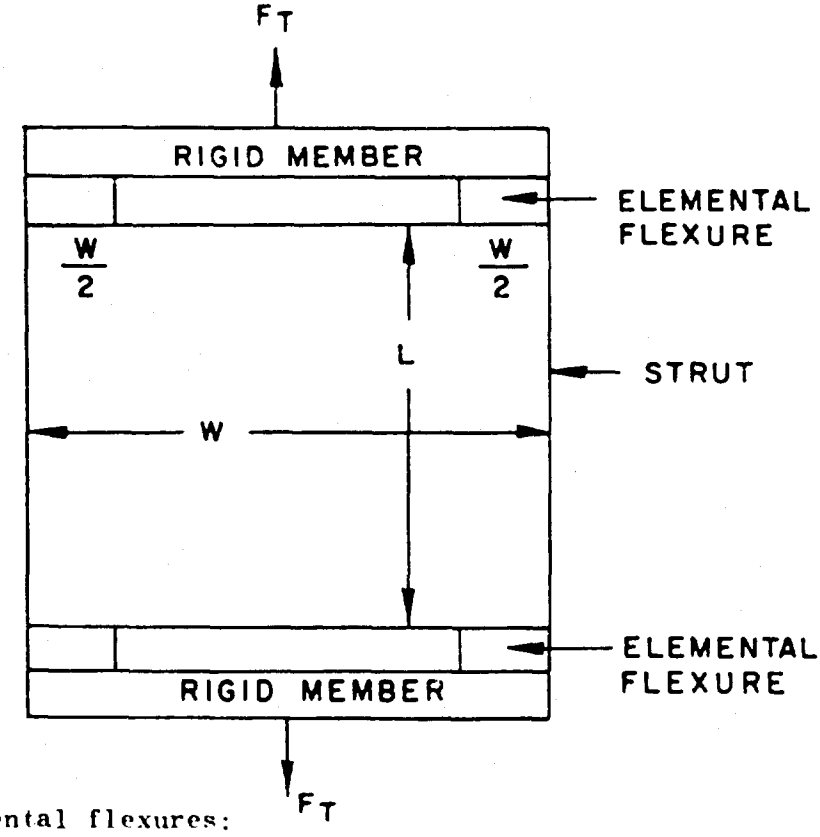

1. Each pair of elemental flexures:

$$E = \frac{F_{T/A}}{\delta'_v/\ell_1} = \frac{F_{T/wt}}{\delta'_v/\ell_1} = \frac{F_T\ \ell_1}{\delta'_v\ wt}$$

Vertical deflection:

$$\delta'_v = \frac{F_T\ \ell_1}{E\ wt}$$

2. Strut:

$$E = \frac{F_{T/A}}{\delta''_v\ /\ L} = \frac{F_{T/WT}}{\delta''_v\ /L} = \frac{F_T\ L}{\delta''_v\ WT}$$

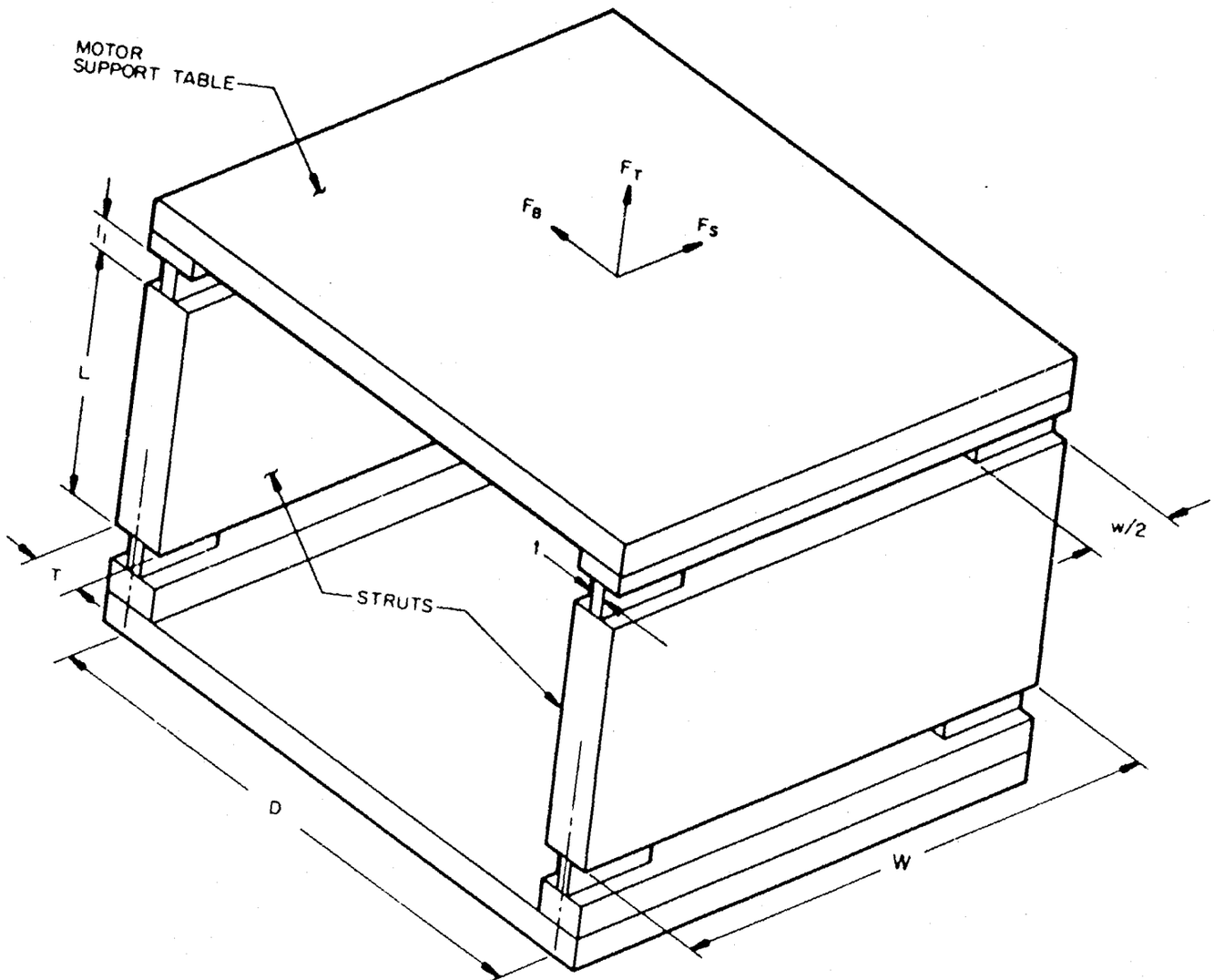

Figure 12. Parallelogram Compression-Type Motor Suspension Flexure System

Vertical Deflection

$$\delta'_v = \frac{F_T L}{E\,WT}$$

3. Total vertical deflection of a flexure-strut combination:

$$\delta_v = 2\,\delta'_v + \delta'_v = \frac{2F_T\,\ell_1}{E\,wt} + \frac{F_T L}{E\,WT}$$

$$\delta_v = \frac{F_T}{E}\left(\frac{2\,\ell_1}{wt} + \frac{L}{WT}\right) \tag{143}$$

Therefore, the vertical stiffness of the combination is:

$$k'_v = \frac{F_T}{\delta_v} = \frac{E}{\frac{2\,\ell_1}{wt} + \frac{L}{WT}} \tag{144}$$

Because two flexure-strut combinations are incorporated in the parallelogram suspension system, the vertical stiffness of the flexure system is:

$$k_v = \frac{2E}{\frac{2\,\ell_1}{wt} + \frac{L}{WT}} \tag{145}$$

Horizontal Longitudinal Stiffness

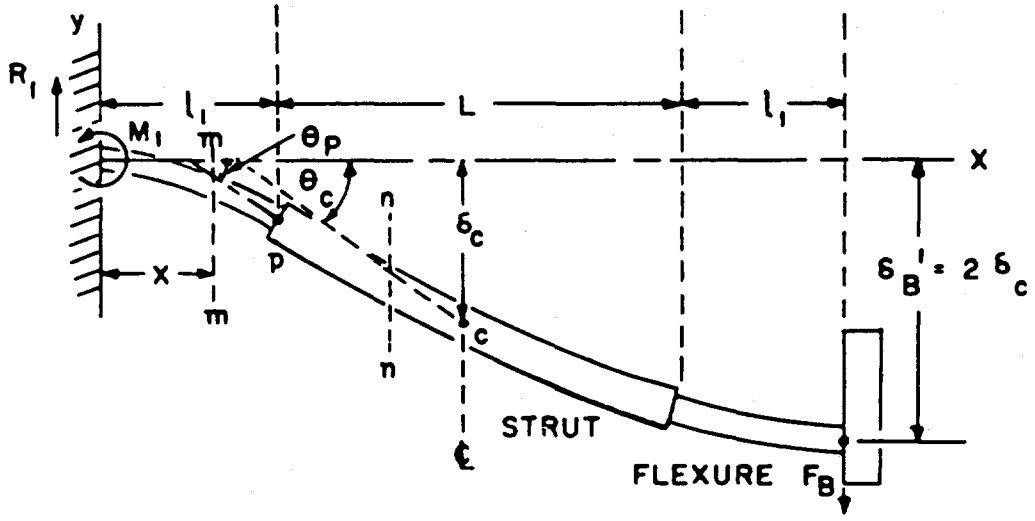

In the case of a composite beam constructed of two relatively short, rather thick, flexure sections separated by a long, thicker strut, all junctions of the sections are builtin and the displacement of the movable support is considered to be translation only (no rotation). The curvature of the entire flexure-strut combination is therefore symmetrical about a line through the center inflection point C, parallel to the planes of the two supports. Consequently, the displacement of the movable support, associated with the bending force F_B, is twice that of the center point C. Considering only bending of the flexures, the vertical reaction at the fixed support is $R_1 = F_B$ and the couple exerted by the wall is $M_1 = -F_B (L + 2\ell_1)$. The bending moment at any cross section mm of the flexure adjacent to the fixed end is $M = M_1 + Rx$. Using the well-known differential equation of the deflection curve of a bent beam,

$$EI_1 \frac{d^2y}{dx^2} = M \tag{146}$$

there is obtained, by substitution for M:

$$EI_1 \frac{d^2y}{dx^2} = -F_B (L + 2\ell_1) + F_B x \tag{147}$$

where I_1 is the moment of inertia of the flexure section about a horizontal transverse axis through its section. A first integration gives the slope equation for the flexure section:

$$EI_1 \frac{dy}{dx} = -F_B (L + 2\ell_1) x + F_B \quad 2 \quad 1 \tag{148}$$

and because $dy/dx = o$ at $x = o$, it follows that $C_1 = o$. A second integration gives the bending deflection equation for the flexure section:

$$EI_1 \; y = -F_B (L + 2\ell_1) \frac{x^2}{2} + F_B \frac{x^3}{6} + C_2 \tag{149}$$

and because $y = o$ at $x = o$, it follows that $C_2 = o$. The slope and deflection of the bent flexure section at the junction point P at the end of the strut are found from the above equations by substituting $x = \ell_1$. Because for small angles $\tan \theta \approx \theta$, it follows that

slope

$$\theta'_p = \left(\frac{dy}{dx}\right)_p = \frac{-F_B\left(L\ell_1 + \frac{3}{2}\ell_1^2\right)}{EI_1}$$

deflection

$$\delta'_p = \frac{-F_B\left(L\ell_1^2 + \frac{5}{6}\ell_1^3\right)}{EI_1} \qquad (150)$$

However, for beams whose thickness is an appreciable fraction (> 1/10) of the length, a substantial additional deflection is produced by shear. At the point P, the slope and deflection due to shear alone are:

$$\theta''_p = -\frac{k\,F_B}{AE_s}$$

$$\delta''_p = -\frac{k\,F_B\,\ell_1}{AE_s} \qquad (151)$$

where

A = cross-sectional area of flexure

E_s = shear modulus

k = numerical factor (3/2 for rectangular section)

Consequently, the total slope and deflection of the flexure at point P due both to bending and shear is:

slope

$$\theta_p = \theta'_p + \theta''_p$$

$$\theta_p = -F_B\left(\frac{L\,\ell_1 + \frac{3}{2}\ell_1^2}{EI_1} + \frac{k}{AE_s}\right)$$

deflection

$$\delta_p = \delta'_p + \delta''_p$$

$$\delta_p = -F_B \left(\frac{L\,\ell_1^2 + \frac{5}{6}\ell_1^3}{EI_1} + \frac{k\,\ell_1}{AE_s} \right) \qquad (152)$$

The deflection of the strut in bending is obtained in similar manner. The vertical reaction at the end of the strut (point P) is $R_2 = F_B$ and the couple exerted by the flexure is $M_2 = -F_B\,(L + \ell_1)$. The bending moment at any cross section nn to the left of the center point C is $M = M_2 + R_2 x$, where x is now the distance of section nn from the end point P. Again, using the differential equation

$$EI_2 \frac{d^2y}{dx^2} = M \qquad (153)$$

there is obtained, by substitution for M:

$$EI_2 \frac{d^2y}{dx^2} = -F_B\,(L + \ell_1) + F_B\,x \qquad (154)$$

where I_2 = the moment of inertia of the strut section about a horizontal transverse axis through its centroid. A first integration gives the slope equation for the strut section:

$$EI_2 \frac{dy}{dx} = -F_B\,(L + \ell_1)\,x + F_B \frac{x^2}{2} + C_1$$

and because

$\frac{dy}{dx} = \theta_p$ at x = o, it follows that

$$C_1 = -F_B \left[\frac{I_2}{I_1} \left(L\,\ell_1 + \frac{3}{2}\ell_1^2 \right) + \frac{k\,EI_2}{AE_s} \right] \qquad (155)$$

and therefore:

$$EI_2 \frac{dy}{dx} = -F_B (L + \ell_1) x + F_B \frac{x^2}{2} - F_B \left[\frac{I_2}{I_1} (L \ell_1 + \frac{3}{2} \ell_1^2) + \frac{k EI_2}{AE_s} \right] \quad (156)$$

A second integration gives the deflection equation for the strut section:

$$EI_2 y = -F_B (L + \ell_1) \frac{x^2}{2} + F_B \frac{x^3}{6} - F_B \left[\frac{I_2}{I_1} (L \ell_1 + \frac{3}{2} \ell_1^2) + \frac{k EI_2}{AE_s} \right] x + C_2$$

and because $y = \delta_p$ at $x = o$, it follows that

$$C_2 = -F_B \left[\frac{I_2}{I_1} (L \ell_1^2 + \frac{5}{6} \ell_1^3) + \frac{k EI_2 \ell_1}{AE_s} \right] \quad (157)$$

and therefore:

$$EI_2 y = -F_B (L+\ell_1) \frac{x^2}{2} + F_B \frac{x^3}{6} - F_B \frac{I_2}{I_1} (L\ell_1 + \frac{3}{2} \ell_1^2) x - F_B \left[\frac{I_2}{I_1} (L\ell_1^2 + \frac{5}{6} \ell_1^3) + \frac{k EI_2 \ell_1}{AE_s} \right] \quad (158)$$

Because the strut thickness-to-length ratio is small ($< 1/20$), deflection due to shear is negligible and the deflection of the bent flexure-strut combination at the center point C is found from the above equation by substituting $x = \frac{L}{2}$. The result is:

$$\delta_c = \frac{-F_B \left[\frac{5}{48} L^3 + \frac{L^2 \ell_1}{8} + \frac{I_2}{I_1} \left(\frac{L^2 \ell_1}{2} + \frac{7}{4} L\ell_1^2 + \frac{5}{6} \ell_1^3 \right) + \frac{k EI_2 \ell_1}{AE_s} \right]}{EI_2} \quad (159)$$

The total deflection, δ'_B, of the flexure-strut combination in the horizontal longitudinal direction, is, by symmetry considerations, twice that of point C, and the stiffness of the combination is, numerically:

$$k'_L = \frac{F_B}{\delta'_B} = \frac{EI_2}{\frac{5}{24}L^3 + \frac{L^2 \ell_1}{4} + \frac{I_2}{I_1}\left(L^2 \ell_1 + \frac{7}{2} L \ell_1^2 + \frac{5}{3}\ell_1^3\right) + \frac{2k\, EI_2\, \ell_1}{AE_s}} \tag{160}$$

Because two flexure-strut combinations are incorporated in the parallelogram suspension system, the horizontal longitudinal stiffness of the flexure system is given as follows, where

$$I_1 = \frac{wt^3}{12}, \quad I_2 = \frac{WT^3}{12}, \quad A = wt, \text{ and } k = \frac{3}{2}$$

have been substituted:

$$k_L = \frac{2\, EWT^3}{\frac{5}{2}L^3 + 3L^2 \ell_1 + 12 \frac{WT^3}{wt^3}\left[L^2 \ell_1 + \frac{7}{2} L \ell_1^2 + \frac{5}{3}\ell_1^3\right] + \frac{3\, EWT^3\, \ell_1}{E_s\, wt}} \tag{161}$$

Horizontal Transverse Stiffness

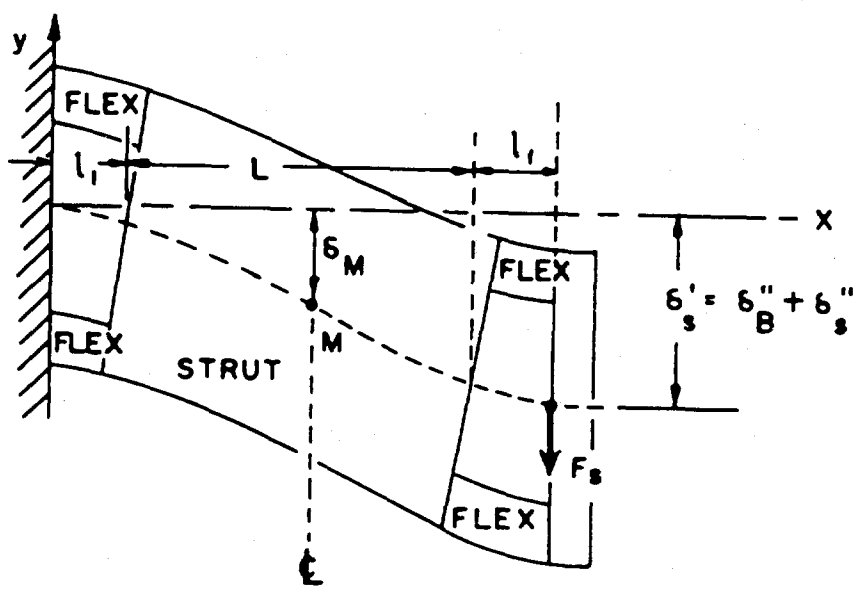

In the case of a beam which has a large thickness at all parts compared to its length, so that the deflection is due both to bending and to shearing, the composite beam consists of relatively short, deep flexures separated by a long, deep strut. All junctions are builtin and the displacement of the movable support is again considered to be one of translation (no rotation). The curvature of the whole flexure-strut combination is therefore symmetrical about a line through the center inflection point M, parallel to the planes of the two supports. The deflection of the flexure-strut combination is due in part to bending, δ''_B , and in part to shear, δ''_S , of both the flexures and the strut. The deflection due to bending can be stated by using the expressions already obtained, with regard to the proper expressions for the moments of inertia I_1 and I_2 which are now

$$I_1 = \frac{1}{2} tw^3$$

$$I_2 = \frac{1}{12} TW^3 \qquad (162)$$

and the expression for the total deflection of a flexure-strut combination due to bending alone:

$$\delta''_B = \frac{-F_S \left[\frac{5}{2} L^3 + 3L^2 \ell_1 + 12 \frac{TW^3}{tw^3} \left(L^2 \ell_1 + \frac{7}{2} L\ell_1^2 + \frac{5}{3} \ell_1^3 \right) \right]}{ETW^3} \qquad (163)$$

The deflection of the flexure-strut combination due to shear is obtained by the use of the expression $dy_1/dx = kF_s/AE_s$ with both the flexures and the strut where:

$\frac{dy_1}{dx}$ = slope of the shear deflection curve of the section considered.

k = numerical factor by which the average shearing stress must be multiplied in order to obtain the shearing stress at the centroid of the cross section. (k = 3/2 for a rectangular section)

F_s = shearing force

A = cross-sectional area of the section considered

E_s = shear modulus of the material

For a single flexure,

$$\left(\frac{dy_1}{dx}\right)_f = \frac{\delta_{s1}}{\ell_1} = -\frac{\frac{3}{2} F_s}{wt\, E_s} \tag{164}$$

and for the strut,

$$\left(\frac{dy_1}{dx}\right)_s = \frac{\delta_{s2}}{L} = -\frac{\frac{3}{2} F_s}{WTE_s} \tag{165}$$

Therefore, for the two-flexure-strut combination, the total deflection due to shear is:

$$\delta_s'' = 2\,\delta_{s1} + \delta_{s2} = -\frac{\frac{3}{2} F_s\, \ell_1}{wt\, E_s} - \frac{\frac{3}{2} F_s\, L}{WTE_s}$$

$$\delta_s'' = -\frac{3F_s}{2\,E_s}\left(\frac{\ell_1}{wt} + \frac{L}{WT}\right) \tag{166}$$

Thus, the total deflection of the combination, due to both bending and shear, is:

$$\delta_s' = \delta_B'' + \delta_s''$$

$$= -F_s \left[\frac{\frac{5}{2} L^3 + 3L^2 \ell_1 + 12 \frac{Tw^3}{tw^3}\left(L^2 \ell_1 + \frac{7}{2} L\ell_1^2 + \frac{5}{3}\ell_1^3\right)}{ETw^3} + \frac{3}{2\,E_s}\left(\frac{\ell_1}{wt} + \frac{L}{WT}\right) \right] \tag{167}$$

Because two flexure-strut combinations are incorporated in the parallelogram suspension system, the horizontal transverse stiffness of the system is:

$$k_T = \frac{2F_s}{\delta_s'} = \frac{2ETW^3}{\frac{5}{2}L^3 + 3L^2\ell_1 + 12\frac{TW^3}{tw^3}\left(L^2\ell_1 + \frac{7}{2}L\ell_1^2 + \frac{5}{3}\ell_1^3\right) + \frac{3ETW^3}{2E_s}\left(\frac{\ell_1}{wt} + \frac{L}{WT}\right)} \tag{168}$$

Rotational Stiffness About Horizontal Transverse Axis

Rotational moments about a horizontal transverse axis displace the flexure system in tension and compression, and because two flexure-strut combinations are equally stressed in opposite directions, the suspension system stiffness expression is:

$$\tau_T = \frac{F_T D}{\delta_v/\frac{D}{2}} = \frac{F_T D^2}{2\delta_v} = \frac{D^2}{2} k_v'$$

$$\tau_T = \frac{D^2 E}{2\left(\frac{2\ell_1}{wt} + \frac{L}{WT}\right)} \tag{169}$$

Rotational Stiffness About Vertical Axis

A transverse couple about a vertical axis displaces the flexure system in shear-bending, and because two flexure-strut combinations are equally stressed in opposite directions, the suspension system stiffness expression is:

$$\tau_v = \frac{F_s D}{\delta_s/\frac{D}{2}} = \frac{F_s D^2}{2\delta_s} = \frac{D^2}{2} k_T' \tag{170}$$

$$\tau_v = \frac{D^2 ETW^3}{5L^3 + 6L^2\ell_1 + 24\frac{TW^3}{tw^3}\left(L^2\ell_1 + \frac{7}{2}L\ell_1^2 + \frac{5}{3}\ell_1^3\right) + \frac{3ETW^3}{E_s}\left(\frac{\ell_1}{wt} + \frac{L}{WT}\right)}$$

(170 Continued)

Rotational Stiffness About Horizontal Longitudinal Axis

This stiffness expression was not developed because moments about this axis are not expected to be encountered in appreciable amounts, and also because the load cell response to torsional moments is negligible.

The flexure system stiffnesses, expressed by the preceding equations, are related to the corresponding load cell stiffnesses by the design requirements based on measurement errors. The complementary B-L-H proposed load cell stiffnesses are given below:

1. Axial stiffness: $k_L' = 1.67 \times 10^6$ lb in.
2. Transverse stiffnesses: $k_v' = k_T' = 10^6$ lb in.
3. Rotational stiffnesses: $\tau_T' = \tau_L' = \tau_v' = 25 \times 10^9$ lb in./rad

The electrical responses of the load cell to transverse loads and bending moments are as follows:

1. A 500-pound transverse load, or a moment of 2500 lb/in., causes a maximum sensitivity change of 0.15% of full scale.
2. Cell responses to torsional (twisting) moments are negligible.

DETERMINATION OF FLEXURE SYSTEM STIFFNESS REQUIREMENTS

The design of the flexure system is largely determined by the anticipated degree of departure from a perfect thrust calibration and measurement system. An ideal system is one in which no-error calibration forces are

imposed exactly on the axis of a noncompliant force-measuring transducer which responds only to axial forces, connected to a suspension system in which the motor thrust axis is perfectly aligned with the ideal transducer. With such a system no errors would result from misaligned calibration links or motor thrust axis, and the load-measuring transducer would identically indicate equal calibration and thrust forces. The linearity of the transducer calibration would be solely dependent upon the transducer linearity itself. However, actual calibration and measurement systems employed for rocket motor thrust determinations must necessarily depart somewhat from the ideal system described, and the purpose of this discussion is to identify the nature of the departures and quantitatively describe their effects upon the calibration and measurement system accuracies.

Identification of Causes of Bending Moments

It should be stated, first, that an accurate employment of a load cell is obtained by merely imposing identical load conditions upon it during calibrations and measurements. With only an accuracy requirement, the presence or absence of transverse forces, along with couple bending and/or twisting moments on the load cell is not material, provided that the transducer loading conditions are duplicated in the calibration and operation of the measurement system. However, the calibrations of such systems are, in general, nonlinear. Accuracy plus linearity in the calibration and use of a system requires considerably more attention to system design detail. All direct-reading electromechanical transducers require axial compliance in some degree for their operation, and they are sensitive in some degree to transverse loads and couple bending moments. The cause of such loads and couple moments is not only fabrication and assembly tolerances, but also operational variables such as shifting motor thrust axes, decreasing motor weight (burning solid propellant) and differential thermal expansions. Because these loads and moments result in calibration nonlinearities and measurement

errors, it is useful to list and quantitatively discuss their sources as follows:

1. Bending moment produced by flexure system axial stiffness
2. Constructionally misaligned calibration and/or motor thrust forces
    a. Horizontally and or vertically offset forces parallel to load cell axis
    b. Forces angularly inclined to load cell axis in the horizontal and/or vertical planes
3. Motor test and environmental conditions
    a. Decreasing motor weight (burning propellant)
    b. Shifting motor thrust axis (unusual propellant combustion)
    c. Vertical and/or horizontal differential thermal expansions

Ten or more sources of load cell bending moment have been identified, and it is useful to regard them as equally probable. As already stated, 2500 lb in. of bending moment on the load cell produces a possible 0.15% change in load cell sensitivity. Load cell sensitivity changes are directly related to calibration and measurement nonlinearities and, therefore, measurement errors. Because it is desirable to limit the total possible error, due to load cell nonlinearities, to values of 0.01% or less, it is appropriate to require that the maximum transverse load and the maximum amount of bending moment necessarily supplied by the load cell with each single source be limited to 10 pounds and 50 lb in. respectively. In the following discussion, the individual sources are examined and the flexure system stiffness requirements are determined on the basis of these limitations.

Flexure System Stiffness Requirements

Flexure system stiffness requirements will be determined on the basis of errors produced by the most unfavorable circumstances of system

construction and operation. Considering first the forces and moments which can occur in a vertical plane containing the load cell and motor axis, in the figure below, the concrete abutment is considered fixed, and the initial motor weight is simply supported on the flexure system beneath with no associated restraining forces or moments supplied by the load cell. If a weight W' is subtracted from the original weight, the changes in flexure force are F_1 and F_2 respectively and the associated transverse load and pure moment supplied by the load cell are R and M, respectively.

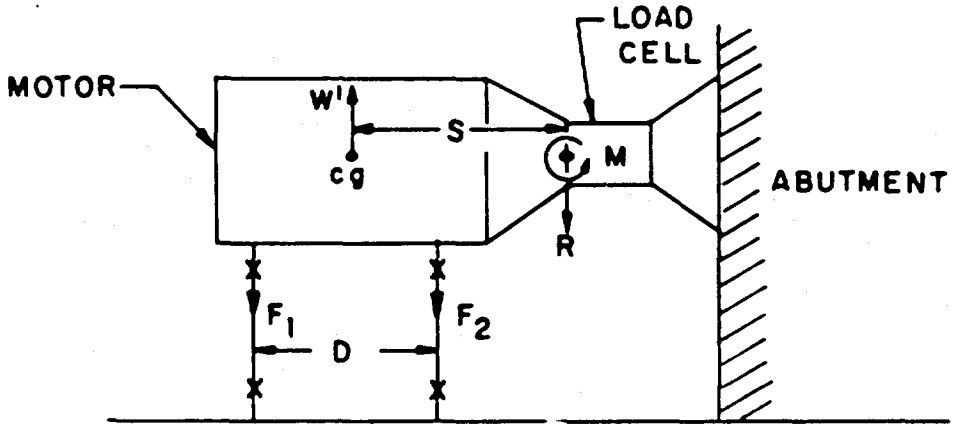

At equilibrium,

$$W' = F_1 + F_2 + R$$

$$RS = (F_1 - F_2)\, D/2 + M \qquad (171)$$

A 70-pound weight change due to burned propellant should be considered, letting S = 24 inches and D = 30 inches. Because both a transverse load and pure moment are supplied by the load cell with this single source, the maximum permissible values of R and M should be 10 pounds and 50 lb in., respectively.

Then:

$$70 = F_1 + F_2 + 10$$

$$240 = (F_1 - F_2)\, D/2 + 50 \qquad (172)$$

Therefore, $F_1 + F_2 = 60$ and the flexure system vertical stiffness is seen to be about six times the load cell transverse stiffness. In the same manner, $(F_1 - F_2)\ D/2 = 190$ and the flexure system rotational stiffness about a horizontal transverse axis is seen to be about four times the load cell bending stiffness.

In the next case, (below), a perfectly aligned 10,000-pound calibrating force compressing the load cell and deflecting the motor flexure suspension system in the thrust direction is considered. Denoting by f the backward force exerted by the flexure system, it is seen that $fh = M = 100$ and for h = 15 inches and M = 100 lb in., $f \doteq 6$ pounds. Therefore, the axial stiffness of the load cell should be at least 1700 times the flexure system horizontal longitudinal stiffness.

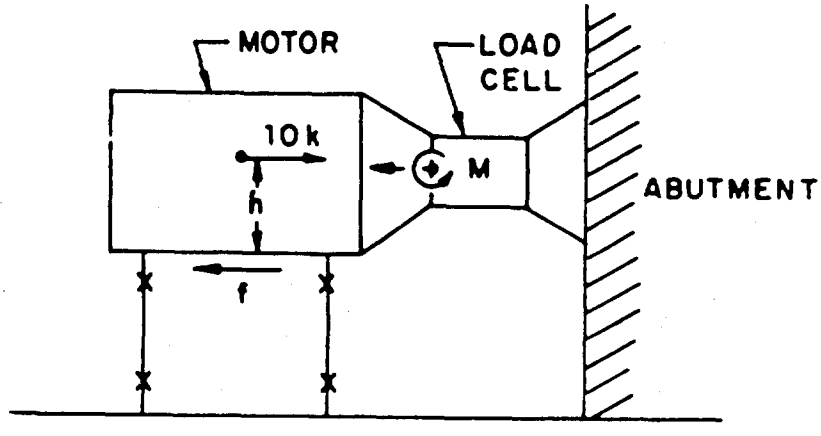

Next, a motor thrust force of 10,000 pounds vertically displaced a distance d from the load cell axis is considered (below):

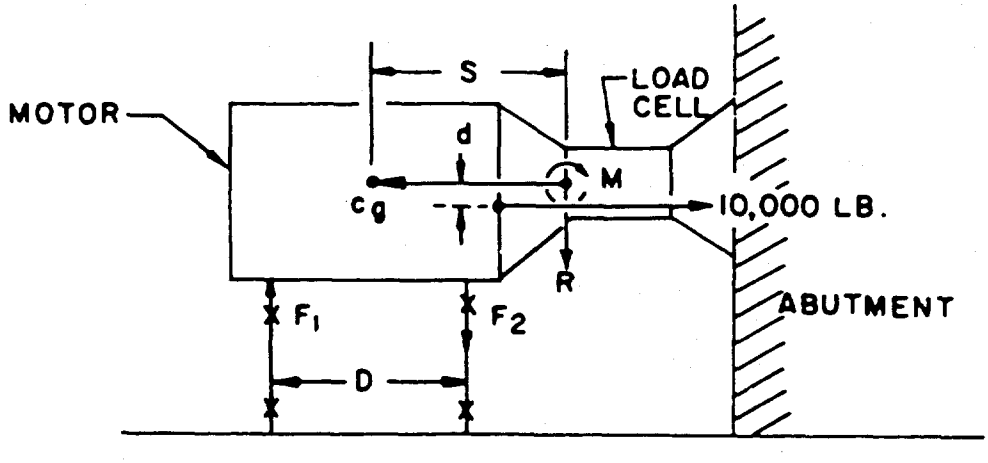

At equilibrium:

$$F_1 - F_2 = R \tag{173}$$

and the moment equation about cg is:

$$10{,}000\ d = (F_1 + F_2)\ D/2 + M + RS \tag{174}$$

Assuming that d = 1/4 inch (abnormally large misalignment) and S = 24 inches,

$$2500 = (F_1 + F_2)\ D/2 + M + 24\ R \tag{175}$$

So that the transverse force R and the bending moment M supplied by the load cell are 10 pounds and 50 lb in., respectively, the flexure system rotational stiffness about a horizontal transverse axis should be 44 times stiffer than the load cell bending stiffness, and the flexure system vertical stiffness should be 15 times the load cell transverse stiffness. By consideration of a 1/4-inch, horizontally displaced, 10,000-pound-thrust force, the same conclusions can be reached regarding the flexure system rotational stiffness about a vertical axis and the transverse longitudinal stiffness.

On the basis of the foregoing considerations of possible misalignments that can occur in motor test operations, the following design criteria are given for the flexure system stiffnesses:

1. Vertical stiffness: about 15 times the load cell transverse stiffness (same for horizontal transverse stiffness)
2. Horizontal longitudinal stiffness: about 1/1700 of the load cell axial stiffness
3. Rotational stiffness about a horizontal transverse axis: about 45 times the load cell bending stiffness (same for rotational stiffness about a vertical axis for transverse couples)

APPLICATION OF THEORY

Flexure System Design

The application of the foregoing flexure system design criteria was made to the Rocketdyne design of a test stand using the BATES motor for propellant studies. The practical use of the flexure stiffness expressions suggests that suitable allowances be made for fabrication equipment limitations. Accordingly, it was reasonable to inquire if flexure dimensions that were reasonable from geometrical and machining standpoints were adequate to provide the desired flexure system stiffnesses. Therefore, a determination of flexure stiffnesses was made on the basis of the following dimensions:

1. Flexure component dimensions, inches:

   $\ell_1 = 1/2$

   $w = 16$

   $t = 1/8$

2. Strut dimensions and spacing, inches:

   $L = 13$

   $W = 16$

   $T = 1/4$

   $D = 30$

3. Material: steel, $E = 30 \times 10^6$ psi and $E_s = 12 \times 10^6$ psi

The flexure system stiffnesses, along with the ratios of flexure system to load cell stiffness that were obtained are listed below:

Vertical Stiffness.

$$k_v = \frac{2E}{\frac{2\ell_1}{wt} + \frac{L}{WT}} = 13.3 \times 10^6 \text{ lb/in.}$$

$$\text{Ratio: } \frac{k_v}{k_v'} = 13.3 \tag{176}$$

Horizontal Longitudinal Stiffness.

$$k_L = \frac{2EWT^3}{\frac{5}{2}L^3 + 3L^2\ell_1 + 12\frac{WT^3}{wt^3}\left(L^2\ell_1 + \frac{7}{2}L\ell_1^2 + \frac{5}{3}\ell_1^3\right) + \frac{3EWT^3\ell_1}{E_s wt}}$$

$$k_L = 1000 \text{ lb/in.}$$

$$\text{Ratio: } \frac{k_L}{k_L'} = \frac{1}{1670} \tag{177}$$

Rotational Stiffness About a Horizontal Transverse Axis.

$$\tau_T = \frac{D^2E}{2\left(\frac{2\ell_1}{wt} + \frac{L}{WT}\right)}$$

$$\tau_T = 3 \times 10^9 \text{ lb in./rad}$$

$$\text{Ratio: } \frac{\tau_T}{\tau_T'} = 120 \tag{178}$$

Rotational Stiffness About a Vertical Axis.

$$\tau_v = \frac{D^2ETW^3}{5L^3 + 6L^2\ell_1 + 24\frac{TW^3}{tw^3}\left(L^2\ell_1 + \frac{7}{2}L\ell_1^2 + \frac{5}{3}\ell_1^3\right) + \frac{3ETW^3}{E_s}\left(\frac{\ell_1}{wt} + \frac{L}{WT}\right)}$$

$$\tau_v = 6.4 \times 10^8 \text{ lb in./rad}$$

$$\text{Ratio: } \frac{\tau_v}{\tau_{v'}} = 25.6 \qquad (179)$$

Horizontal Transverse Stiffness.

$$k_T = \frac{2ETW^3}{\frac{5}{2}L^3 + 3L^2\ell_1 + 12\frac{TW^3}{tw^3}\left(L^2\ell_1 + \frac{7}{2}L\ell_1^2 + \frac{5}{3}\ell_1^3\right) + \frac{3ETW^3}{2E_s}\left(\frac{\ell_1}{wt} + \frac{L}{WT}\right)}$$

$$k_T \doteq 3 \times 10^6 \text{ lb/in.}$$

$$\text{Ratio: } \frac{k_T}{k_{T'}} \doteq 3 \qquad (180)$$

Although this last ratio is only 3, compared to the requirement of 15, it is considered adequate in view of the magnitude (1/4 inch) of the assumed thrust misalignment.

Because the obtained ratios of flexure system stiffness to load cell stiffness compare very favorably with the desired ratios, determined on the basis of measurement errors, the stated flexure dimensions are used in the suspension system design.

Flexure Bending Stress and Column Strength

Because the flexure system supports the motor and motor mount assembly, an examination of the design was made with respect to flexure bending

stresses and column strength. Considering the flexure system diagram given in the figure below, the maximum bending stress of the flexure occurs at the junction point, A, with the strut. Its value is obtained as follows:

$$M = \frac{EI\theta}{\sqrt{\frac{EI}{P}}\sin\left(\frac{\ell_1}{\sqrt{\frac{EI}{P}}}\right)} \qquad (181)$$

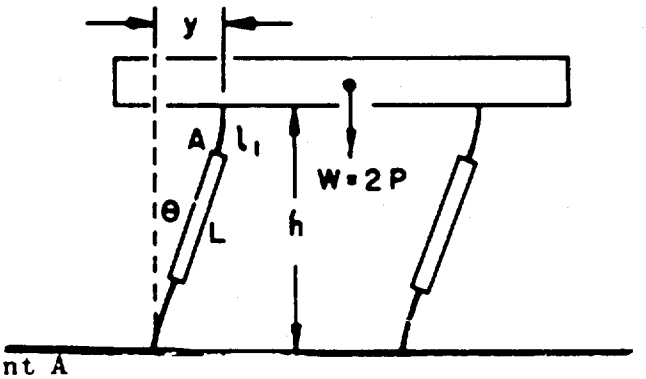

where

M = bending moment at point A

I = flexure moment of inertia

θ = angle of deflection of the system = y/h

P = axial load on flexure

ℓ_1 = flexure length

but

$$M = \frac{SI}{t/2} \qquad (182)$$

where

S = bending stress on flexure surface

t = flexure thickness

Therefore, by equating the two expressions for M and solving for the stress S, there is obtained:

$$S = \frac{y\sqrt{3PE}}{h\sqrt{wt}\sin\left(\frac{2\ell_1\sqrt{3P/E}}{t\sqrt{wt}}\right)} \qquad (183)$$

and for y = 0.006 inch, h = 14 inches, P = 275 pounds, E = 30×10^6 psi, w = 16 inches, t = 1/8 inch, and ℓ_1 = 1/2 inch, the result is:

$$S \doteq 15 \text{ psi} \qquad (184)$$

With regard to column buckling, the expressions for the critical loads, P_c, which cause buckling of long columns are given as follows for various end attachment conditions:

1. One end fixed, one end free: $P_c = \frac{\pi^2 EI}{(2\ell)^2}$
2. Both end pinned: $P_c = \frac{\pi^2 EI}{\ell^2}$
3. One end fixed, one end pinned: $P_c = \frac{\pi^2 EI}{(0.7\ell)^2}$
4. Both ends built in: $P_c = \frac{\pi^2 EI}{(0.5\ell)^2}$

where:

E = Young's modulus of elasticity

I = moment of inertia of cross section about a transverse axis

ℓ = column length

The application of these expressions in discussions of flexure and strut design requires a judgment not only of the applicable expression, but also of its limit of applicability.

Single Flexure. Considerations of the end conditions of an elemental flexure lead to the use of the expression $P_c = \frac{\pi^2 EI}{(2\ell_1)^2}$ in order to remain on the conservative side of critical loading. The limit of applicability in calculations can be established by dividing the expression by the cross-sectional area, A, and letting $r = \sqrt{I/A}$. Then because the critical stress is $S_{cr} = P_{cr}/A$, there is obtained

$$S_{cr} = \frac{P_{cr}}{A} = \frac{\pi^2 E}{4(\frac{\ell_1}{r})^2} \qquad (185)$$

This equation is applicable as long as the stress S_{cr} remains within the proportional limit. For structural steel with a proportional limit of 30,000 psi and $E = 30 \times 10^6$ psi,

$$\frac{\ell_1}{r} = 50 \tag{186}$$

Consequently, the critical load for a steel flexure with one end fixed and one end free, having $\frac{\ell_1}{r} \geq 50$, is calculated from $P_c = \frac{\pi^2 EI}{(2\ell_1)^2}$

Now, because

$$r = \sqrt{I/A} = \sqrt{\frac{wt^3}{12wt}} = \frac{t}{2\sqrt{3}}$$

$$\frac{\ell_1}{r} = \frac{2\ell_1\sqrt{3}}{t} \tag{187}$$

For the flexure dimensions $\ell_1 = 1/2$ inch and $t = 1/8$ inch, the slenderness ratio is:

$$\frac{\ell_1}{r} = \frac{1.7}{1/8}$$

$$\frac{\ell_1}{r} = 13.6 \tag{188}$$

Because $\frac{\ell_1}{r} < 50$, the flexure will not fail in buckling.

Strut. Consideration of the end conditions of a strut separating two elemental flexures leads to the use of the expression $P_c = \frac{\pi^2 EI}{L^2}$ to

remain on the conservative side. Thus, for a proportional limit of 30,000 psi for steel, it follows that:

$$\frac{L}{r} = 100 \tag{189}$$

Consequently, the critical load for a steel strut with both ends pinned, having $\frac{L}{r} \geq 100$, is calculated from $P_c = \frac{\pi^2 EI}{L^2}$.

For the strut dimensions L = 13 inches and T = 1/4 inch, the slenderness ratio is:

$$\frac{L}{r} = 177 \tag{190}$$

Because $\frac{L}{r} > 100$, the strut will fail in buckling before it fails in compression. However, for a strut with the stated dimensions, P_c = 37,000 pounds or 135 times the normal weight supported by each strut.

Differential Thermal Expansion

It is useful to investigate the possible vertical differential expansion of the concrete abutment and the steel-aluminum motor mount and suspension system. With reference to the figure below, the vertical expansion are calculated and compared.

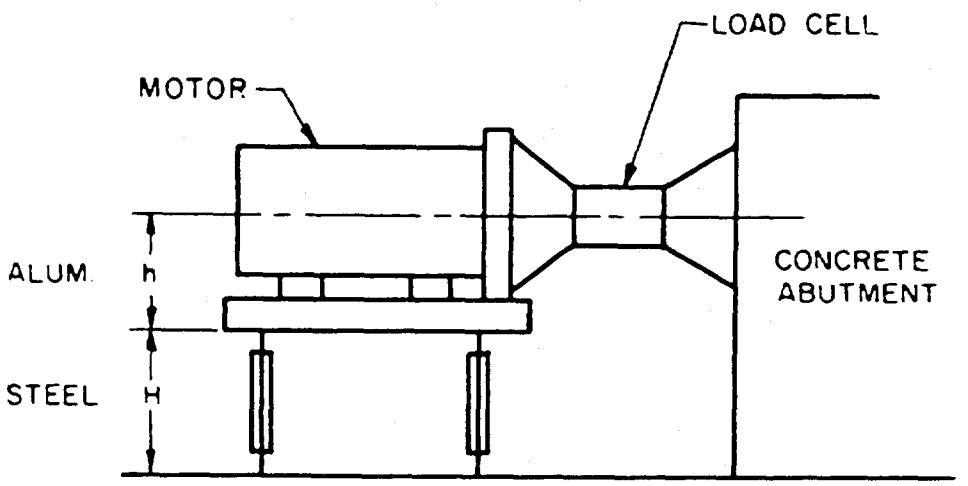

If the load cell attach bolts are removed and the whole system is heated, the vertical shift of the motor centerline is:

$$E_{M-F} = (H \alpha_s + h \alpha_a) \Delta t \qquad (191)$$

where

H = initial height of steel flexure system

h = initial height of aluminum motor mount assembly

α_s = thermal coefficient of expansion of steel

α_a = thermal coefficient of expansion of aluminum

Δt = temperature change

The vertical shift of a point of the concrete originally on a level with the motor centerline is:

$$E_c = (H + h) \alpha_c \Delta t \qquad (192)$$

Using the following values (from the Handbook of Chemistry and Physics, 1960-61)

$\alpha_s = 10.0 \times 10^{-6}$ in./in. degree C (5.6×10^{-6} in./in./degree F)

$\alpha_a = 24.0 \times 10^{-6}$ in./in./degree C (13.3×10^{-6} in./in./degree F)

$\alpha_c = 10 - 14 \times 10^{-6}$ in./in. degree C (6.7×10^{-6} in./in./degree F)

and $H + h = 32$ inches, $H = 18$ inches, and $H = 14$ inches, and using the average value of α_c, for a 25 F temperature rise there is obtained:

$E_{M-F} = 0.007$ inch

$E_c = 0.0055$ inch

Therefore, the indicated differential expansion of 0.0015 inch will result in a slight up-bending of the local cell, producing a transverse

force on the load cell. However, no change in the electrical calibration of the load cell will occur because the load cell will be rotationally positioned to electrically cancel the signals produced by the stresses accompanying transverse loads and bending moments in a vertical plane.

SYSTEM AND COMPONENT DESCRIPTION

The thrust total impulse measurement system is generally described in two ways, functionally and constructionally (Fig. 13 through 15).

FUNCTIONAL

The solid-propellant motor, when fired, produces a thrust force which compresses a strain-gage load cell, producing a d-c voltage which is directly and accurately proportional to the thrust level. This d-c voltage equivalent of the motor thrust controls the generation of a train of pulses with a repetition rate directly proportional to the d-c voltage, and, therefore, the motor thrust. An electronic counter records the number of pulses produced during the propellant burning time, and the total pulse count is directly proportional to the thrust total impulse of the burned propellant. The calibration of the entire electromechanical system is accomplished by using hydraulic pressures produced by accurate, remotely operated, dead weights and supplied to a precision piston to produce accurate static forces. The transmission of these forces to the motor support is accomplished by two long tie rods extending through a concrete retaining abutment. The total impulse calibration of the entire system is accomplished by counting the number of pulses generated in one second by a specific calibration force on the motor support table. The calibration constant is obtained by dividing the number of pulses generated in one second by the value of calibration force. To obtain the most accurate use of the measurement system, calibrations are made immediately before and after each motor firing.

CONSTRUCTIONAL

The general configuration of the mechanical system and components of the 20- by 5- by 5-foot, 22,000-pound, two-piece test stand is shown in Fig. 13 . The large, 13-foot, 18,000-pound section consists of the following.

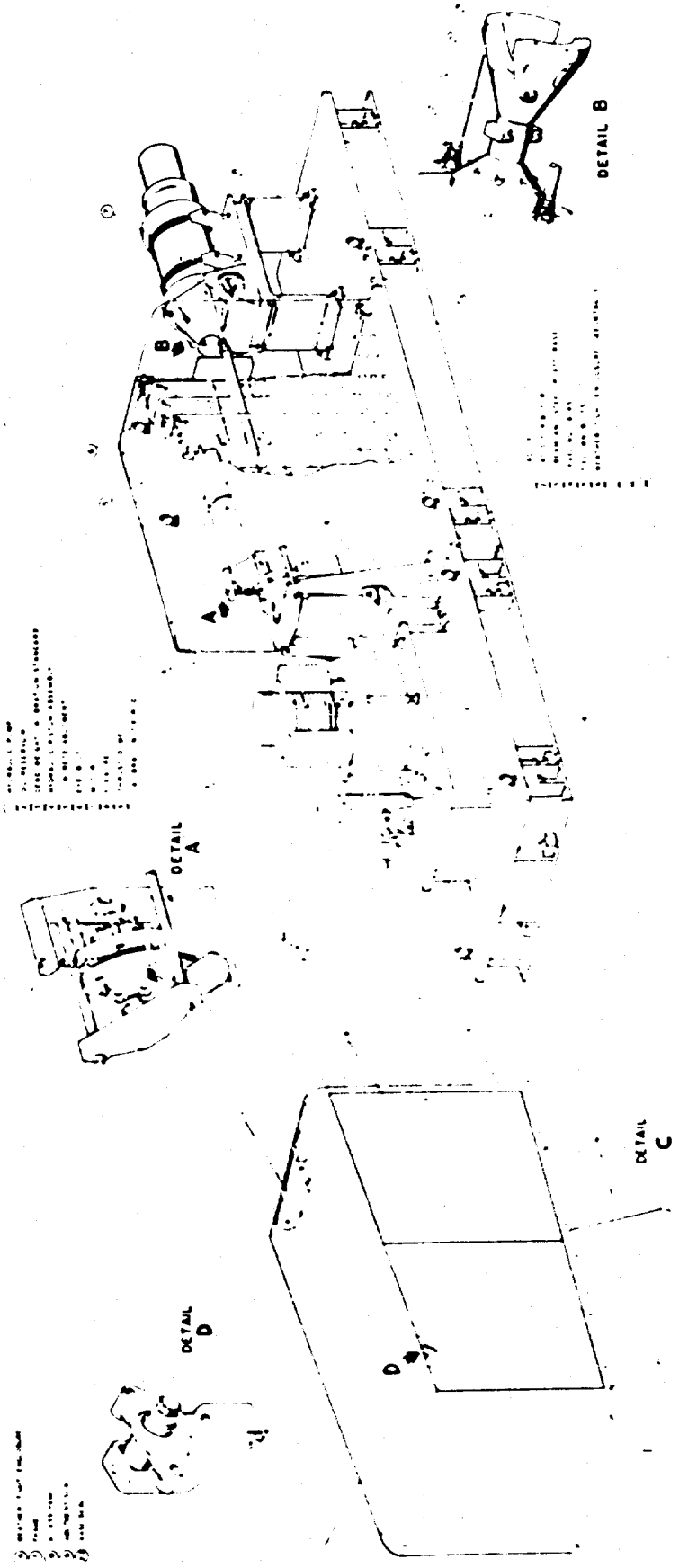

Figure 13. Test Stand Solid-Propellant Total Impulse Measurement System

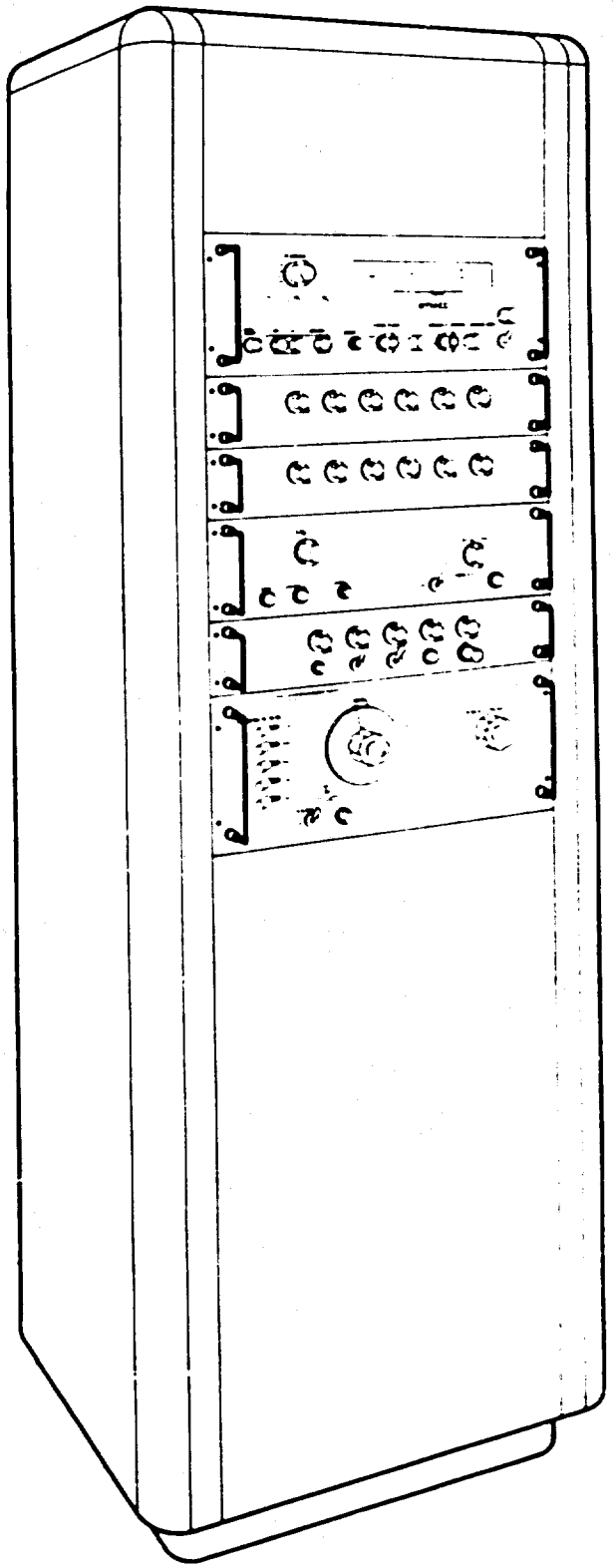

Figure 14. Electronic Equipment Cabinet

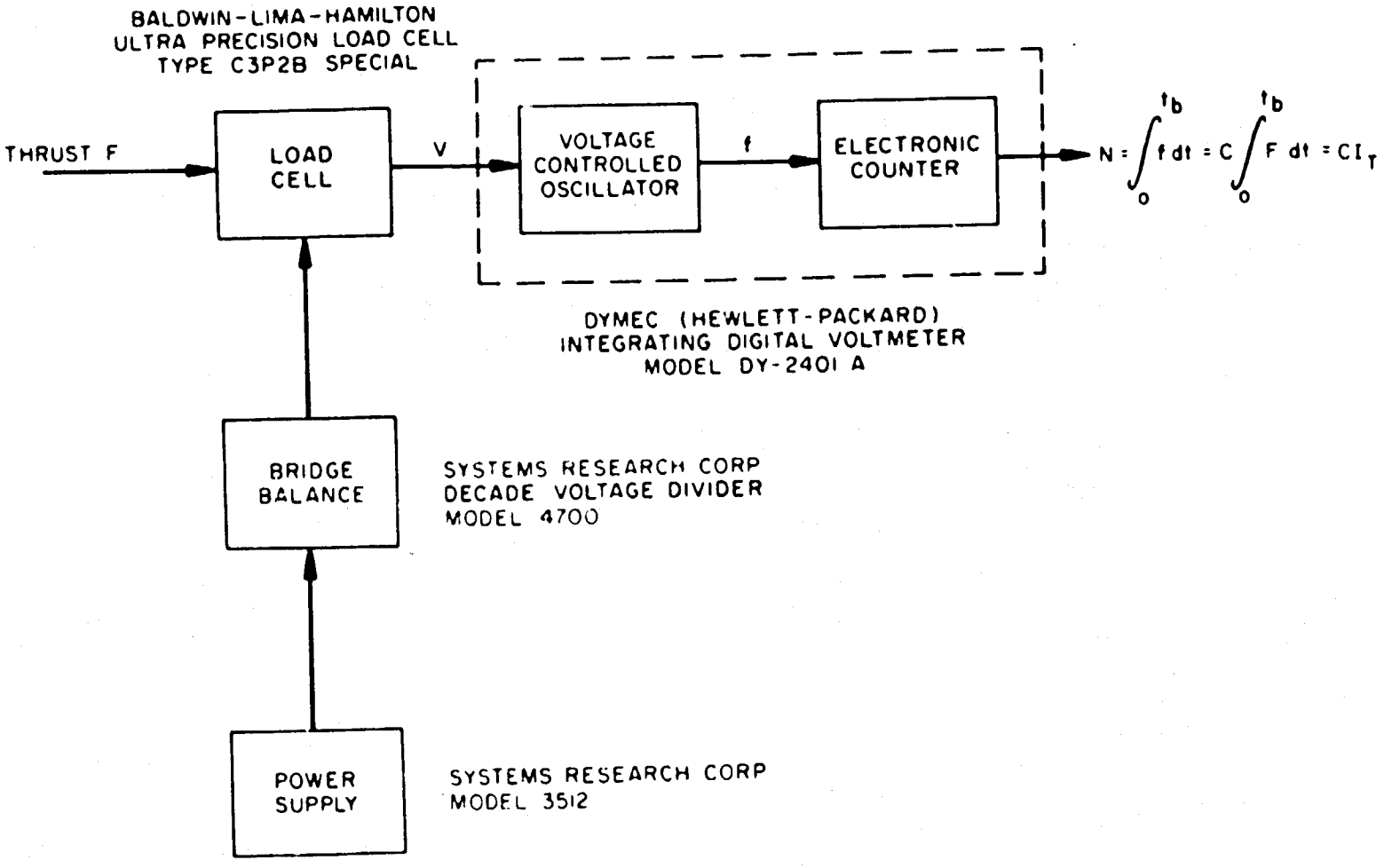

Figure 15. Electrical Block Diagram, Solid-Propellant Total Impulse Measurement System

Motor Support System

The solid-propellant motor is directly supported by two adjustable aluminum support blocks that enable alignment with the load cell axis. The support blocks are supported by a welded aluminum I-beam and plate assembly which includes a braced thrust plate in direct contact with the head end of the motor. The entire assembly is supported by a steel compression-type parallelogram flexure system which is compliant in the thrust direction and rigid in and about the vertical and transverse coordinate axes. Leveling jacks at the bottom of the flexures enables the initial alignment of the motor-mount assembly during construction of the system.

Thrust Dome Assembly

Motor thrust forces are conducted to and away from the load cell transducer by a conical-steel load collector and a load distributor, respectively. Symmetrical minimum-size slots enable the installation and removal of propellant igniters in the motor head.

Concrete Abutment and I-Beam Frame

Motor thrust forces are transferred to a welded I-beam supporting frame by a 5- by 4- by 4-foot, 11,500-pound reinforced-concrete block. Forces enter the block through 12- by 12- by 2-1 2-inch imbedded steel plates and are transferred to the supporting frame through a 2-inch-thick steel base plate. Reinforcing rods, 3/4-inch diameter, are spaced at 6-inch intervals from top to bottom and are welded to the base plate. The 10-inch-high, I-beam frame is constructed of three lengthwise sections welded together by I-beam cross beams. Six tiedown bolts connect this frame to the test pad.

Calibration Piston Assembly and Tie Rods

The hydraulic piston assembly is supported from the concrete abutment and supplies coaxial calibration forces to the motor-mount assembly by means of two rods extending through clearance holes in the concrete abutment.

The smaller, 7-foot-long, 4000-pound, section of the two-piece test stand consists of the following:

Master Pressure Standard (Dead Weight Tester)

This unit produces the accurate hydraulic pressures transmitted to the calibrating piston. The production of the pressures is accomplished by the placing of dead weights, with remotely controlled lifters, on a piston in a hydraulic cylinder.

A hydraulic pump, operated either by a hand wheel or an electric motor, maintains the proper supply of oil in the closed hydraulic system.

Weather-Tight Enclosure

The precision calibration system is protected from dirt and water by an air- and water-tight enclosure containing two sealed access panels on each side.

The general configuration of the electrical system and its components is shown in Fig. 14 . The enclosure contains the load-cell power supply and bridge balance, the integrating digital voltmeter which performs the electronic integration of the thrust-time curve, control equipment for the operation of the calibration system, and equipment which enables satisfactory tape recording and playback of the pulses produced by the voltage-to-frequency converter section of the integrator.

REALISTIC ERRORS

A realistic error breakdown of the entire measurement system is presented in Table 3.

TABLE 3

REALISTIC ERROR BREAKDOWN
(Entire Measurement System)

Load Cell	
Linearity, %	0.03
Hysteresis, %	0.02
Repeatability, %	0.01
Temperature (10 F), %	0.02
Bridge Balance	
Resolution (1μv), %	0.02
Power Supply	
Stability (2 C) %	0.01
Time-drift, %	0.01
Integrating Voltmeter	
Linearity, %	0.005
Stability, %	0.01
Calibrator	
Accuracy, %	0.05
Mechanical Misalignment	
Total Error, %	0.01
Dynamic Response to Rapid Transients	
Total Error, %	0.01
Root-sum-square error, % less than	0.08

LOAD CELL

The precise determination of the motor thrust-time curve depends directly on the quality of the transducer which converts motor thrust to an equivalent electrical voltage. The need for the greatest possible accuracy and linearity of this transducer is evidenced by the over-all system error limit of 0.1% in the measurement of the area under the BATES motor thrust-time curve (total impulse). Efforts to fulfill this need to the greatest possible degree led to direct technical discussions with the Baldwin-Lima-Hamilton Corporation, Waltham, Massachusetts. The result of these technical negotiations was a proposed design of a load cell with an accuracy exceeding that of the Baldwin-Lima-Hamilton precision units. The performance specifications are as follows:

Model: Special C3P2B (double bridge)
Full scale: 10,000-pounds compression
Full scale output: 3-mv/v input (±0.15%)
Input resistance: 350 ohms nominal
Nonlinearity (terminal method): less than 0.03% full scale
Hysteresis: Less than 0.02% full scale
Repeatability: Less than 0.01% full scale
Temperature effects:

1. On zero output: less than 0.15% full scale/100 F
2. On sensitivity: less than 0.08% of load per 100 F

Full-scale deflection: less than 0.006 inch

Important additional calculated data of this unit were obtained concerning mechanical stiffness to transverse loads, bending and twisting moments, and are as follows:

Mechanical

1. The transverse stiffness is in the order of 1×10^6 lb/in. in any direction for a load applied at the top of the cell (5 inches from the base).

2. The torsional stiffness is in the order of 20×10^6 lb in./rad

3. The bending stiffness for a couple applied to the end of the cell, tending to bend the axis of the cell, is in the order of 25×10^6 lb in./rad in any direction

Electrical

1. The cell response to a 500-pound transverse load is a maximum span (sensitivity) change of ±0.15% of full scale, and this change increases and decreases sinusoidally as the direction is rotated about the cell.

2. Cell response to torsion will be negligible

3. A moment of 2500 lb in. applied at the end of the cell has the same effect as item 1.

These mechanical and electrical data enabled an adequate design analysis to be made of a suitable motor-suspension flexure system. Figure 16 shows the dimensions of the load cell and the detail of the special heavy end mounting plates containing alignment center holes and threaded holes for bolted attachments.

POWER SUPPLY

The low over-all system error limit of 0.1% in the measurement of thrust total impulse imposes severe requirements on the load cell bridge excitation voltage. Measurement-system accuracy is directly related, through the load cell sensitivity, to the power-supply stability. Efforts to obtain a suitable strain gage power supply led to technical negotiations with the Systems Research Corporation, Van Nuys, California. The result of these discussions was a proposed new design of power supply with performance specifications as follows:

Model: 3512
Input power: 95-135 vac, 50 cycle

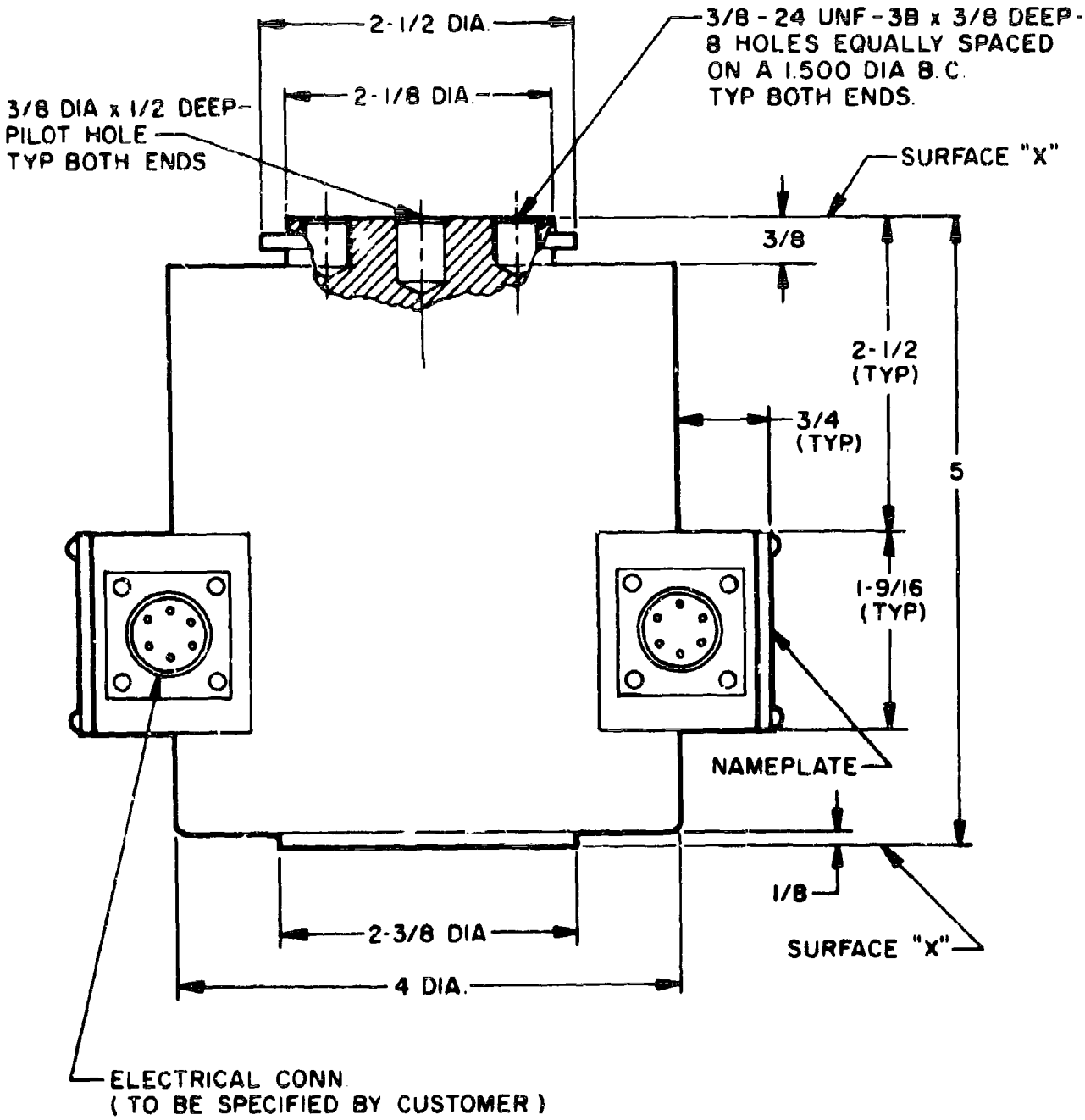

GENERAL NOTES

1. BEARING SURFACES "X" ARE LAPPED AND ELECTROPLATED WITH LEAD .001/.002 THK.

Figure 16. Load Cell

Output: Digitally selectable 0 to 18 vdc, 0 to 200 milliamperes
Regulation: 0.01% NL-FL and 95 to 135 vac
Ripple: 0.05 millivolt rms
dc isolation: 10,000 megohms
Stability: 0.005% C
Noise at bridge (350 ohms): 2μv
Overload protection: fused
Overvoltage protection: limits output voltage to 18 vdc
Current regulation: available by jumpering at rear chassis
Size: 3-1/2- by 19- by 10-inches

This supply has a solid-state construction incorporating balanced differential amplifiers and temperature compensated zener circuitry for stability. Output voltage is digitally selected in 1-millivolt steps by means of decade switching of precision voltage dividers connected in a Kelvin-Varley arrangement. By accurate selection of close-tolerance resistors, superior accuracy is obtained and resolution to five significant figures or one part in 100,000 is more than adequate for the application. Two excitation outputs are available at the rear terminals. Isolation to ground is extremely high as a result of design care in the layout of the circuitry components and the unit is made completely floating with reference to ground. Design care is also taken to keep capacitive coupling to a minimum. Excellent isolation to line is achieved by using transformers with a completely box-shielded primary. Special features of overload protection are included to limit the supply output to 18 volts, regardless of conditions, as a result of zener diode effecting the feedback loop to the regulating series pass transistors. Low ripple is achieved by heavy negative feedback coupled with preregulator filtering. The digital programming portion of these units provides a precision operation and excellent application where exact power settings are required. Operation is simple because the voltage desired appears immediately at the rear terminals after selecting the five front panel knobs. This is a distinct advantage over a continuously variable control because it takes time to reach the voltage setting desired as well as expensive additional readout equipment. The additional advantage is that any specific value of voltage can be selected giving operational

simplicity and elimination of error. This feature of excellent repeatability is useful in applications of repeating test conditions. Figure 17 shows the general front panel configuration.

BRIDGE BALANCE

The over-all system error limit of 0.1% also imposes severe requirements on the circuitry employed for the load cell output zero signal control. Bridge balance must be accomplished with a resolution of approximately 1 microvolt if load cell signal errors of 0.01% are not to be exceeded with 1500-pound thrust levels. The Systems Research Corporation, Van Nuys, California, proposed a design of an adequate unit with performance and description as follows:

Model 4700
Input: Three wires to bridge
Resolution: Balance to microvolt with 350-ohm bridge
Size: 3-1/2 by 19- by 6 inches

Six front panel mounted controls will allow nulling bridge unbalances to ±5%. Precision-tolerance resistors of excellent long-term stability are used throughout. Quality switches of low-contact resistance ensure excellent repeatability. As in the power supply, the system used is decade switching of precision voltage dividers connected in a Kelvin-Varley arrangement. Terminals are provided for a limiting resistor if desired, otherwise these terminals are jumpered.

Figures 18 and 19 show the front panel configuration and circuit design and respectively.

INTEGRATING DIGITAL VOLTMETER

The measurement of the area under a thrust-time curve is readily accomplished by the use of a voltage-to-frequency converter and a counter. A thrust (F) on the load cell produces a dc voltage (V) into the converter,

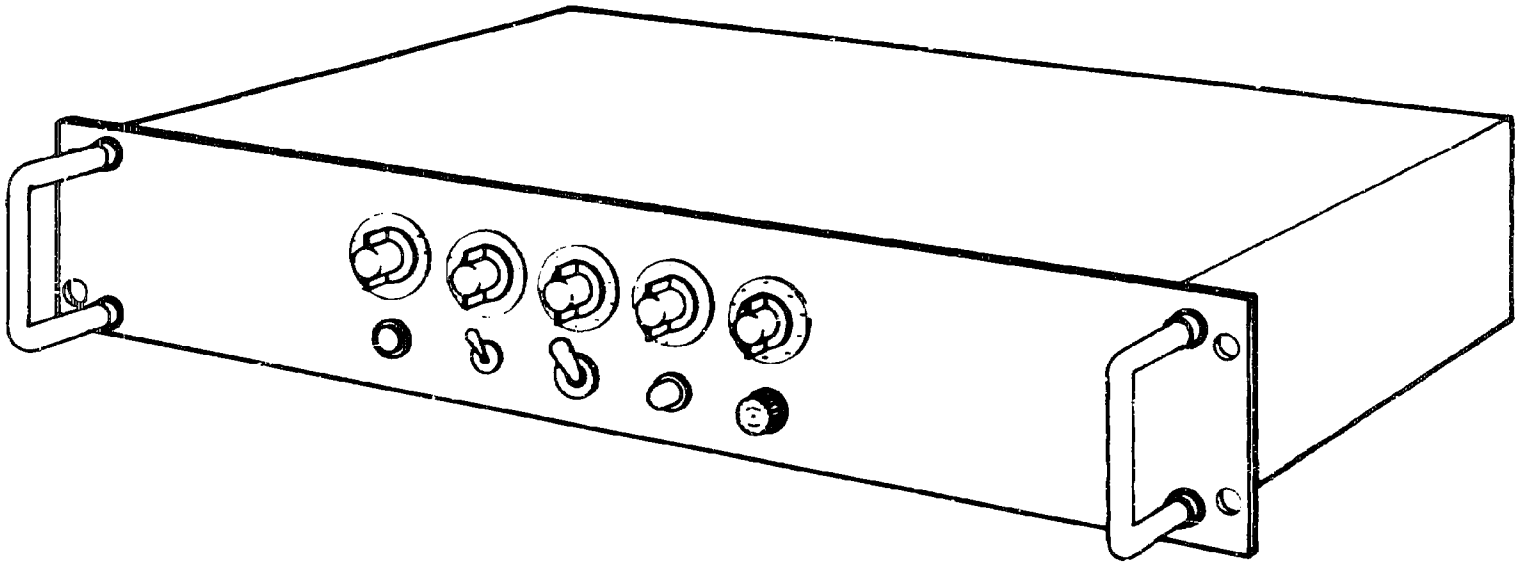

Figure 17. Power Supply

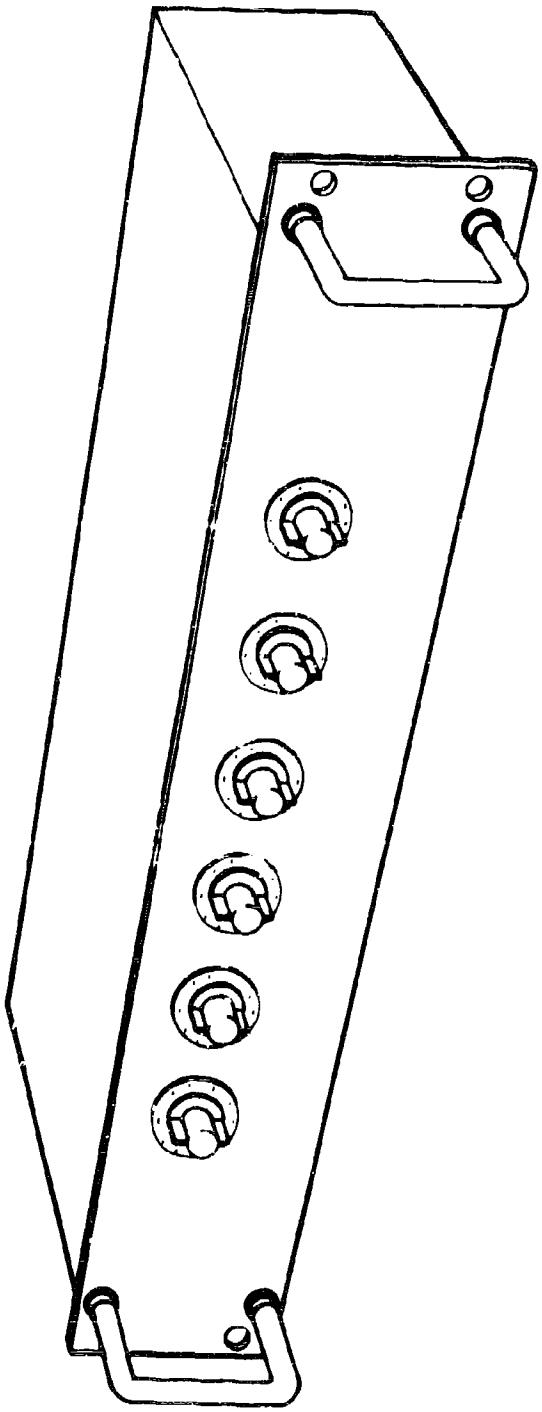

Figure 18. Bridge Balance

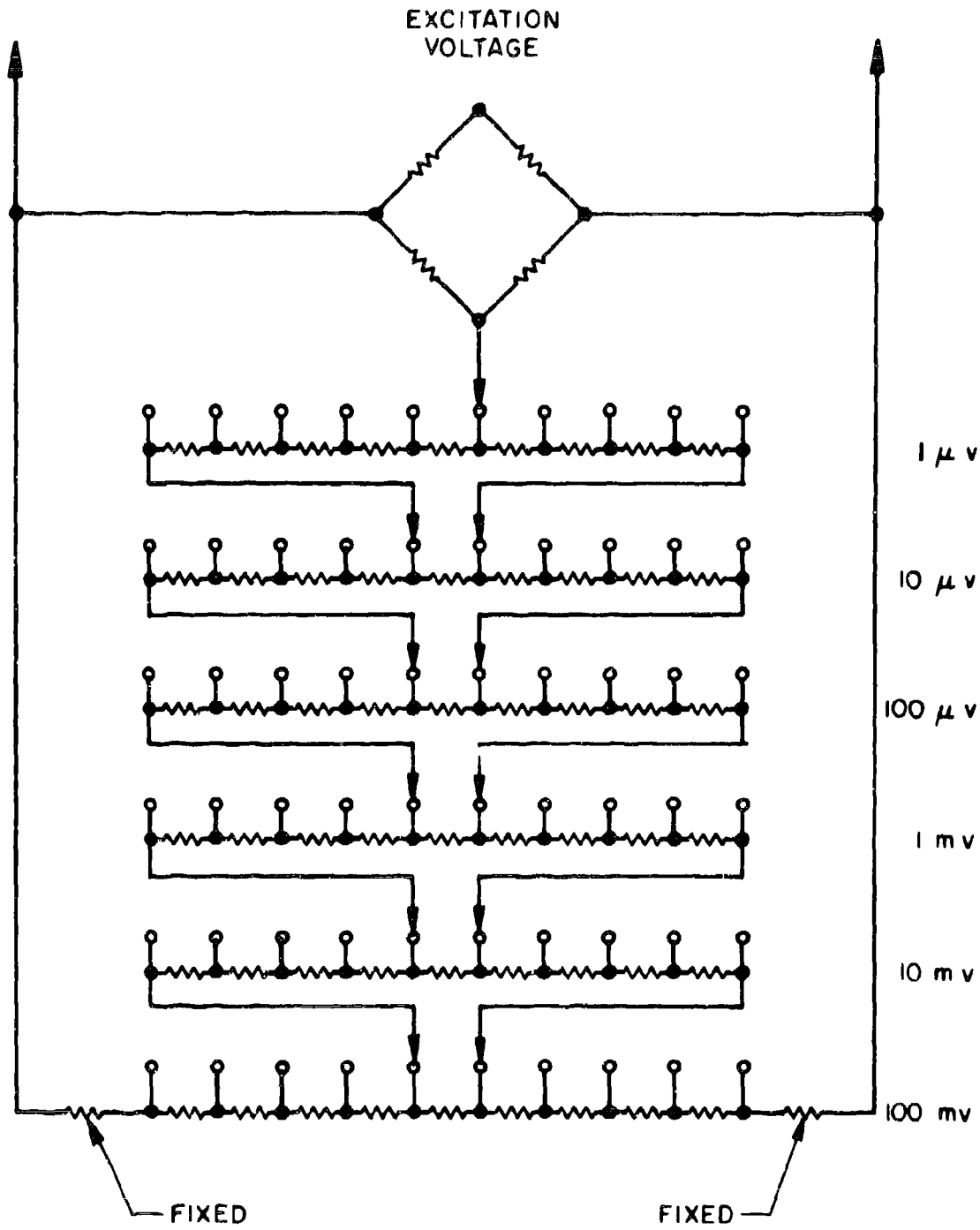

Figure 19. Bridge Balance Circuit Design

which in turn produces a pulse repetition frequency (f), and the individual pulses are electronically counted. As a result, the total number of counts (N) is proportional to the time integral of the force (total impulse). Mathematically, this is expressed as

$$N = \int_o^{t_b} f\,dt = C_1 \int_o^{t_b} V\,dt = C_1 C_2 \int_o^{t_b} F\,dt$$

therefore

$$N = CI_T$$

where

$$C = C_1 C_2$$

and

$$I_T = \int_o^{t_b} F\,dt$$

To comply with an over-all system error limit of 0.1% in the total impulse measurement, the linearity and stability of the integrating equipment must be of the highest possible degree. Also, the total number of counts obtained with the expected minimum thrust (1500 pounds) during an expected minimum burning time interval (2 seconds) must be sufficiently great so that one count represents a negligible error when compared to 0.1% of the total number of counts obtained. If one count is required to be only 0.01% of the total number obtained (with the minimum thrust and time conditions), then the total number must be at least 10,000 or 5000 pps. Consequently, any converter-counter combination which yields 5000 pulses per second, with the minimum thrust levels to be encountered, is adequately sensitive for the application. Linearity of the converter-counter combination, like the load cell transducer, must be the greatest possible because nonlinearities occurring anywhere in the system produce errors in the total impulse measurement.

The Dymec Model DY-2401 A integrating digital voltmeter, manufactured by the Dymec Division of Hewlett-Packard Company, fulfills these requirements when used in conjunction with the special Baldwin-Lima-Hamilton load cell. Its superior linearity (0.005% is obtained at the expense of sensitivity (0.1 vdc yields 100,000 pps), but because the special Baldwin-Lima-Hamilton load cell produces 54 millivolts with 10,000-pounds force, its sensitivity is sufficient to produce the described negligible error (0.01% with minimum thrust and time conditions) with the one-count resolution common to high-quality electronic counters, as the following statements demonstrate:

vco sensitivity is 100 millivolts ⟶ 100,000 pps
load cell 10,000 ⟶ 54 millivolts ⟶ 54,000 pps
1500 ⟶ 8.1 millivolts ⟶ 8100 pps
0.01% of 1500 ⟶ $8.1 \cdot 10^{-4}$ millivolts ⟶ 0.8 pps

Therefore, in 2 seconds the total count is 1.6. Consequently, the Baldwin-Lima-Hamilton load cell and Dymec integrating digital voltmeter combination sensitivity and resolution are consistent with the assigned error limitation of 0.01%.

The performance features and specifications of the Dymec 2401 A unit include the following:

1. Better than 140-decibel effective common mode rejection at all frequencies, including dc
2. Active integration minimizes error caused by superimposed noise and provides average reading of input over sampling period
3. Five-digit readout provides up to one part in 100,000 reading resolution. Minor changes accommodate 10^6 counts.
4. 0.005% linearity, stability ±0.03% of full scale per day on most sensitive range (0.1 vdc) with constant temperature and ±10% line voltage change
5. Temperature sensitivity ±0.002% of reading per degree-centigrade on the most sensitive range (0.1 vdc)

Figure 20 shows the front panel configuration.

CALIBRATION SYSTEM

From a measurement accuracy standpoint, the most important single component of the entire measurement system is the equipment used for calibration. The accuracy, linearity, repeatability, stability, and all other instrumentation performance parameters, can be determined only by reference to an accepted standard. The over-all error of the system can be no less than the error incurred in its calibration. Efforts to obtain the most precise force standard possible for this purpose led to direct technical negotiations with the Ruska Instrument Corporation, Houston, Texas. The result of these discussions was a proposed design for a combined master pressure standard and a precision hydraulic piston for the production of six forces in the 0 to 10,000-pound range. To obtain the most accurate calibration of this equipment possible it was also proposed that this equipment be calibrated by the National Bureau of Standards, Washington, D. C.

The operating principle of this equipment is the production of accurate hydraulic pressures by means of precision dead weights supported by a vertical piston, and the transmission of these pressures to a second precision piston oriented to use the accurate output forces with the equipment to be calibrated. The application of this principle to the calibration of a horizontal thrust measuring system constitutes the most accurate method known for this purpose, because it eliminates all pivots, bell cranks, bearings, flexures, lever arms, etc., necessary to produce horizontal forces with dead weights alone. The operational flexibility of this equipment in the Bates motor test stand enables remotely controlled calibrations of the entire measurement system to be made immediately before and after a motor firing, with all controls mounted on a single panel and located with the remaining electronic equipment of the system. The calibration equipment control wiring will enable operating it from either the test stand or the control room.

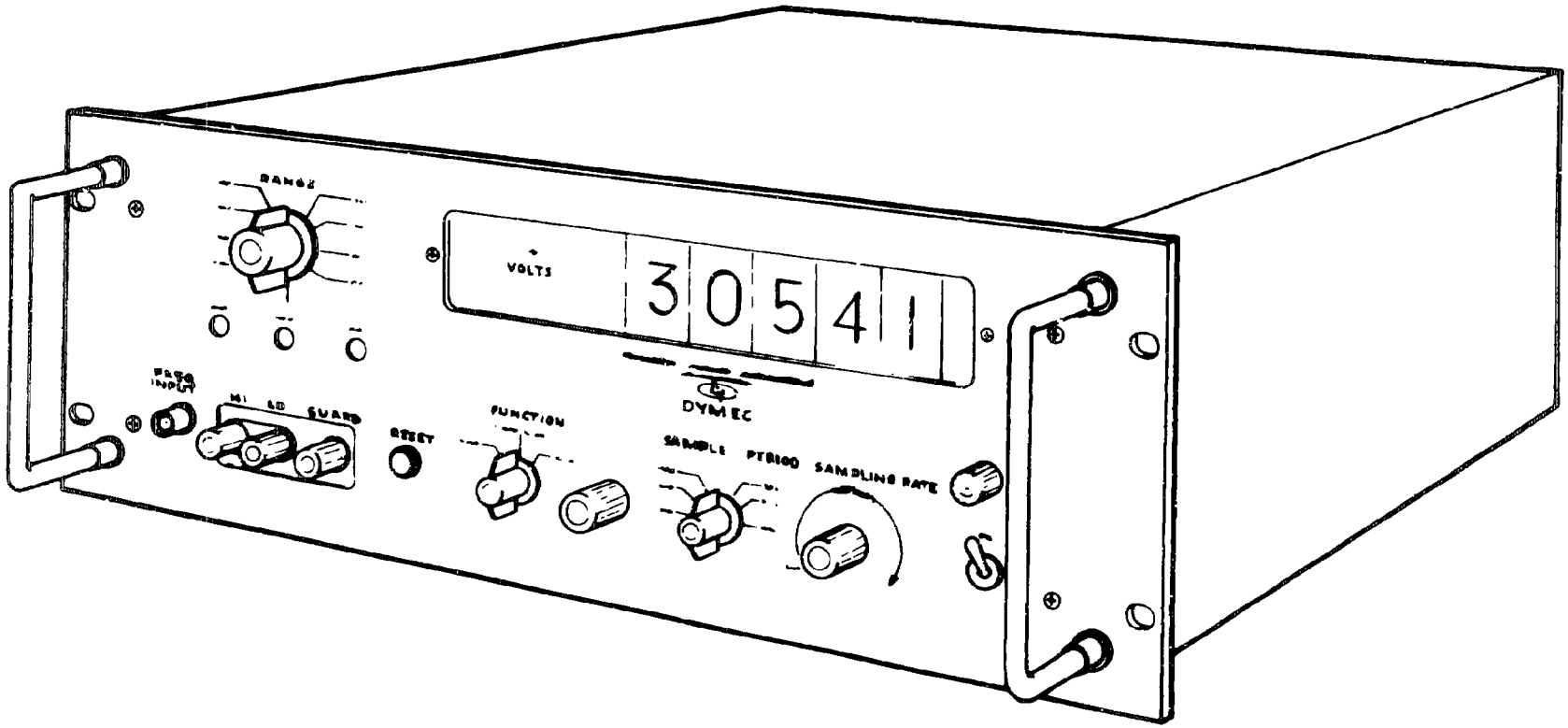

Figure 20. Integrating Digital Voltmeter

The specifications of the equipment include:

1. Six calibration points: 1000-, 2000 , 4000-, 6000-, 8000-, and 10,000-pounds force (dead weights manufactured to the local g value at Edwards Air Force Base test site).
2. Accuracy of each force point: ±0.05%
3. Resolution: 0.02% of full scale
4. Float time of dead weight gage and force piston cylinder shall be at least 1 minute for each calibration point
5. Hydraulic pump capacity shall be sufficient to provide at least one complete calibration (ascending and descending), including any leakage, without refilling
6. Visual means shall be provided at the control console to indicate when the dead weight gage is floating and a calibration point may be taken
7. Weights shall be applied in ascending or descending order selectable through a multiposition switch
8. The piston cylinder of both the dead weight gage and force piston cylinder shall be of the same material.

Figure 21 shows this equipment.

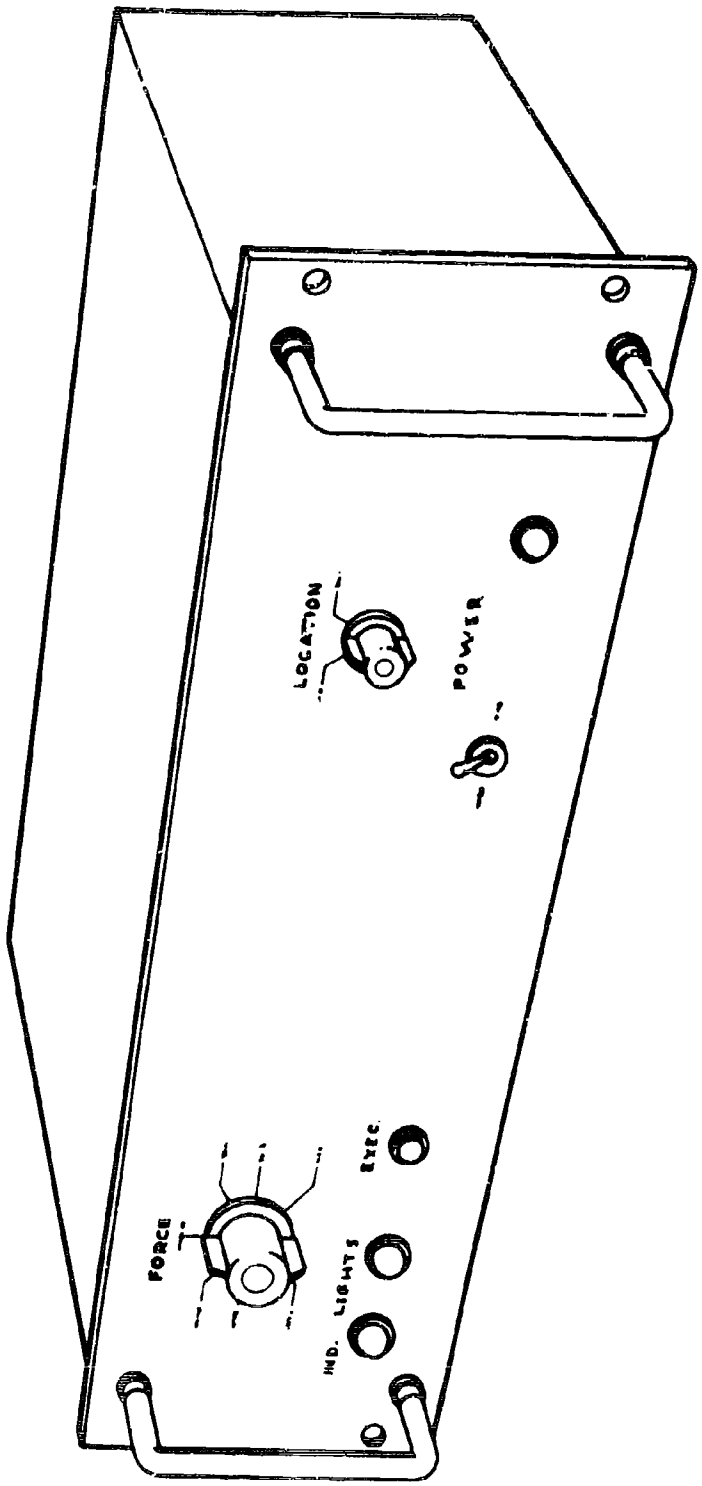

Figure 21. Calibration System Control Panel

CALCULATION OF COMPLETE SPRING SYSTEM

The mathematical analyses described in preceding discussions provided the initial justification of the detailed design of the entire measurement system. However, practical consideration of system and component fabrication and assembly, system calibration, and motor installation and operation, require some deviation from the simple, ideal image of the system as a 1- or 2-degree-of-freedom system. These deviations were held to a minimum, however, not only to design the system as close as possible to the systems which are more amenable to mathematical analysis but, more important, because the simpler the system the fewer sources of error.

It is useful, therefore, to estimate the stiffness and weights of the designed components so that a more accurate picture may be obtained of the dynamic system. The purpose in such an effort is to (1) determine how close the designed system came to the simpler models used in the mathematical analyses, (2) provide a more accurate basis for possible additional analyses, if needed, and, (3) identify possible sources of undesirable dynamic performance which can be corrected by minor changes during fabrication and assembly.

CALCULATION OF COMPONENT STIFFNESS

Concrete Abutment

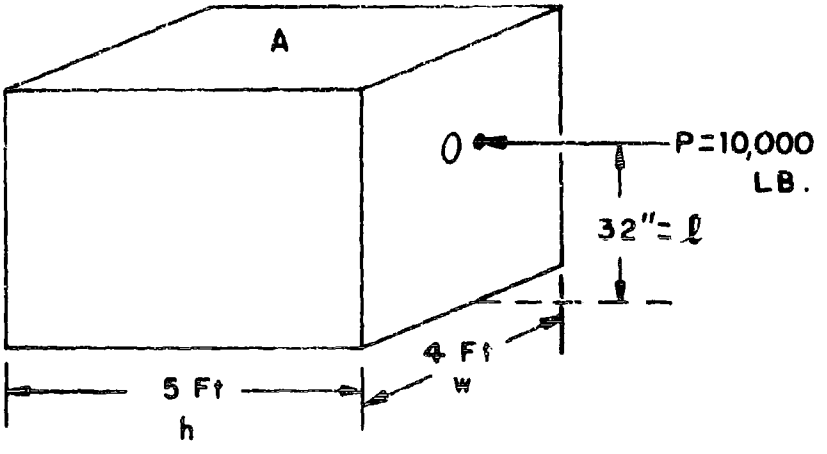

The deflection of the concrete abutment, fixed at the base, is obtained by the use of the following equation (Ref. 8):

$$\delta = P\left(\frac{\ell^3}{3EI} + \frac{k\ell}{AE_s}\right)$$

where

δ = deflection of point 0 relative to base
P = static load (10,000 pounds)
E, E_s = concrete modulus of elasticity (3×10^6 psi) and shear (1.35×10^6 psi)
I = moment of inertia ($1/12\ wh^3$)
k = constant (3/2 for rectangular cross sections)
ℓ = length of beam (32 inches)
A = cross section parallel to base

Substitution of these values into the equation yields the value of stiffness of the concrete abutment.

$$k_c = \frac{P}{\delta} = 7.27 \times 10^8 \ \frac{lb}{ft}$$

Because load cell stiffness is $k = 2.04 \times 10^7 \frac{lb}{ft}$

The stiffness ratio is

$$\frac{k_c}{k} = \frac{7.27 \times 10^8}{2.04 \times 10^7}$$

$$= 3.56 \times 10$$

$$\frac{k_c}{k} = 35.6$$

Load Distributor (Steel)

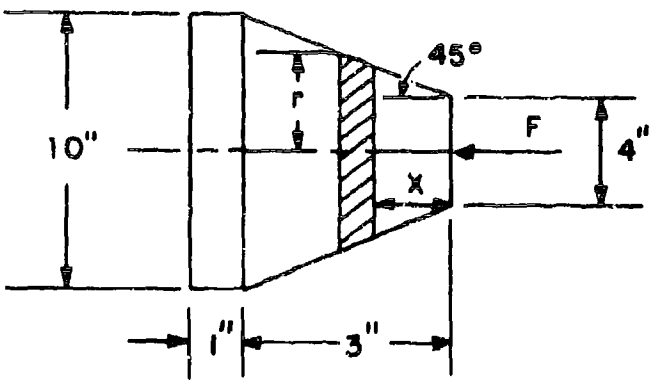

Conical Part. Area of elemental cross hatched circular slice $dA = \pi r^2$

$$E = \frac{F/dA}{d\delta/dx} = \frac{F\ dx}{dA \cdot d\delta} = \frac{F}{d\delta}\ \frac{dx}{\pi r^2}$$

$$\therefore\ d\delta = \frac{F}{\pi E}\ \frac{dx}{r^2}$$

The total axial deflection (δ) of the conical part associated with force (F) is

$$\delta = \frac{F}{\pi E} \int_0^3 \frac{dx}{(x + 2)^2}$$

$$\delta = \frac{F}{\pi E} \left(\frac{3}{10}\right)$$

Cylindrical Part. Cross-sectional area is

$$A = \frac{\pi d^2}{4}$$

$$E = \frac{F/A}{\Delta/t} = \frac{Ft}{\Delta \cdot A}$$

$$\therefore\ \Delta = \frac{Ft}{EA}$$

Total deflection of load distributor obtained with force (F) is

$$\delta + \Delta = \frac{3F}{10\ \pi E} + \frac{Ft}{EA} = F\left(\frac{3}{10\ \pi E} + \frac{t}{EA}\right)$$

Substituting the appropriate values yields the stiffness value

$$k_{LD} = \frac{F}{\delta + \Delta} = 336 \times 10^7 \text{ lb/ft}$$

The stiffness ratio is

$$\frac{k_{LD}}{k} = \frac{336 \times 10^7}{2.04 \times 10^7} = 165$$

Load Collector (Thrust Dome)

The stiffness of this component was estimated to be approximately 1/4 the stiffness of the load distributor. Therefore

$$\frac{k_{LC}}{k} \doteq 40$$

Rocket Motor Case

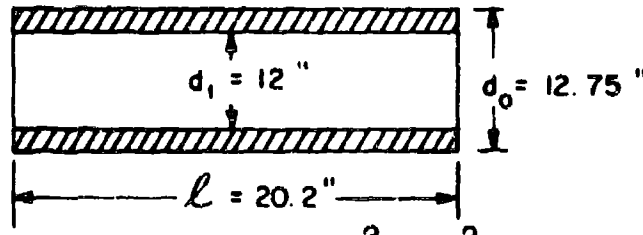

$$k_M = \frac{EA}{\ell} = \frac{(30 \times 10^6)\ \pi\ (d_o^2 - d_1^2)}{4\ (20.2)}$$

$$k_M = 25.2 \times 10^7 \text{ lb/ft}$$

Stiffness ratio is

$$\frac{k_M}{k} = \frac{25.2 \times 10^7}{2.04 \times 10^7} = 12.2$$

DIAGRAM OF COMPLETE SYSTEM

On the basis of the estimated component stiffnesses and weights, the complete spring-mass system is given below. Damping values are those regarded as nominal in the computer program.

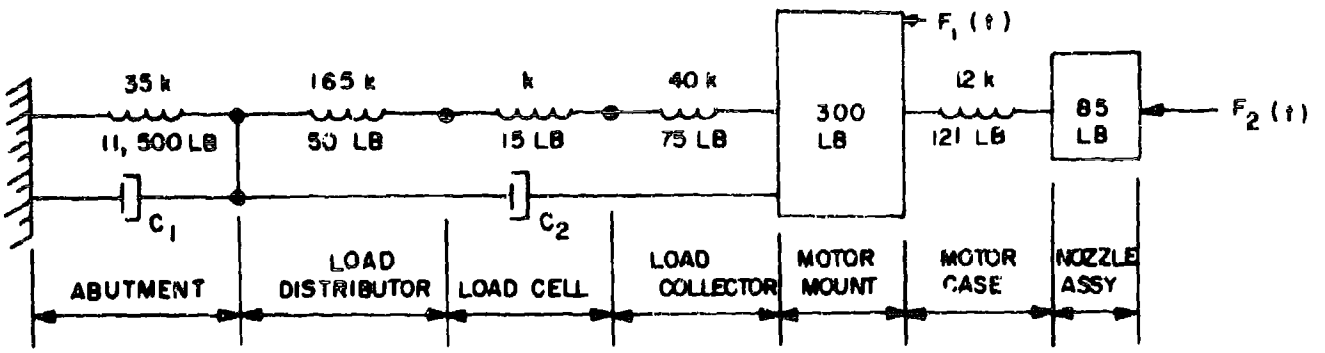

The model (nominal) used in the computer program was:

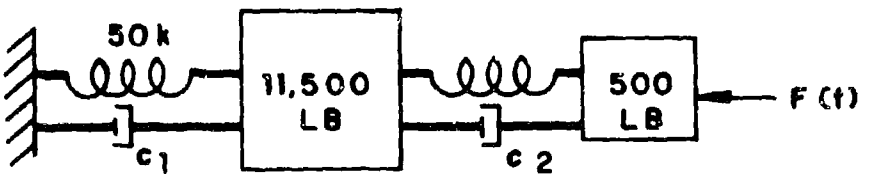

The two-degree-of-freedom model used in the computer analysis is a simplification of the actual system. Lumped masses were used in the model which were comparable to the distributed masses of the concrete abutment and solid propellant motor.

The load distributor and collector springs were omitted from the computer model altogether, and the distributed spring and masses of the motor were simply lumped as a mass. Nevertheless, it is felt that the two-degree-of-freedom computer model represented the essential features of the system, because the computer results showed the impulse error sensitivity to abutment stiffness to be very slight. Therefore, the unification of the load distributor and abutment springs is entirely reasonable. The correctness of the unification of load collector and motor springs and masses into one single mass (500 pounds) is not so apparent. To further complicate the assessment of the computer model correctness, the motor thrust is not all applied at one location. Approximately 70% of it (F_1 (t) in the detailed diagram) is applied at the head-closure end of

the motor case, and the remaining 30% (F_2 (t) in the diagram) is applied at the nozzle assembly and it is transmitted to the head end through the comparatively compliant rocket motor case (12 times the stiffness of the load cell). Consequently, the dynamic behavior of the part of the actual system between the load cell and the motor nozzle could conceivably be quite different from that of the lumped mass representing it in the computer studies. However, most of the misrepresentation is associated with the motor hardware, which is outside the test stand design and therefore beyond Rocketdyne design control. It is felt that the dynamic behavior of the motor hardware should receive additional attention in the future evaluations of the constructed measurement system.

VCO PULSE MODIFIER FOR TAPE PLAYBACK

Because a standard tape recorder cannot record and playback pulses of short duration with good fidelity, it is necessary to modify the pulse characteristic at the input and/or output of the recorder. The reason for this is that the upper frequency limit of the recorder is near the natural ringing frequency of the head, which causes the system to ring electrically when activated by a pulse. Therefore, when a pulse is recorded, the playback of that pulse will be a damped oscillatory wave with a frequency equal to the ringing frequency of the system, and the rate of decay (damping) determined by the Q of the system. If the playback pulse is being read by a counter, it is quite possible to obtain more than one count per initial pulse because the excursions of the immediate subsequent ringing can be of sufficient amplitude to activate the counter. The amplitude resolution of the counter cannot be predictably set to discriminate between the first and the second cycles of the damped wave because a slight change in playback pulse amplitude will cause the counter to either miss or to produce multiple counts.

A possible method of solving this problem has been tested at Rocketdyne and proved practical. The pulses can be first modified to a constant amplitude and duration of about 6 volts and 4 microseconds by use of a monostable multivibrator (one-shot). These pulses can be recorded on a tape recorder with a flat frequency response of at least 100 kilocycles such as an Ampex FR-100 used on direct record mode. Figure 22A shows a train of three pulses as they would be fed to the recorder, and Fig. 22B shows the approximate characteristic of the playback. Figure 23A shows one of the playback pulses expanded on a shorter time base. This signal can be fed to two parallel circuits as shown in Fig. 24 (the 10 kilocycle hipass filter is present to remove most of the noise). The signal of Fig.23A can be fed to one side of the summing amplifier, and through a delay network to the other side. In this way the two signals which will be added together look like the wave forms of Fig.23A and 23B. The delay

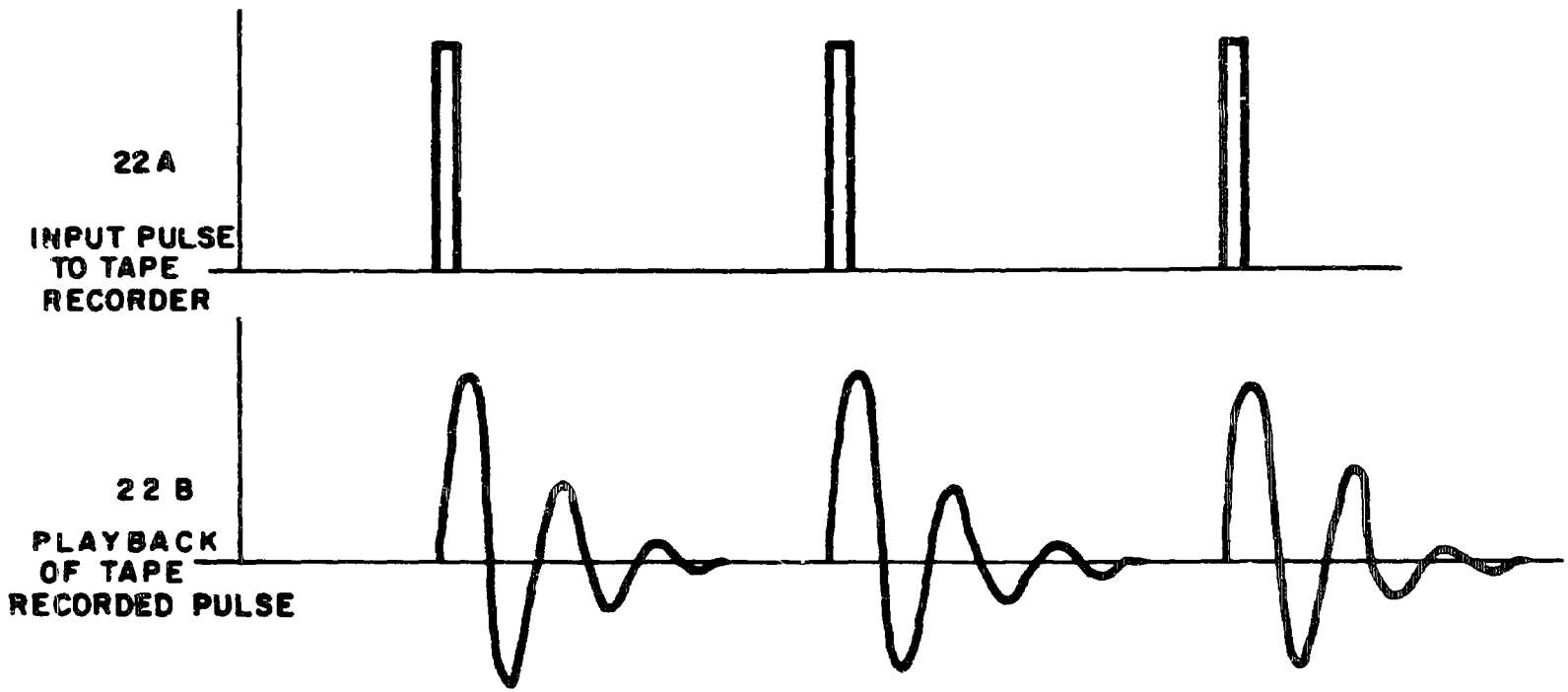

Figure 22. Tape Recorder Input and Played-back Signals

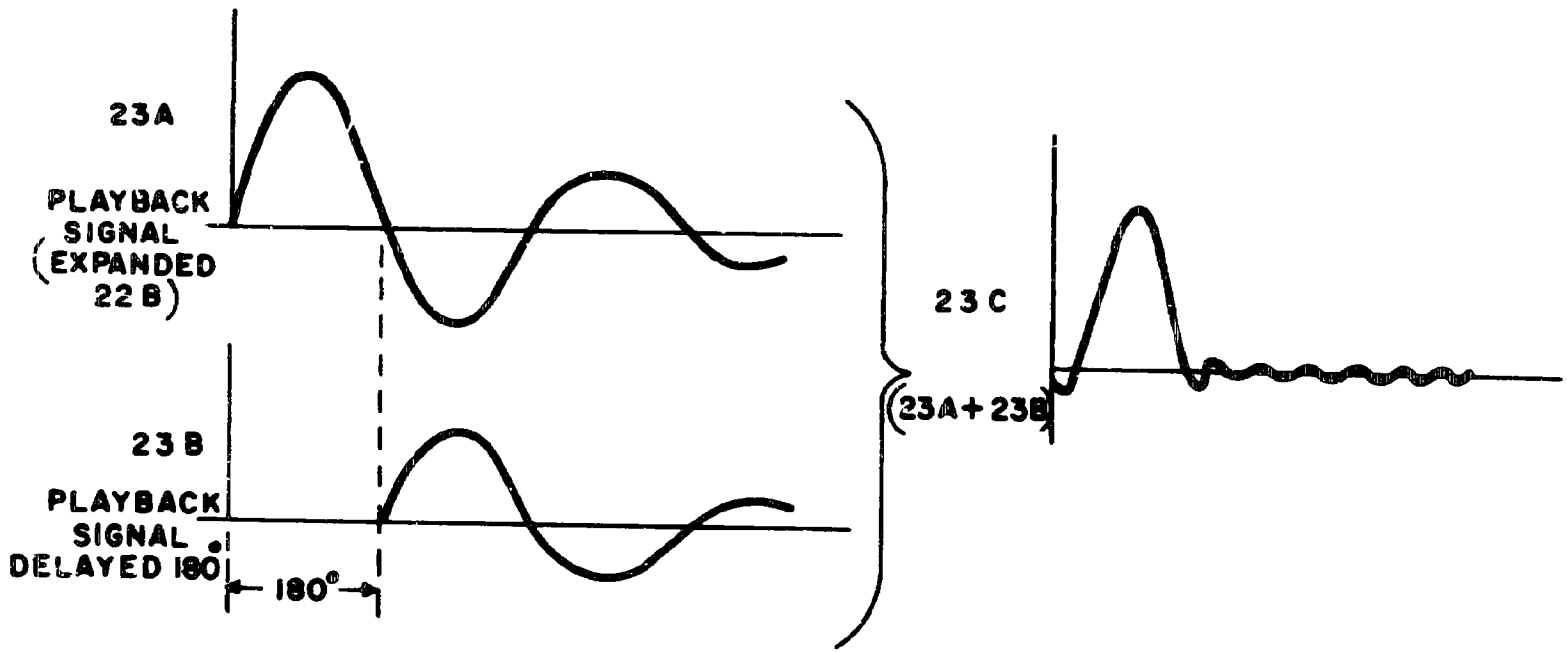

Figure 23. Played-back and Delayed Signals

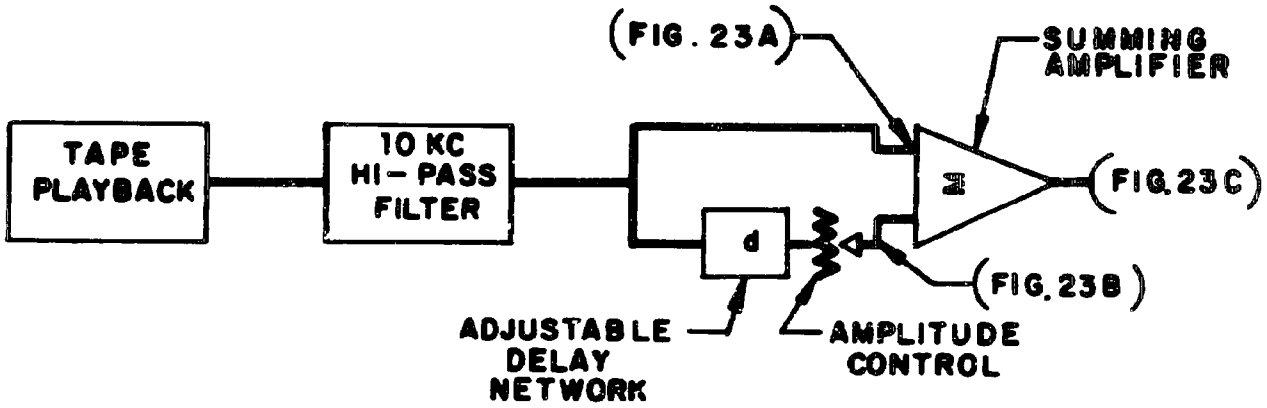

Figure 24. Block Diagram of Play-back Signal Modifier

can be adjusted until 180 degree phase shift is produced (for 100 kilocycles this will be 5 microseconds) and the amplitude adjusted until the first half-cycle of the delayed signal (23B) is equal and opposite to the second half-cycle of the original signal. When these conditions exist, all succeeding half-cycles will cancel and the sum of the two signals (Fig.23C) will be zero except for the first half-cycle, thus effectively recreating a single pulse. (Some small amplitude trash will remain as a result of harmonics, but will be negligible.) The delay network must be adjustable near 5 microseconds and some amplitude control is necessary because no two tape recorders will produce the same wave form on playback. However, once set for any particular recorder, no further adjustment should be needed unless the system is to be used with another recorder. Figure 25 shows the general appearance of this unit.

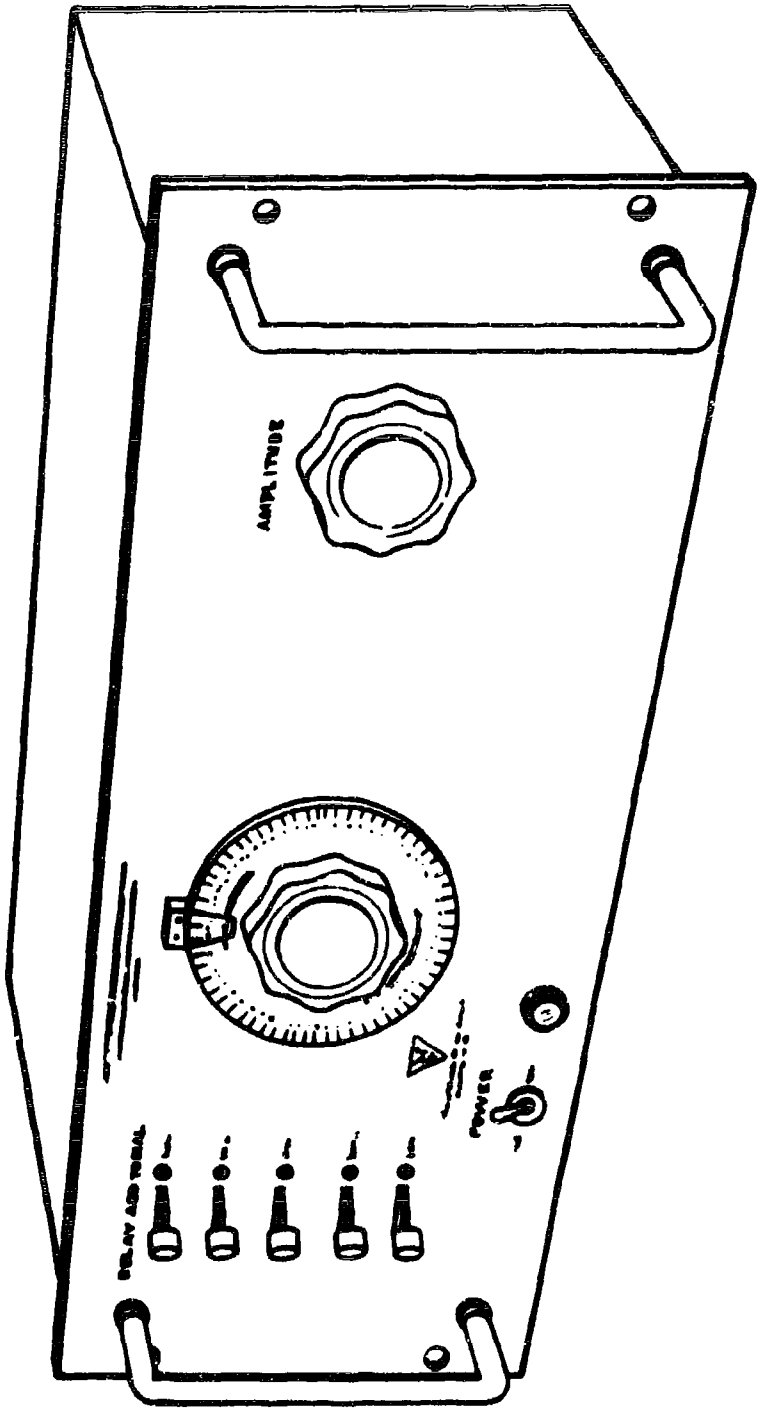

Figure 25. VCO Pulse Modifier

REFERENCES

1. R-3612P, Design, Development, and Fabrication of a Solid-Propellant Total Impulse Measurement System, Rocketdyne, a Division of North American Aviation, Inc., Canoga Park, California, 18 May 1962.

2. James, H. M., N. B. Nichols, and R. S. Phillips: Theory of Servomechanisms, McGraw-Hill Book Co., 1947.

3 Timoshenko, S.: Vibration Problems in Engineering, McGraw-Hill Book Co., 1st Edition, 1928.

4. Timoshenko, S. and D. H. Young: Advanced Dynamics, McGraw-Hill Book Co., 1st Edition, 1948.

5. Timoshenko, S.: Strength of Materials, 3rd Edition, Vol. 1, D. Van Nostrand Co., 1956.

6. Hildebrand: Introduction to Numerical Analysis, McGraw-Hill Book Co., 1956.

7. Henrici: Discrete Variable Methods in Ordinary Differential Equations, John Wiley and Sons, Inc.

8. Timoshenko, S. and D. H. MacCullough: Elements of Strength of Materials, 3rd Edition, D. Van Nostrand Co., 1949.

DISTRIBUTION LIST

U. S. Department of the Interior 1
Bureau of Mines
4800 Forbes Avenue
Pittsburgh, Pennsylvania 15213
Attn: M. M. Dolinar, Repts Librarian
Explosives Research Center

Central Intelligence Agency 1
2430 E Street, N. W.
Washington, D. C. 20505
Attn: OCD, Standard Dist.

Office of the Director of Defense 1
Research and Engineering
Washington, D. C. 20301
Attn: W. E. Sheehan, Office of Asst.
Dir. (Chemical Technology)

Nat'l Aeronautics and Space Admin. 1
Lewis Research Center
21000 Brookpark Road
Cleveland, Ohio 44135
Attn: Library

John F. Kennedy Space Center, 1
NASA
Cocoa Beach, Florida 32931
Attn: Library

Nat'l Aeronautics & Space Admin. 1
Manned Spacecraft Center
P. O. Box 1537
Houston, Texas 77001
Attn: Library

Nat'l Aeronautics & Space Admin. 1
George C. Marshall Space Flight
Center
Huntsville, Alabama 35800
Attn: Library

Nat'l Aeronautics & Space Admin. 3
Langley Research Center
Langley Air Force Base
Virginia 23365
Attn: Library

Nat'l Aeronautics & Space Admin. 1
Washington, D. C. 20546
Attn: Office of Technical Information
& Education Programs, Code
ETL

Scientific & Tech. Info Facility 2
P. O. Box 5700
Bethesda, Maryland 20014
Attn: NASA Representative

Nat'l Aeronautics & Space Admin. 1
Washington, D. C. 20546
Attn: R. W. Ziem (RPS)

Nat'l Aeronautics & Space Admin. 1
Goddard Space Flight Center
Greenbelt, Maryland 20771
Attn: Library

Defense Documentation Center 20
Cameron Station
Alexandria, Virginia 22314

RTD (RTNP) 1
Bolling AFB
Washington, D. C.

Arnold Eng. Development Center 1
Attn: AEOIM
Air Force Systems Command
Tullahoma, Tennessee 37389

AFRPL (RPR) 1
Edwards, California 92523

AFRPL (RPM) 1
Edwards, California 92523

AFFTC (FTBAT-2) 1
Edwards AFB, California 93523

Office of Research Analysis (OAR) 1
Attn: RRRT
Holloman AFB, New Mexico 88330

AFRPL (RPFDE) 33
Edwards, California 92523

Air Force Missile Test Center 1
Attn: MTBAT
Patrick Air Force Base, Florida 32925

Wright-Patterson AFB, Ohio 1
45433
Attn: AFML(MAAE)

Commanding Officer 1
Ballistic Research Laboratories
Aberdeen Proving Ground, Maryland
Attn: AMXBR-1
21005

Commanding Officer 1
Harry Diamond Laboratories
Washington, D.C. 20438
Attn: AMXDO-TIB

Commanding Officer 1
U.S. Army Research Office (Durham)
Box CM, Duke Station
Durham, North Carolina 27706

Commanding Officer 1
U.S. Army Chemical Research &
Development Laboratories
Edgewood Arsenal, Maryland 21010
Attn: Chief, Physicochemical
Research Division

Commanding Officer 1
Frankford Arsenal
Philadelphia, Pennsylvania 19137
Attn: Propellant & Explosives
Section, 1331

Commanding Officer 1
Picatinny Arsenal
Dover, New Jersey 07801
Attn: Library

Commanding Officer 1
Picatinny Arsenal
Liquid Rocket Propulsion Laboratory
Dover, New Jersey 07801
Attn: Technical Library

U.S. Army Missile Command 4
Redstone Scientific Info. Center
Redstone Arsenal, Alabama 35808
Attn: Chief, Document Section

Commanding General 1
White Sands Missile Range
New Mexico 88002
Attn: Technical Library

Bureau of Naval Weapons 2
Department of the Navy
Washington, D.C. 20360
Attn: DLI-3

Bureau of Naval Weapons 2
Department of the Navy
Washington, D.C. 20360
Attn: RMMP-2

Bureau of Naval Weapons 1
Department of the Navy
Washington, D.C. 20360
Attn: RMMP-3

Bureau of Naval Weapons 1
Department of the Navy
Washington, D.C. 20360
Attn: RMMP-4

Bureau of Naval Weapons 1
Department of the Navy
Washington, D.C. 20360
Attn: RRRE-6

Commander 2
U.S. Naval Missile Center
Point Mugu, California 93041
Attn: Technical Library

Commander 2
U.S. Naval Ordnance Laboratory
White Oak
Silver Spring, Maryland 20910
Attn: Library

Commander 5
U.S. Naval Ordnance Test Station
China Lake, California 93557
Attn: Code 45

Commander (Code 753) 2
U.S. Naval Ordnance Test Station
China Lake, California 93557
Attn: Technical Library

Superintendent 1
U.S. Naval Postgraduate School
Naval Academy
Monterey, California

Commanding Officer 1
U.S. Naval Propellant Plant
Indian Head, Maryland 20640
Attn: Technical Library

Commanding Officer 1
Office of Naval Research
1030 E. Green Street
Pasadena, California 91101

Director (Code 6180) 1
U.S. Naval Research Lab.
Washington, D.C. 20390
Attn: H. W. Carhart

Director 1
Special Projects Office
Department of the Navy
Washington, D.C. 20360

Commanding Officer 1
U.S. Naval Underwater Ordnance Station
Newport, Rhode Island 02844
Attn: W. W. Bartlett

Aerojet-General Corporation 1
P.O. Box 296
Azusa, California 91703
Attn: F. M. West, Chief Librarian

Aerojet-General Corporation 1
11711 South Woodruff Avenue
Downey, California 90241
Attn: Florence Walsh, Librarian

Aerojet-General Corporation 3
P.O. Box 1947
Sacramento, California 95809
Attn: Technical Information Office

Aeronutronic Div. Philco Corp. 1
Ford Road
Newport Beach, California 92600
Attn: Dr. L.H. Linder, Manager
Technical Information Dept.

Aeroprojects, Inc. 1
310 East Rosedale Avenue
West Chester, Pennsylvania 19380
Attn: C.D. McKinney

Aerospace Corporation 2
P.O. Box 95085
Los Angeles, California 90045
Attn: Library-Documents

Allied Chemical Corporation 1
General Chemical Division
Research Lab., P.O. Box 405
Morristown, New Jersey 07960
Attn: L.J. Wiltrakis, Security Officer

Amcel Propulsion Company 1
Box 3049
Asheville, North Carolina 28802

American Cyanamid Company 1
1937 W. Main Street
Stamford, Connecticut 06902
Attn: Security Officer

IIT Research Institute 1
Technology Center
Chicago, Illinois 60616
Attn: C.K. Hersh, Chemistry Div.

ARO, Inc. 1
Arnold Engrg. Dev. Center
Arnold AF Station, Tennessee 37389
Attn: Dr. B.H. Goethert
Director of Engrg.

Atlantic Research Corporation 2
Shirley Highway & Edsall Road
Alexandria, Virginia 22314
Attn: Library

Atlantic Research Corporation 1
Western Division
48-506 Easy Street
El Monte, California
Attn: H. Niederman

Battelle Memorial Institute 1
505 King Avenue
Columbus, Ohio 43201
Attn: Report Library, Room 6A

Bell Aerosystems 1
Box 1
Buffalo, New York 14205
Attn: T. Reinhardt

The Boeing Company 1
Aero Space Division
P.O. Box 3707
Seattle, Washington 98124
Attn: R.R. Barber, Lib. Ut. Ch.

Chemical Propulsion Information 3
Agency
Applied Physics Laboratory
8621 Georgia Avenue
Silver Spring, Maryland 20910

Defense Metals Information Ctr. 1
Battelle Memorial Institute
505 King Avenue
Columbus, Ohio 42301

Douglas Aircraft Co., Inc. 1
Santa Monica Division
3000 Ocean Park Boulevard
Santa Monica, California 90405
Attn: Mr. J.L. Waisman

The Dow Chemical Company 1
Security Section
Box 31
Midland, Michigan 48641
Attn: Dr. R.S. Karpiuk, 1710 Bldg.

E.I. duPont deNemours & Co. 1
Eastern Laboratory
Gibbstown, New Jersey 08027
Attn: Mrs. Alice R. Steward

Esso Research & Engineering Co. 1
Special Projects Unit
P.O. Box 8
Linden, New Jersey 07036
Attn: Mr. D.L. Baeder

General Dynamics/Astronautics 1
P.O. Box 1128
San Diego, California 92112
Attn: Library & Information
Services (128-00)

General Electric Company 1
Flight Propulsion Division
Evendale
Cincinnati, Ohio 45215

Hercules Powder Company 1
Allegany Ballistics Laboratory
P.O. Box 210
Cumberland, Maryland 21501
Attn: Library

Hercules Powder Company 1
Research Center
Wilmington, Delaware 19899
Attn: Dr. Herman Skolnik, Manager
Technical Information Division

Jet Propulsion Laboratory 1
4800 Oak Grove Drive
Pasadena, California 91103
Attn: Library (TDS)
Mr. N. E. Devereux

Arthur D. Little, Inc. 1
15 Acorn Park
Cambridge, Massachusetts 02140
Attn: W. H. Varley

Lockheed Propulsion Company 3
P. O. Box 111
Redlands, California 92374
Attn: Miss Belle Berlad, Librarian

Marquardt Corp. 1
16555 Staticoy Street
Box 2013 - South Annex
Van Nuys, California 91404

Martin Company 1
Baltimore, Maryland 21203
Attn: Science - Technology
Library - Mail 398

Minnesota Mining & Manufacturing 2
Co.
900 Bush Avenue
St. Paul, Minnesota 55106
Attn: Code 0013 R & D
VIA: H. C. Zeman
Security Administrator

Monsanto Research Corporation 1
Boston Labs., Everett Station
Chemical Lane
Boston, Massachusetts 02149
Attn: Library

New York University 1
Dept. of Chemical Engineering
New York, New York 10053
Attn: P. F. Winternitz

North American Aviation, Inc. 1
Space & Information Systems Div.
12214 Lakewood Boulevard
Downey, California 90242
Attn: W. H. Morita

Rocketdyne 3
6633 Canoga Avenue
Canoga Park, California 91304
Attn: Library, Dept. 596-306

Rohm & Haas Company 1
Redstone Arsenal Research Division
Huntsville, Alabama 36808
Attn: Librarian

Space Technology Laboratory, 2
Inc.
1 Space Park
Redondo Beach, California 90200
Attn: STL Tech. Lib. Doc.
Acquisitions

Texaco Experiment Incorporated 1
P. O. Box 1-T
Richmond, Virginia 23202
Attn: Librarian

United Technology Center 1
P. O. Box 358
Sunnyvale, California 94088
Attn: Librarian

Thiokol Chemical Corporation 1
Alpha Division, Huntsville Plant
Huntsville, Alabama 35800
Attn: Technical Director

Thiokol Chemical Corporation 1
Alpha Division
Space Booster Plant
Brunswick, Georgia 31500

Thiokol Chemical Corporation 1
Elkton Division
Elkton, Maryland 21921
Attn: Librarian

Thiokol Chemical Corporation 1
Reaction Motors Division
Denville, New Jersey 07834
Attn: Librarian

Thiokol Chemical Corporation 1
Rocket Operations Center
P. O. Box 1640
Ogden, Utah 84401
Attn: Librarian

Thiokol Chemical Corporation 2
Wasatch Division
P. O. Box 524
Brigham City, Utah 84302
Attn: Library Section

Union Carbide Chemicals Co. 1
P. O. Box 8584 (Technical Center)
South Charleston, West Virginia
25303 Attn: Dr. H. W. Schulz

United Aircraft Corporation 1
Pratt & Whitney Fla. Res. & Dev. Ctr.
P. O. Box 2691
W. Palm Beach, Florida 33402
Attn: Library

United Aircraft Corporation 1
Corporation Library
400 Main Street
East Hartford, Connecticut 06118
Attn: Dr. David Rix

General Electric Company 1
Apollo Support Department
P. O. Box 2500
Dayton Beach, Florida 32015

British Defence Staff * 4
British Embassy
3100 Massachusetts Avenue
Washington, D. C. 20008
Attn: Scientific Information Officer

Defence Research Member * 4
Canadian Joint Staff (W)
2450 Massachusetts Avenue
Washington, D. C. 20008

Commanding Officer 1
Ammunition Procurement & Supply
Agency
Joliet, Illinois 60400
Attn: Engr. Library

AFRPL (RPCS) 1
Edwards, California 93523

Callery Chemical Company 1
Research & Development
Callery, Pennsylvania 16024
Attn: Document Control

Ethyl Corporation 1
P. O. Box 3091
Istrouma Branch
Baton Rouge, Louisiana 70805

Hercules Powder Company 1
Bacchus Works
Magna, Utah 84044
Attn: Librarian

Hynes Research Corporation 1
308 Bon Air Avenue
Durham, North Carolina 27704

Walter Kidde Company 1
675 Main Street
Belleville, New Jersey 07109
Attn: Security Librarian

Olin Mathieson Chemical Corp. 1
Marion, Illinois 62959
Attn: Research Library
Box 508

Olin Mathieson Chemical Corp. 1
Research Library 1-K-3
275 Winchester Avenue
New Haven, Connecticut 06511
Attn: Mail Control Room
Miss Laura M. Kajuti

Pennsalt Chemicals Corporation 1
Technological Center
900 First Avenue
King of Prussia, Pennsylvania 19406

Purdue University 1
Lafayette, Indianna 47907
Attn: M. J. Zucrow

Rocketdyne, A Division of 1
North American Aviation, Inc.
Solid Propulsion Operations
P. O. Box 548, McGregor, Texas
76657
Attn: Library

Shell Development Company 1
1400 53rd Street
Emeryville, California 94608

Southwest Research Institute 1
Department of Structural Research
8500 Culebra Road
San Antonio, Texas 78228
Attn: Dr. Robert C. DeHart, Director

Texaco, Inc. 1
P. O. Box 509
Beacon, New York 12508
Attn: Dr. R. E. Conary, Manager

Los Alamos Scientific Laboratory 1
University of California
P. O. Box 1663
Los Alamos, New Mexico 87544

Headquarters, U. S. Air Force 1
Washington, D. C.
20330
Attn: AFRSTD

AFRPL (RPCL) 1
Edwards, California 93523

Callery Chemical Company 1
Research & Development
Callery, Pennsylvania 16024
Attn: Document Control

Chem. Research & Dev. Center 1
FMC Corporation
P. O. Box 8
Princeton, New Jersey 08540
Attn: Security Officer

Ethyl Corporation 1
P. O. Box 3091
Istrouma Branch
Baton Rouge, Louisiana 70805

Hynes Research Corporation 1
308 Bon Air Avenue
Durham, North Carolina 27704

Walter Kidde Company 1
675 Main Street
Belleville, New Jersey 07109
Attn: Security Librarian

Olin Mathieson Chemical Corp. 1
Research Library 1-K-3
275 Winchester Avenue
New Haven, Connecticut 06511
Attn: Mail Control Room
Miss Laura M. Kajuti

Pennsalt Chemicals Corporation 1
Technological Center
900 First Avenue
King of Prussia, Pennsylvania 19406

Purdue University 1
Lafayette, Indiana 47907
Attn: M. J. Zucrow

Shell Development Company 1
1400 53rd Street
Emeryville, California 94608

Southwest Research Institute 1
Department of Structural Research
8500 Culebra Road
San Antonio, Texas 78228
Attn: Dr. Robert C. DeHart, Director

Texaco, Inc. 1
P. O. Box 509
Beacon, New York 12508
Attn: Dr. R. E. Conary, Manager

* Reports prepared under a Department of the Air Force contract or project will be transmitted VIA:

Headquarters
Air Force Systems Command
Attn: SCS-41(3-1833)
Andrews Air Force Base
Washington, D. C. 20331